PIAF

Vincent Henneken

Product-internal assembly functions

A novel micro-assembly concept applied to optical interconnects

Proefschrift

ter verkrijging van de graad van doctor
aan de Technische Universiteit Delft,
op gezag van de Rector Magnificus prof.dr.ir. J.T. Fokkema,
voorzitter van het College voor Promoties,
in het openbaar te verdedigen op vrijdag 5 december 2008 om 10.00 uur

door

Vincent Adrianus HENNEKEN

werktuigkundig ingenieur
geboren te Leidschendam

Dit proefschrift is goedgekeurd door de promotoren:

Prof.dr. U. Staufer
Prof.dr. P.M. Sarro

Copromotor: dr.ir. M. Tichem

Samenstelling promotiecommissie:

Rector Magnificus,	voorzitter
Prof.dr. U. Staufer,	Technische Universiteit Delft, promotor
Prof.dr. P.M. Sarro,	Technische Universiteit Delft, promotor
Dr.ir. M. Tichem,	Technische Universiteit Delft, copromotor
Prof.dr. A. Boisen,	Danmarks Tekniske Universitet, Denemarken
Prof.ir. H.M.J.R. Soemers,	Universiteit Twente
Prof.dr.ir. R. Dekker,	Technische Universiteit Delft
Dr.ir. H. de Waardt,	Technische Universiteit Eindhoven
Prof.dr.ir. J. van Eijk	Technische Universiteit Delft, reservelid

The research described in this PhD thesis has been financially supported by the Dutch government programme IOP Precision Engineering as part of the project IPT02310 Technologies for in-package optical fibre-chip coupling.

ISBN 978-90-9023430-4

Acknowledgments

In pursuing a PhD, of course there are many moments of working on your own, but when looking back I particularly remember all the valuable discussions and the pleasant contact with everybody I shared place, time, and thought with. Just too many people to mention have contributed to the work presented in this thesis, or have played a significant role in making my past years into very enjoyable ones.

First of all, I would like to express my gratitude to my promoters Urs Staufer and Lina Sarro for their pleasant discussions and valuable input during different stages in my project. Urs, I'm sure I would have enjoyed working with you for a longer time. Lina, thank you for being so cooperative and practical.

My special gratitude goes out to my daily supervisor Marcel Tichem, for offering me such an interesting project and convincing me that doing a PhD would be 'just something for me'. Furthermore, his support was invaluable, particularly during the years that our group was lacking a professor.

I also would like to thank all my (former) colleagues within TU Delft who shared their experience, thoughts and ideas with me, and who contributed in creating an enjoyable and stimulating working environment. Incredible, how much knowledge is 'hidden' in such a diverse and international organization like TU Delft!

Within the department PME, I would like to thank my fellow PhD researchers, in particular my room mates Defeng and Iwan, but also my close colleagues in the former PMA group Jeroen Derkx, Marcel Achtsnick, Tolga, Viktoria, Peiyuan, Pi, and Rogier. I would also like to mention my recent

room mates Marcello, Friedi ;) and Hans, as well as my colleagues of the Mechatronics group, for their pleasant company during my last months after moving to the laboratory.

With regard to my project, I would like to thank Warner Venstra for paving some of the way, and Fredrik Creemer, Hans Goosen, Sander Paalvast, Gih-Keong Lau and Matthijs Langelaar for their valuable input during many discussions. Huug de Waardt and Johan van Zantvoort of TU/e and Jan Mink (www.2mel.nl) are also acknowledged for their input in various discussions.

A special thanks is due to the DIMES ICP team, and especially Wim van der Vlist and Wim Wien for their advice and for carrying out careful processing, packaging, and delicate wire bonding. Without your help the demonstrators could not have been realized! Ms. C. Thanner of EV Group Austria is kindly acknowledged for spray coating some of the critical wafers. Furthermore, I thank Harry and Jos for their technical assistance in the laboratory, also on behalf of my students.

I really enjoyed coaching students, and I am indebted to all who have contributed to my research: Sven van den Bedem (MSc assignment), Reimer Hettema, Kun Liu, Roel Engelen, Ronald Plak, Reinout Swane, Michel Jansen, Kees Buring (MSc), Michiel Berkheij (MSc), Derk Luik, Wouter Sassen (MSc), and Henk van der Burgh (MSc). Particularly I would like to mention Wouter Sassen, whom I managed to persuade to stay and help a few months more after his graduation. Working towards a 'common goal', first also with Henk, and later together, I really enjoyed very much!

Finally, I would like to thank my parents, family and friends for all their interest and attention. Most of all, I thank Addie, for her love, support, encouragement, and patience over the past few years. I promise I will not do it again!

Vincent Henneken

Delfgauw, October 2008

Contents

Abbreviations

2-D	Two-dimensional
3-D	Three-dimensional
AuSn	Gold-tin
CTE	Coefficient of thermal expansion
DBR	Distributed Bragg reflector
DFB	Distributed feedback
DIMES	Delft Institute of Microsystems and Nanoelectronics
DOF(s)	Degree(s) of freedom
DRIE	Deep reactive ion etching
DWDM	Dense wavelength division multiplexing
EDFA	Erbium doped fibre amplifier
FEA	Finite element analysis
FTTH	Fibre-to-the-home
IC	Integrated circuit
InGaAsP	Indium gallium arsenide phosphide
KOH	Potassium hydroxide
LD	Laser diode
LED	Light emitting diode

LIGA	Lithography, electroforming, and moulding
LPCVD	Low-pressure chemical vapour deposition
MEMS	Micro electro mechanical system
MST	Microsystem technology
PbSn	Lead-tin
PCB	Printed circuit board
PIAF	Product-internal assembly functions
PWS	Post-weld shift
PZT	Lead zirconate titanate
SCARA	Selectively compliant assembly robot arm
SDA	Scratch drive actuator
Si	Silicon
SiN	Silicon nitride
SiOB	Silicon optical bench
SMA	Shape memory alloy
SMD	Surface mount device
SOI	Silicon-on-insulator
SEM	Scanning electron microscope
TEC	Thermoelectric cooler
TEOS	Tetraethoxysilane
UV	Ultraviolet
VCSEL	Vertical cavity surface-emitting laser
VOA	Variable optical attenuator
ZnO	Zinc oxide

1

Introduction

This chapter provides a brief introduction to the research covered in the present thesis: *micro-assembly using product-internal assembly functions* (PIAF). First, the effect of the continuing technological miniaturization on assembly demands is briefly introduced in Section 1.1, opening up opportunities for the novel micro-assembly method investigated here, which is subsequently introduced. In Section 1.2, the objective and the main research questions are introduced, followed in Section 1.3 by an explanation of the approach taken in the investigation. Finally, the structure of the thesis is outlined in Section 1.4.

1.1 The effect of miniaturization on assembly demands

In the past decades, miniaturization has been an important driving force in the development of technology. For example consumer products have become smaller and smaller, and at the same time function densities have increased dramatically.

This miniaturization trend has a significant effect on production. It brings challenges to both part manufacturing and the assembly of these smaller parts into composed products. Assembly of miniature parts is commonly referred to as *micro-assembly*. Micro-assembly is the assembly of small products with a high accuracy, in the range of 0.1-20 μm, having overall dimensions of about 0.5-30 mm, and with part features in the order of

10-100 μm. Along with the miniaturization trend, micro-assembly gains in importance in the assembly domain.

In addition to reducing overall part and product dimensions, the fabrication tolerances and the positioning requirements also become stricter. Assembly is performed manually or (semi-)automatically. When scaling down to smaller dimensions and at the same time moving towards higher accuracies, it becomes increasingly difficult to fulfil the stricter requirements using these conventional assembly methods. Assembly times increase and the costs constitute a larger part of the overall production cost than in the case of macro-scale products.

The fact that conventional assembly methods have increasing difficulty to fulfil the tighter demands posed to micro-assembly asks for the use of possible alternative methods to perform micro-assembly. The present thesis covers the feasibility study regarding one of these methods: *micro-assembly using product-internal assembly functions*, PIAF for short.

The PIAF method

This method distinguishes itself from other methods by the fact that part of the assembly functionality is included into the product subject to assembly. The process is started with a coarse assembly step, to prepare for the product-internal assembly process. The functions that apply for integration in the product are (1) controlled positioning of the component, (2) sensing the position of the component, and (3) fixation of the component in the final position, see Figure 1.1.

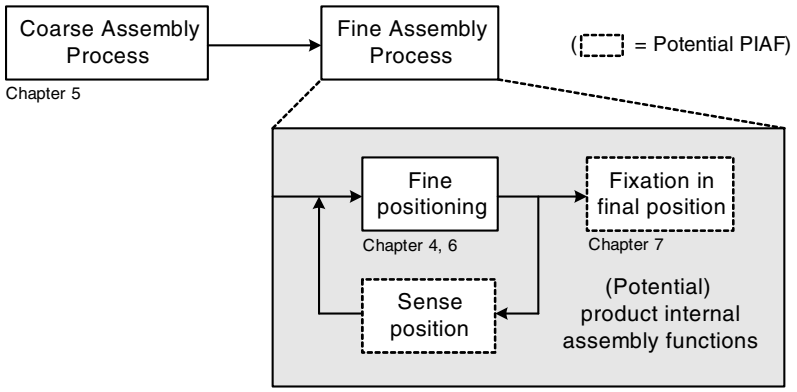

Figure 1.1 Schematic function overview of micro-assembly using product-internal assembly functions (including the chapter numbers in which the indicated sub-functions are discussed)

Although adding functionality to the product likely increases its cost, the overall cost may actually be *de*creased because it reduces the required accuracy of the preceding coarse assembly step. Moreover, it may positively influence assembly yield and cycle time, and possibly result in higher assembly accuracies.

Microsystem technology (MST) - comprising lithography-based techniques from the integrated circuit (IC) domain for selectively depositing and removing material on wafers - is selected as enabling technology for creating the product-internal functionality. This technology was selected based on its capability to create very small structures with extremely high accuracies at potentially low cost, resulting from its possibility of batch processing. The processing also has limitations: a restricted set of techniques is available and processing is predominantly planar, posing challenges to the design of the often required 3-D structures.

Although a small number of MST-based devices have been found in literature that can be categorized as example implementations of the PIAF method, this method of micro-assembly to date has not been investigated in a comprehensive manner. When considering the potential advantages and the apparent drawbacks, it is not evident whether the PIAF method could become a viable alternative for existing micro-assembly methods. This has formed the most important motivation for this research.

1.2 Objective and research questions

The focus in the investigation has been mainly on the technical feasibility of the method, involving whether and how the required functionality can be realized. This is a necessary precondition for the economic viability of the method, which concerns if and under which conditions the method can be an attractive alternative compared to competitive methods. Although it would be valuable to make statements about the economical applicability of the method, this is very complicated, since reliable quantitative estimates of costs and sales volumes would be required, both for the PIAF method and for alternative methods, which are extremely difficult to obtain. Therefore, only a limited assessment of its economic viability is presented in the concluding chapter of this thesis.

Technical aspects for investigation are for example the possibilities of the product-internal functions, such as attainable actuation forces and ranges, but also the achievable number and configuration of different positioning actuators. Integration issues also need to be considered, as the PIAF functionality should be included into the product without or only minimally affecting its primary functionality. Finally, bringing the component to be

assembled into contact with the MST-based internal assembly functionality - which is most likely fragile - also requires investigation.

The research has an exploratory character; therefore the main objective of the research has been defined as follows:

To explore the technical feasibility of using MST-based product-internal assembly functions for the purpose of micro-assembly.

Research questions related to this objective are:

- *What is the portion of assembly functionality to be performed product-internally? How (and to what degree) is the product-internal assembly functionality integrated in the overall system?*
- *What methods are available for coarse placement and fixation of the part?*
- *What methods/technologies are available for product-internal fine positioning of the part?*
- *What methods/technologies are available for sensing the relative position of the part?*
- *What methods/technologies are available for final fixation of the part?*
- *How does the product-internal assembly functionality interact with the primary device functionality? What interactions and trade-offs exist between the coarse and fine assembly functionality? How do the fine positioning and the fixation functionality interact?*

Internal position sensing is not part of the investigation to limit the complexity and size of the project. Instead, for the product case under investigation - introduced in the next section and discussed in more detail in Chapter 3 - it is reasoned that position sensing takes place conventionally using external means.

The remaining research questions are treated in detail in the present thesis, starting with the first one in Chapter 3 by making initial decisions on how the product-internal assembly functionality should be combined with the primary device functionality for the product case under investigation.

1.3 Research approach: designing for a specific product case

It was decided to make the investigation more concrete by developing product-internal assembly functions for a specific product case. The selected

product case was the accurate assembly of an optical fibre with respect to a laser diode in a realistic coupling configuration for telecommunication applications. This case was selected based on its industrial relevance and the assembly challenge in aligning at very tight tolerances in order to maximize light coupling between the components. The strictest tolerances are in the plane perpendicular to the propagation direction of the light and can be as small as 0.1 μm for the most demanding situations.

Following from the decision to focus the investigation on the fibre coupling case, the problem statement and the research questions presented in the previous section were narrowed down towards the content of this case. The problem statement for the fibre coupling case is as follows:

In what way can MST-based product-internal assembly functions best be used for accurately assembling an optical fibre with respect to an optical chip in the selected fibre-chip coupling case?

The related research questions are a further specification of the ones written above, and are therefore not repeated here.

By developing product-internal assembly functions for a specific product case, we obtain valuable insights in what is exactly involved in applying this concept. However, it should be realized that it is only possible to draw conclusions about the case being considered; it is not allowed to extend these conclusions to other cases without verifying the validity. Scientific research is generally considered to be composed of explorative research followed by evaluative research in a cyclic manner; in the exploration phase observations are made, aimed at development of a theory and/or formulation of hypotheses (*induction*). In the evaluation phase, these assumptions or hypotheses are used as starting point for making predictions about other cases (*deduction*), which are then tested by collecting observations that either confirm or falsify the expectations. Combined they expand the knowledge about the subject under investigation; see *e.g.* Christiaans *et al.* (2004). From this viewpoint the presented explorative case study is an essential first step in a possible broader investigation into the technical feasibility of the PIAF concept, aiming to result in a better understanding and assumptions about the issues involved, which may be verified in an evaluative investigation with regard to validity for a wider application field.

Design process

The development of product-internal assembly functionality is a typical example of a mechanical design process. In literature various sources on design methodology can be found, with often little difference in the described methodology. The present project loosely follows the design approach as presented by Pahl and Beitz (1996), in which the design process

is split up into four main phases: *problem analysis*, *conceptual design*, *embodiment design* and *detail design*.

First, during the problem analysis, the design problem is analyzed and all demands and wishes are gathered in a requirements list, which serves as a starting point for the following design steps. In the conceptual design phase, suitable solution principles are found for all sub-functions and combined into concept variants, which are evaluated against criteria derived from the requirements list. Subsequently, during the embodiment and detail design phase the technical design is developed from the concept, in accordance with technical and economical considerations, ultimately aiming to lead to an overall solution that best fulfils the initial task set out at the start of the design process.

The design process used in the present research project largely followed the here described procedure, starting with the problem analysis in Chapter 3. The design problem was elaborated and an overview of the relevant requirements was drawn up. Next, described in Chapters 4 through 7, solution principles for the main considered sub-functions *fine positioning*, *coarse assembly* and *fine fixation* were investigated and developed in a step-wise approach, increasing in complexity from 1-D to 2-D fine positioning, and ultimately leading to a proposed overall design, presented in Chapter 7. Demonstrators were developed and realized at the Delft Institute of Microsystems and Nanoelectronics (DIMES) of the TU Delft.

In the thesis, relatively much attention is paid to finding and developing solution principles on sub-function level, due to the relative immaturity and lack of standardization of the used technology. For example, MST-based actuators for internal fibre positioning required dedicated development. Moreover, this is an important aspect in the underlying PIAF feasibility investigation. For applying PIAF, typically the same sub-functions should be fulfilled regardless of the product case involved. Therefore, the discussed solution principles may be used for other cases for which PIAF should be applied and have a broader relevance than for the considered fibre coupling case only.

Although the selection and development of solution principles for the individual sub-functions is presented sequentially in Chapters 4 to 7, the actual steps took place more in parallel. Additionally, the solution principles were not only evaluated on sub-function level, but also on system level to ensure good compatibility with the other parts of the system.

1.4 Structure of the thesis

The chapters in this thesis are grouped into three parts, as shown in Figure 1.2. In Part I, comprising the first two chapters, the research focus is outlined. In the present chapter, the research goal and questions were defined, and the approach for the investigation was explained. Following, the background and motivation of the research is further elaborated and the PIAF concept is discussed in more detail in Chapter 2.

Part II, encompassing Chapters 3 through 7, is dedicated to the design and development of product-internal functionality for the fibre coupling product case. In Chapter 3, the first design choices regarding the device configuration are explained and the requirements overview for the internal assembly functionality is presented. Following, in Chapter 4, an MST-based actuation principle is selected for positioning the fibre tip in the chosen product case, and test results are presented of 1-D in-plane embodiments for this actuation principle. In Chapter 5, a design is proposed for the coarse assembly process that should precede the final fine positioning of the fibre, after which the design, fabrication and testing results of the developed MST-based 2-D fibre concept are presented in Chapter 6. In Chapter 7 the selection, development, and test results of the fibre fine fixation functionality are presented, together with adaptations to the 2-D positioning functionality to enable integration into a single chip. Their joint performance is discussed based on experimental and modelling results.

Finally, in Part III, consisting of Chapter 8, the results achieved in the project are discussed and the application potential of the PIAF method is evaluated, after which the chapter is concluded with suggestions for further research.

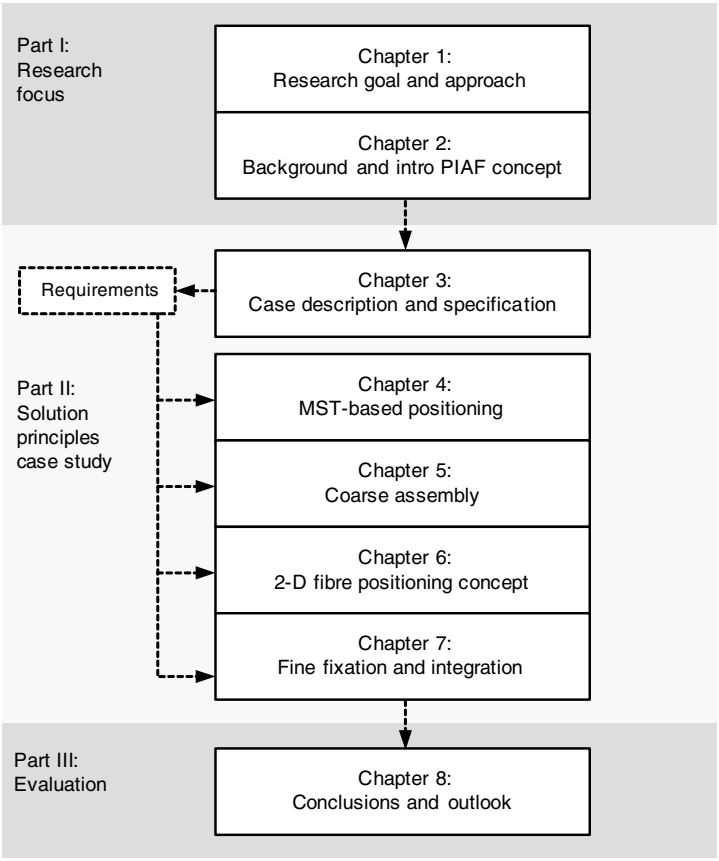

Figure 1.2 Structure of the thesis

2

Background and introduction PIAF concept

In this chapter, the novel concept of using MST-based product-internal assembly functions for the purpose of micro-assembly is discussed, along with relevant background information and examples.

In Section 2.1, background information is provided about assembly in general and micro-assembly in particular, and the main challenges regarding micro-assembly are outlined. The possibilities and limitations of currently used and researched micro-assembly methods are discussed in Section 2.2, followed in Section 2.3 by an in-depth treatment of the novel micro-assembly concept investigated in this research. Finally, the selection of MST as technology enabler for the PIAF concept is more elaborately explained in Section 2.4, accompanied by an overview of MST-based PIAF and PIAF-related examples from literature.

2.1 Micro-assembly as research area

In recent history a gradual shift in focus of academic research has taken place from the conventional assembly domain (also called *macro*-assembly) towards *micro*-assembly, very much in parallel to a major technological trend in the last decades: *miniaturization*. In the following subsections, a brief introduction into assembly is provided, followed by a discussion of the relevance of micro-assembly and specific challenges in the micro-assembly sub domain.

2.1.1 Assembly terminology and characteristics

Assembly is defined in Webster's dictionary as the fitting together of manufactured parts into a complete machine, structure, or unit of a machine. The necessity of assembly originates from the need for separation of parts. In Willemse (1997), seven fundamental reasons were formulated that give rise to the need for part separation, the most important of which are:

- (relative) motion possibilities;
- fabrication considerations;
- different material properties.

A comprehensive treatment of the assembly terminology and their definitions is provided in Vos (2001). Assembly can be considered the final part of the product creation process. Discrete parts are fabricated from raw materials (*fabrication* or *part-manufacturing*) and subsequently combined into composed products using assembly. *Production* in this thesis denotes the area that includes fabrication, assembly, and all product creation related fields such as product design and production planning. The assembly process consists of a sequence of assembly operations. In a basic assembly cycle typically the assembly operations *feed-grip-move-mount* take place, however a multitude of other terms are also used in describing assembly operations. For example, the terms *connect*, *mount*, *fit*, and *join* are used as synonyms. They all represent the process of making a connection between parts (Baartman 1995, p.11). The same holds for the slightly different but related terms *fasten*, *fixate* and *fix*, which are used to describe the putting a part securely in place or in a desired position.

Manual versus automatic assembly

A main classification of industrial assembly is based on the level of automation that is being applied. In many occasions, assembly can be performed manually, requiring hardly any tools or machines. However, both economical and technical motives for automation can be distinguished. Willemse (1997) has identified five different possible reasons for assembly automation:

- rationalizing of production, *viz.* productivity gain or cost savings;
- elimination of monotonous tasks;
- improved quality control and less rejects;
- miniaturization beyond human handling capabilities;
- special environmental conditions, such as clean rooms or handling in hazardous environments, such as nuclear systems.

Based on individual product and production requirements, the entire range from completely manual assembly to fully automatic assembly may be encountered in industry. The most important parameters for determining the appropriate level of automation for a given situation are *production volume* and *product complexity* (Vos 2001). Generally, a higher level of automation is warranted only at higher production volumes and lower product complexity.

Despite significant efforts to improve this issue, up to now automated assembly is still relatively inflexible compared to manual assembly. An important bottleneck preventing successful implementation of flexible automation is embedded in the products themselves. Assembly is not taken into account in the design, making the majority of present-day products unfit for flexibly automated assembly (Willemse 1997). Therefore, assembly automation is only considered feasible if the required investment pays off within a few years, ideally within the expected production duration the initial investment is set out for. Potential long-term advantages of automation are mostly not considered since they are outside the time scope of the financial calculations.

Issues limiting high-level automation from becoming more widespread are found both on the demand and the supply side. Especially in the consumer product market the demands on the assembly process have grown considerably, due to market developments and increasing competition. Generally, over the past years, production series have become smaller due to shorter product life cycles and a trend towards increased product differentiation, which can only partly be addressed by applying a modular product design (Doll and Vonderembse 1991)[1]. An example of a high degree of differentiation combined with short life cycles can be seen in the mobile phone market, in which market leader Nokia alone offers over 100 models worldwide and has launched 30 new models in the first half of 2008 only (Nokia 2008). On the supply side, automation should compete with an increased availability of cheap labour. In many industries, shifting assembly to low-to-medium-wage countries has taken a high rise in recent years, for a large part to South-East Asia but for example also to Eastern European countries. Nevertheless, in some situations technical or economical reasons exist for selecting some form of automation to perform (part of) the assembly process.

[1] A trend also characterized as 'low-volume/high-mix'.

2.1.2 Challenges in micro-assembly

One of the strongest driving forces in technology development in recent decades has been *miniaturization*. The aims in product miniaturization are to increase the function density of products, to achieve new product possibilities, or to improve energy efficiency or material usage (Tichem and Karpuschewski 2002). This has led to the emerging of more and more miniature-sized products, so-called *micro-products*. Assembly associated to composed products of this type is often referred to as *micro-assembly*.

Micro-assembly is the assembly of small products with high accuracy. In literature, no single clear definition of micro-assembly is given. In this thesis, micro-products are characterized as having overall part-and product dimensions in the range of about 0.5-30 mm, with part features in the range of 10-100 μm.[1]

Generally, the demanded accuracy in positioning is high. The required accuracy in relative position of features of parts may vary from 10-20 μm down to 0.1 μm for the most demanding applications. This accuracy should be maintained after parts are joined, *e.g.* by gluing or soldering.

Micro-products can either be stand-alone products, or can be applied in larger-scale systems. Example application fields are (Tichem and Karpuschewski 2002):

- photonics and optoelectronics, *e.g.* fibre(-array) to chip coupling, optical switching;
- biomedical instruments, *e.g.* for tissue handling, surgery, endoscopy and catheterisation;
- consumer electronics, *e.g.* disk drives, reading head actuators, mechanisms in video cameras;
- automotive industry, *e.g.* the application of micro-systems in engine systems or safety systems;
- production engineering, *e.g.* micro sensors for process monitoring and micro grippers for assembly.

Micro-products include both highly miniaturized mechatronic systems which originate from the mechanical engineering discipline, as well as so-called *hybrid microsystems*, which originate in the semiconductor domain.[2]

[1] Although representing an interesting emerging field of investigation, structures in the nanometre range are not included, since they comprise only a relatively small portion of the overall micro-product portfolio which do not yet require industrial assembly.

Increasingly, it can be seen that micro-products also comprise of parts from both technology domains. From this viewpoint, the area of micro-products and micro-assembly can be considered as a field in which these traditionally separate technology domains meet. In Figure 2.1 a schematic overview is shown of micro-products with their associated fabrication technology domains.

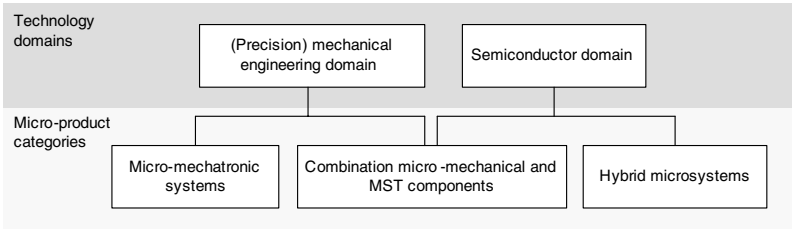

Figure 2.1 Micro-product categories with their associated technology domains

Interest in micro-assembly, also as part of academic research, has been fuelled by the increased availability of micro-products. Specific challenges that are met in the micro-assembly area are mostly related to the small dimensions and the high demanded accuracies involved. According to Reinhart and Höhn (1997) the main challenges associated to the manipulation and assembly of micro parts can be summarized as follows:

- Tolerance problems: exceptionally small assembly tolerances are permissible, which, depending on the application, lie between 0.1 and 20 μm.
- Force problems: with reducing product dimensions, the relative influence of physical effects that operate on the objects change. Forces related to surface interactions - electrostatic forces, surface tension forces and Van der Waals forces - start to prevail over gravity, which scales with the volume of objects (Fearing 1995, Arai *et al.* 1995). This may result in uncontrolled part behaviour, *e.g.* repulsion of the micro part or sticking of the part to the gripper. In addition, due to small contact areas, even low forces may exceed the allowable surface pressure and consequently damage the components, which are often very fragile.

[2] In the USA, but also in other regions, these are mainly referred to as *Micro Electro Mechanical Systems* or *MEMS*; in Europe the term *Microsystem Technology* (MST) is used to describe the associated technology domain. The latter term is also used in the present thesis for this purpose. A more elaborate introduction into MST is provided in Section 2.4.

- Interference factors: *e.g.* vibrations, temperature changes or contamination can cause positioning errors or have an adverse effect on product quality.
- Variety of models: a notable feature of micro-products is their large number of different models. Any system for automated assembly of micro-products therefore should be suitably flexible.

Due to the specific challenges related to micro-assembly, usually lower assembly speeds and yields are achieved than in the macro domain. Micro-assembly cost is therefore typically relatively high. According to information from industrial companies it is often between 60 and 90% of the total product cost (Tichem and Karpuschewski 2002). Consequently, a natural approach is to try to avoid micro-assembly altogether by employing a higher level of integration than with conventional size products. However, critical micro-assembly steps become increasingly unavoidable.

2.2 Micro-assembly methods and research

In this section, the main methods currently employed and being researched to perform micro-assembly tasks are briefly discussed. For a more extensive overview the reader is referred to Böhringer *et al.* (1999) and Van Brussel *et al.* (2000).

2.2.1 Current micro-assembly approaches

Approaches currently used for performing micro-assembly tasks in industry are based on downscaling or otherwise adapting macro-scale assembly solutions. Both manual and automated assembly solutions are employed, of which manual assembly is still widely used because of its unsurpassed flexibility. Usually, the sensor and actuator skills of the human operators are improved by providing them with appropriate tools or equipment, ranging *e.g.* from tweezers and microscopes to vision systems and mechanisms which increase the sensitivity for the operators' movements.

A difficulty in manual handling of micro-parts is the loss of direct hand-eye co-ordination (Van Brussel *et al.* 2000). The microscopes and tools limit the ability to directly see and sense the objects to be handled. The tools have less degrees of freedom than the human hand and the assembly and grasping forces are generally too small to be sensed by a human operator.

A method under investigation to solve the lack of force feedback for accurate positioning under contact is by so-called haptic micro-assembly using master-slave tele-operation systems equipped with force sensors. In such

systems the position of the master arm, manipulated by the operator, is scaled down and used to control the position of the slave. The forces measured by the slave system are amplified and transferred to the master arm. Haptic micro-assembly systems are in a research stage and are not yet commonly applied in industry.

Since manual micro-assembly tasks are very demanding on the human operators performing them, they are time-consuming and costly, and frequently give rise to quality problems (Reinhart and Höhn 1997). In certain challenging cases, demands on the assembly process supersede the capabilities of human operators, despite the use of supporting sensor and actuator systems.

Accuracy of manipulators

To overcome the problems related to the limited capabilities of human operators, employment of automated assembly solutions is a logical approach. However, as indicated in the previous section, the demanded positional accuracies in the micro-assembly domain typically are much stricter than for macro-scale assembly. This degree of precision is beyond the calibration range of conventional open-loop assembly devices used in industry. Conventional multi-link robots typically have a repeatability in the order of 100 μm, which is much higher than the defined 20-μm upper threshold for micro-assembly. Examples of state-of-the-art SCARA[1] robots especially designed for micro-handling are the twin-arm RP series MELFA robots by Mitsubishi Electric, which have a repeatability of at best ± 5 μm in the horizontal plane and ± 10 μm vertically at a pick-and-place cycle period less than 0.5 s (Mitsubishi 2008).

A common approach to improve the assembly accuracy is by employing closed-loop vision feedback. Particularly in the highly specialized assembly of electronic components onto printed circuit boards (PCBs) this is very successful. These so-called pick-and-place operations on surface mount devices (SMDs) essentially consist of a 2-D problem, which is well-solved using highly specialized equipment optimized for high throughput and low cost-per-placement. For example, the AX-201 module of the Dutch assembly machine supplier Assembléon is capable of placing up to 18,000 SMD components per hour on a board with a 3-sigma placement accuracy of 20 μm (Assembléon 2008).

Frequently, however, micro-assembly tasks are not restricted to 2-D operations only. In those cases, the manipulator should have sufficient accuracy

[1] *Selectively Compliant Assembly Robot Arm*: common assembly robot configuration with a higher compliance in the horizontal plane to facilitate vertical assembly motions such as typical peg-in-hole insertions.

in a 3-D workspace, making the manipulation problem considerably more challenging. The application of force sensors for feedback purposes is researched, but up to now hardly applied in industry. If accuracies down to the sub-μm range are required, then typically precision positioning stages need to be applied that take care of the final positioning over a small range in a limited number of directions.

Current micro-part gripping

Typical problems in micro-assembly are related to the way the part can be gripped. Conventionally, mechanical grippers are used for manipulating macroscopic objects. Together with vacuum-based gripping this is the main applied method in industry when scaling down to the micro-domain. Due to the fragility of many micro-parts the force applied by the gripper should be precisely controlled. Many kinds of mechanical micro-grippers have been built; see Van Brussel *et al.* (2000) for examples.

A vacuum gripper is very simple as it consists mainly of a soft thin tube or pipette connected to a vacuum pump, making this kind of gripper cheap and easy to replace. Gripping electrical components for PCB assembly typically takes place using vacuum. The smallest standardized passives nowadays handled by pick-and-place machines have a footprint of 0.01×0.005 inch (254×127 μm), hence their name '01005'-components. Naturally, an approximately flat non-permeable top surface is necessary for successful vacuum gripping.

A particular problem when using vacuum for manipulating micro-parts is that the tube has to be very thin and, therefore, is easily obstructed by small particles. More generally, to reduce the influence of interference factors, handling and assembly of micro-parts should be carried out in clean rooms or local clean areas. Furthermore, it is important to take precautions to reduce the effect of adhesive forces. Example measures are a reduction of the contact surface area, or performing assembly in a humidity-controlled environment (Tichem and Karpuschewski 2002). In addition, part releasing strategies may be required to ensure the correct placement of a micro-part at the end of the gripping cycle, for example by applying an auxiliary tool to press the micro-part on the substrate while releasing and retracting the gripper.

2.2.2 Micro-assembly research directions

The difficulties in performing micro-assembly tasks have stimulated research into improved or alternative micro-assembly methods, mainly oriented at:

- alternative micro-gripping methods;
- micro-factories;
- batch assembly methods.

Alternative methods for micro-gripping

Upon scaling to smaller dimensions, alternative gripping principles uncommon to the macro-domain may be applied. A wide range of gripping principles could apply; see Tichem *et al.* (2004) for an overview. Examples are liquid solidification-based micro-gripping as investigated by Lang (2008), and capillary gripping, researched *e.g.* by Lambert (2005), which is attractive for its automatic centring of the component to the gripper surface and its compliance in the horizontal plane during assembly.

Micro-factories

The idea that micro-sized manipulators may have better performance for handling small parts at a fraction of the cost than macro-sized manipulators has invoked academic research on so-called *micro-factories* (Alting *et al.* 2003): extremely miniaturized manufacturing systems, usually of an overall table top size. Assembly equipment such as micro-robots can form part of such micro-factories or operate as stand-alone units. In industry the emergence of smaller assembly robots may occasionally be seen. However true micro-factories have not been developed beyond their infancy and are as yet observed in research projects only.

Batch assembly

In the micro-domain operations may be executed on batches of parts, such that the handling effort could be distributed over multiple parts. Böhringer *et al.* (1999) distinguished two main categories of batch or *parallel* micro-assembly as they called it:

- Deterministic: the relationship between part and its destination is known in advance. Examples are (flip-chip) wafer-to-wafer transfer, micro-gripper arrays or pre-adjusted assembly magazines (Van Brussel *et al.* 2000);
- Stochastic, also referred to as *self-assembly*: the relationship between the part and its destination is unknown or random.

Self-assembly in this sense is defined as the spontaneous organization of molecules or objects into stable aggregates under equilibrium conditions (Srinivasan *et al.* 2002). Their working principle can be based on *e.g.* geometry, electrostatic or magnetic attraction, or on a difference in hydrophobic or hydrophilic adhesion. Often using photolithographic techniques, bind-

ing sites are prepared on the micro-parts and receptor sites are made on the target where the parts are to be assembled. Although self-assembly methods seem appealing for their simplicity, none of them are 100% reliable which lowers yield, limiting their practical applicability. They are expected to have better potential when used in support of pick-and-place operations, acting as *self-alignment* functionality for improved position accuracy, for example by means of electrostatic attraction such as researched by Kurniawan *et al.* (2008).

In addition to the micro-assembly methods mentioned so far, several other approaches for micro-assembly have been proposed, which are discussed in more detail by Van Brussel *et al.* (2000). Examples are distributed micro-motion arrays and various non-contact manipulation methods. One particular interesting method is on-the-machine assembly, as presented by Langen *et al.* (1995), in which the tool is first produced, and the product is subsequently machined and assembled on the same machine, without repositioning.

Despite all efforts in micro-assembly methods, assembly of micro-products is still immature and generally costly. So far, parts are typically assembled using functionality which is located outside the product to be assembled; so, there is a distinct separation between product and production equipment, such as manipulators, grippers, and sensors being employed for the assembly process. The alternative concept of micro-assembly using product-internal assembly functions - topic of this thesis - is discussed in the remaining two sections of this chapter.

2.3 The PIAF concept: product-internal assembly functions

As indicated in Chapter 1, the potential advantages of the novel method to perform micro-assembly using product-internal assembly functions are difficult to asses without careful consideration in further detail. Therefore, it technical feasibility has been investigated in a research project in the Laboratory for Micro and Nano Engineering (MNE) at the Delft University of Technology, of which the present thesis is the principal result.

In the PIAF method assembly functionality is created as an integral part of the product, and it remains part of this product after assembling. The method is applied in a two-stage approach. In the first stage, coarse assembly of components is achieved using product-external assembly functions, typically by a (semi-)automatic production machine or a human operator.

This involves all assembly steps in order to prepare for and facilitate the product-internal assembly process. The final, accurate assembly is subsequently performed with aid of the in-product assembly functions.

Function decomposition

In Figure 2.2 the schematic function structure is shown. The functions that apply for integration in the product are (1) controlled positioning of the component, (2) sensing the position of the component, and (3) fixation of the component in the final position. It should be remarked here that not necessarily all functions shown in Figure 2.2 as part of the PIAF functionality have to be included in the product.

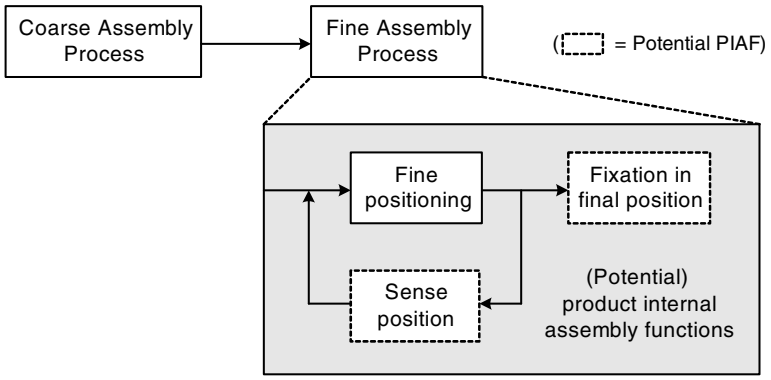

Figure 2.2 Schematic function structure micro-assembly using product-internal assembly functions (repetition of Figure 1.1)

In the research project, it was decided that at least the fine positioning should be performed using internal functionality, since this is the most logical candidate for integration into the product. Internal position sensing on the other hand was not included into the investigation to limit the complexity and size of the project. Instead, for the product case under investigation, position sensing was decided to be performed conventionally using external means, and is therefore not further considered. The remaining three subfunctions are treated in Chapters 4 through 7, starting with the central aspect fine positioning.

Potential PIAF benefits versus drawbacks

The benefits that are generally aimed for are lower overall product costs and a higher product quality by reducing the amount of delicate, time-consuming micro-operations by human operators and expensive production machines. Although adding functionality to the product is likely to increase cost, by lowering the required assembly accuracy of the preceding 'coarse'

assembly step the *overall* assembly cost may actually be decreased. In addition, it may positively influence assembly yield and cycle time, and possibly result in higher assembly accuracies.

The fact that operator involvement is in principle not needed in the final phase, not only reduces the labour cost contribution, but also potentially allows for parallelization of activities (Tichem *et al.* 2003). During the (automatic) final assembly, the operator can take care of other parts of the production chain, *e.g.* start with the preparation of a new package.

In addition to lower overall costs and higher quality, also improved or additional functionality may perhaps be realized using this method. For example by some smart sensing and control strategy it may become possible to actively compensate for any (sub-μm) position errors, which might occur during operation of the system, *e.g.* due to temperature differences. This even provides the prospect of realisation of new generations of systems, with totally new and unrivalled functionality. So-called 'smart systems' [1] could potentially be created, *i.e.* systems that do not only contain functionality for their primary purpose, but also functionality to be self-supportive, *e.g.* self-assembly, self-calibration or self-testing. The overall system performance could be improved in terms of for instance speed, reliability, accuracy, intelligence, or communication.

Of course, the complexity of the product increases due to the added functionality. For example, electrical interfacing is needed to allow for its activation. Negative consequences for product cost, size, and development time, with possibly longer lead times as a result, should naturally be reduced to a minimum. A comparative overview of assembly using product-external versus product-internal assembly functions is given in Table 2.1.

Permanent fixation or continuous position control

Finally, for maintaining the component in the desired position, two possibilities exist: either the component is definitively fixed after final alignment, or continuous control of the component position is applied during product life, see Table 2.2.

When applying permanent fixation, usually part of the position accuracy is lost during the fixation step. Moreover, the long-term stability of the fixation is limited, which may cause problems in situations demanding high

[1] The term '*smart*' can have various meanings, depending on its context. In this case it is used to refer to systems that can adapt to their environment without human intervention.

	Method	
Phase	Product-external assembly functions	Product-internal assembly functions
Package preparation	+ lower product complexity	- higher product complexity - potentially higher preparation effort
Final alignment	- expensive mechinery / delicate manual labour - low yield and long cycle time	+ low cost assembly functions + reduced operator involvement (possibility to parallelize activities) + potentially increased yield and reduced cycle time + potentially increased accuracy

Table 2.1 Final alignment using product-external versus product-internal assembly functions

Fixation after alignment	**Continuous control during product life**
+ no internal sensing functionality needed	+ no fine fixation step required
+ no power consumption during product life	+ can compensate for errors
- loss of position accuracy during fixation	- internal sensing functionality required
- sub-µm stability very challenging	- position trace-back needed after power failure
	- power consumption during product life

Table 2.2 Comparison fixation after final alignment versus continuous control during product life

accuracies. However, if continuous position control is chosen, then internal sensor functionality is needed, increasing the complexity of the overall system. On the other hand, stability issues in this option are far less critical, because the functionality is capable of compensating for errors during operation. An important demand is that the system can retrieve its position after a power failure. Finally, a consequence of continuous position control during product life is that energy needs to be fed to the system, which should of course be kept to a minimum.

For the product case under investigation the option including fixation after positioning was selected, since position sensing was decided to be performed product-externally. This so-called 'fix-and-forget' approach is also the procedure of choice among commercial laser diode manufacturers, as in

existing telecommunication laser diode modules the components generally are fixed relative to each other.

2.4 MST as technology enabler for PIAF

In this section, first the selection of MST as technology enabler for the PIAF method is discussed in Subsection 2.4.1, followed by examples of MST-based PIAF and PIAF-related devices from literature in Subsections 2.4.2 and 2.4.3, respectively.

In this thesis, a relatively strict definition of PIAF is used, in the sense that the product-internal functionality should deal with the positioning and/or fixation of *discrete components* as part of an assembly procedure. The limitation to discrete components was made to include the challenging aspect of placing components in contact with the typically fragile internal assembly functionality, which is one of the aspects that are most interesting from research perspective.

In literature on MST-based devices containing controllable moving structures, a number of MST-based devices are found that are closely related. However, they do not fall under the PIAF definition indicated above, because they either do not perform discrete part manipulation, or they have a purpose other than assembly. This is schematically shown in Table 2.3. Examples of these categories of PIAF-related devices are discussed in Subsection 2.4.3, because of their high degree of similarity to PIAF devices.

	Discrete part manipulation	**Internal structure manipulation**
Assembly	**PIAF; Subsection 2.4.2**	PIAF-related; Subsection 2.4.3
Non-assembly	PIAF-related; Subsection 2.4.3	Not discussed

Table 2.3 Classification of MST-based devices containing controllable moving structures in relation to PIAF

In addition to these two categories of PIAF-related examples, naturally also many MST-based device examples exist in which manipulations are performed on integrated features and are not intended for assembly. This is in fact by far the largest category, mostly comprising optical systems employing beam steering for various purposes such as optical switches, variable optical attenuators, tunable lasers, and micro mirror devices for projection displays. These examples are not further detailed here, since the level of similarity to PIAF devices is lower than with the previous two categories. For

examples of these types of devices the reader is referred to the review papers by Walker (2000) and Lin and Goldstein (2002).

2.4.1 MST for PIAF

Of the many available methods to fabricate miniature components, microsystem technology is selected as enabling technology for creating the product-internal assembly functionality which should be included in the product to be assembled. In accordance to the observation for micro-products in Subsection 2.1.2, development of new manufacturing technologies follows three main paths (Alting *et al.* 2003):

- downscaling of existing manufacturing processes (mainly from the precision engineering domain);
- use and up-scaling of MST processes (from the semiconductor domain);
- development of new technologies in the overlapping fields of existing technologies (*e.g.* new combinations of processes and materials, such as focused ion beam machining of silicon or micro replication by hot embossing in polymers).

It is however expected that scaling down macro-world production methods and technologies will reach its limits, or will not be efficient for micro-scale systems, similarly to some new combinations of processes and materials, due to *e.g.* very low material removal rates. They may nevertheless be selected for specific applications based on their ability to create fully 3-D micro-parts. MST-based manufacturing processes related to the semiconductor domain on the other hand are based on 2-D or planar technologies. This implies the construction of components or products on or in initially flat wafers, for which silicon is the most commonly used base material. MST devices and integrated circuits are formed by creating patterns in layers of the wafer. Pattern transfer consists of a photolithographic transfer of the desired pattern to a photosensitive film covering the wafer, followed by a chemical or physical process to remove or add material in order to create the pattern. This cycle is then repeated until the desired component has been fabricated. Bonding techniques can also be utilized to extend the structures produced by silicon micromachining techniques into stacked multi-substrate structures. For a broad overview of available MST-based processing technologies the reader is referred to *e.g.* Madou (2002).

MST-based technologies are very promising for creating product-internal assembly functionality, based on two specific advantages:

- capability to create very small structures at extremely high accuracies;

- possibility of batch-wise processing (potential of low-cost production).

Although both during the photolithography steps as well as the subsequent process steps inaccuracies are introduced into the geometry of the micro-product, these errors are typically very small, in the order of a few microns at maximum. Together with very small attainable feature sizes, this renders MST-based processing highly suitable for fabrication of many micro-components.

Particularly the possibility to achieve low cost is considered important for application of the PIAF method, since the functionality remains part of the product after the assembly. Using MST-based technologies, typically hundreds to thousands of products, depending on the size, can be processed at the same time on a single wafer, which can measure up to 300 mm in diameter. This makes the process potentially low-cost, especially if large production volumes are required.

For the above reasons it was decided to focus the feasibility study to product-internal assembly functions that are fabricated using MST-based processing technologies. At least the fine positioning functionality was decided to be performed using MST-based processing techniques, and finally the fine fixation functionality was also based on MST, as is shown in Chapter 7.

Beside distinct benefits of MST-based processing over other fabrication methods, it naturally also has some difficulties. Limitations lie mainly in the processing capabilities: only a relatively small number of processing techniques is available that work in combination with a restricted set of materials. Of these, the use of silicon as base material offers the largest choice in processes available, making it still the dominant starting material for most MST-based micro-components. Also, the typical planar nature of the processes restricts the geometrical freedom available to the designer.

A further drawback is the particularly large know-how required to develop functionality using this technology. In contrast to the more standardized IC manufacturing, a feature of this manufacturing technology is the low level of standardization in used processes and materials that may be incompatible with each other. MST-based components generally use monolithic designs in which all components are fabricated in one sequential process. The process sequence must be carefully considered in order to prevent possible problems when combining different process steps. Therefore the designer and product developer have to possess considerable knowledge about alternative materials and production technologies to be able to develop the optimal product for a given situation. This also means that although the micro-components might be quite cheap to produce, still substantial efforts and costs have to be made in the development stage. Conse-

quently, cost-effective production is only possible for sufficiently high volumes.

The above reasons have until quite recently hampered MST technology from widespread application in commercial products. Nevertheless, recent years have brought an explosive growth in new MST devices ranging from accelerometers, oscillators, micro optical components, to micro-fluidic and biomedical devices. As the major boost into widespread use a few years ago originated predominantly from the automotive industry, with the airbag sensor being one of the first high volume applications, nowadays this role is largely taken over by consumer electronics applications. Motion sensors, silicon-based microphones, gyroscopes and accelerometers are examples of MST components that have become cheap and rugged enough to start to find a widespread use in consumers' cell phones, digital cameras, gaming devices, laptops and other devices. For example, dual axis integrated gyroscopes for image stabilization purposes are nowadays being shipped for less than € 2 per unit and can be produced in thousands on a single six-inch wafer including integrated electronics.

Interest is now also slowly shifting towards more complicated, increasingly hybrid microsystems that combine sensors, actuators, computation and communication in single micro devices. Seen in this view, the addition of MST-based functionality to the product to facilitate the final assembly can be considered a logical next step.

2.4.2 MST-based PIAF examples

A limited number of examples utilizing product-internal assembly functions have been found in literature, both MST-based as well as non MST-based. Most of these examples deal with applications in the optical domain, since these applications pre-eminently require very strict positioning accuracies that are very difficult to achieve using conventional assembly methods.

Examples of commercially used products employing PIAF generally contain deformable mechanisms for adjusting the relative part position either by external manipulation (Koster (2000, p. 245 and p. 273-276) or laser adjustment (Hoving 1997, Mobarhan *et al.* 2000). These examples are non MST-based and have limited possibility of further miniaturization, therefore they were not selected in our investigation for micro-assembly.[1]

An overview of relevant MST-based PIAF examples from literature is shown in Table 2.4. The majority of the examples deal with positioning functionality, whereas a few are directed to product-internal fixation functionality. Strictly, the first two examples, by Jebens *et al.* (1989) and Aoshima *et al.*

Reference	Application	Internal assembly functionality	Actuation principle	Positioning range	Configuration	Comments
Jebens *et al.* (1989)	Fibre alignment	2-D fibre positioning	Electrostatic		In-plane	Not MST-based, single-point diamond machining
Aoshima *et al.* (1992)	Fibre alignment	2-D fibre positioning	Piezoelectric	> 20 µm at 130 V	Perpendicular to fibre direction	Not MST-based, discrete piezoactuators
Kikuya *et al.* (1993)	Fibre alignment	2-D fibre positioning	Electrostatic	10x10 µm	In-plane	Combined with UV curable adhesive (~ 1 µm position shift)
Gerlach *et al.* (1997)	Fibre alignment	2-D fibre positioning + position sensor	Electromagnetic / piezoelectric		In-plane	Glued-on piezo elements, discrete photodetector for optical coupling detection by measuring cladding light (measurement resolution not stated)
Haake *et al.* (1998)	Laser-fibre alignment	3-D fibre positioning	Electrothermal	In-plane free displacement > 30 µm, out-of-plane 120 µm	In-plane	Expensive X-ray LIGA, combined functionality not shown
Unamuno *et al.* (2005)	Fibre alignment	1-D fibre positioning	Electrothermal		In-plane	Combined with UV curable adhesive
Shakespeare *et al.* (2005)	Fibre alignment	2-D fibre positioning	Shape memory alloy		In-plane	Sputter-deposited shape memory alloy, results not stated
Luetzelschwab *et al.* (2005)	Fibre alignment	2-D fibre positioning	Electrostatic	> 60 µm at 300 V	Through-plane	Combined with UV curable adhesive
Pétremand *et al.* (2007)	Laser-fibre alignment	2-D lens positioning + locking	Electrostatic	± 25-30 µm	2-D in-plane movable platform	Low damping, locking accuracy and stability not stated
Saitou *et al.* (2000)	Part positioning	1-D part positioning	Resonant vibration		In-plane	Final part position and orientation defined by integrated fixture
Li *et al.* (2005)	Fibre alignment	Adjustable fibre holding platform	-		In-plane	Adjustable fibre position by selectively laser trimming pre-tensioned SiN strings keeping fibre holding block in place
Datta *et al.* (2003)	Fibre alignment	Heater for solder remelting	-		In-plane	Solder melting and resolidification to enable external fibre fine positioning
Su and Lin (2005)	Cap placement	Heater for thermal bonding	-			Local heating for thermally bonding cap over liquid-filled cavity without influencing the encapsulated liquid

Table 2.4 Overview of MST-based PIAF examples in literature

(1992), are not MST-based, however they were considered relevant, and therefore included. Jebens *et al.* were the first to propose a 2-D internal fibre tip positioning system. This system was based on electrostatic actuation; a metal-coated fibre could theoretically be attracted in two dimensions by applying voltages of around 10 V on separate electrodes on the two sides of a V-groove fabricated by single-point diamond machining. Aoshima *et al.* (1992) showed an early 2-D fibre alignment device with discrete piezoactuators capable of over 20 μm displacement in both directions at up to 130 V.

The first MST-based PIAF example was proposed by Kikuya *et al.* (1993), in which the silicon V-grooves were made using wet anisotropic etching, see Figure 2.3.

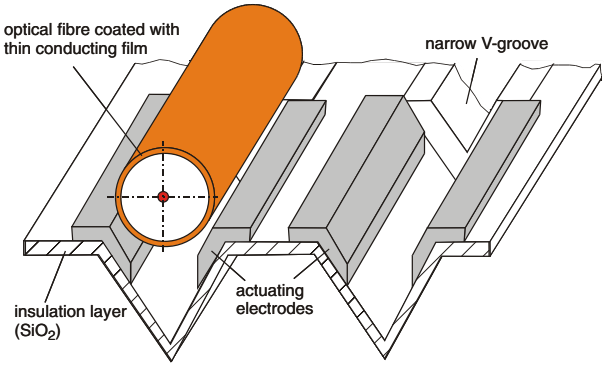

Figure 2.3 Schematic view of the 2-D electrostatic fibre tip positioning device by Kikuya *et al.* (1993)

A positioning range of 10×10 μm was demonstrated for voltages of around 60 V in air. Also movement when immersed in UV-curable epoxy adhesive was tested, which was cured afterwards, resulting in a post-curing position shift of about 1 μm. Gerlach *et al.* (1997) presented two 2-D fibre positioning devices actuated either electromagnetically or by using glued-on piezo elements. In these systems also an optical sensor was included for alignment detection, which was based on measurement of the light intensity coupled into the fibre cladding.

Haake *et al.* (1998) proposed the use of on-chip electrothermal microactuators for in-package 3-D fine positioning of a fibre tip relative to a laser

[1] In addition, laser adjustment is still relatively unpredictable. Since it is promising for larger-size components, however, this process has been investigated further in a parallel project which was conducted at the Eindhoven University of Technology (IOP programme Precision Engineering, project number IPT02310A 'Laser adjust supported fibre array alignment and fixation').

diode. The proposed device measured 5×4×0.5 mm, however miniaturization of the system was claimed to be feasible. The thermal actuators were fabricated by patterning a thick electroplated nickel layer using X-ray LIGA.[1] Individual in- and out-of-plane electroplated nickel thermal actuators were tested. The in-plane actuators were capable of delivering more than 30 μm free displacement at 0.45 W and the out-of-plane silicon/nickel bimorph actuators over 120 μm at 0.3 W. The in-plane actuators were measured to be able to provide > 40 mN over the whole actuation range at a fixed back deflection of 5 μm. However, overall combined device performance was not shown. Fixation of the fibre in the final position was proposed by methods like soldering or gluing. See Figure 2.4 for a schematic view of one of the presented three axis in-package micro aligner concepts.

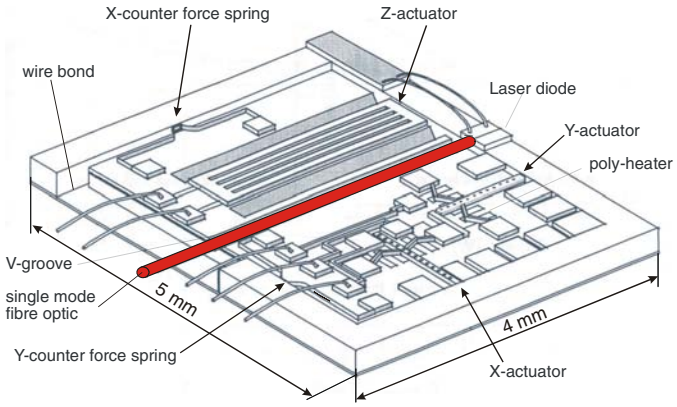

Figure 2.4 3-D in-package electrothermal fibre optic micro-aligner (Haake *et al.* 1998)

Other fibre tip positioning devices were shown by Unamuno *et al.* (2005), Shakespeare *et al.* (2005), and Luetzelschwab *et al.* (2005), employing electrothermal, shape memory alloy, and electrostatic actuation, respectively. Recently, Pétremand *et al.* (2007) have reported a 2-D lens positioning device for laser-fibre coupling, consisting of a 2×2.7 mm silicon bulk micromachined chip with a 2-D in-plane movable platform, being positioned by two unidirectional electrostatic comb drive actuators combined

[1] The German acronym *Lithographie*, *Galvanoformung*, *Abformung*, which stands for lithography, electroforming, moulding. This process relies upon highly expensive synchrotron-based deep X-ray lithography and is therefore a rarely used process. It is capable of defining extremely high aspect ratio structures up to over 1 mm thick in polymer material, usually PMMA, which is exposed and subsequently developed and removed, after which nickel is electroplated in the open areas, which may become part of the final product or be used as mould for replication steps to follow.

with a motion conversion mechanism to obtain ± 25-30 μm *x-y* range of motion, see Figure 2.5. An optical lens was assembled and glued onto the mobile platform to focus and steer the light coming from a laser diode placed under the positioning chip and couple it into an optical fibre above the positioning chip placed normal to the chip surface.

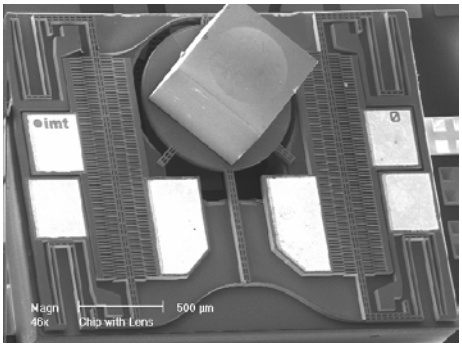

Figure 2.5 Electrostatic *x-y* positioning stage with assembled silicon lens (Pétremand *et al.* 2007)

Once the desired position was reached, the movable platform could be locked in place by applying a voltage between the movable platform and the base of the chip. Depending on the electrical current and the voltage applied, the locking was either temporary or permanent.

The energy for the desired action can also be supplied in other forms than via electricity. Saitou *et al.* (2000) described the alignment of micro-parts using so-called vibromotors, see Figure 2.6. The surface micromachined micro-actuators were activated by applying a proper external vibration frequency. The micro-parts were positioned with low accuracy within a predefined space on the wafer, after which the vibromotor pushed the micro-part into its final position, which was defined by a frame on the wafer.

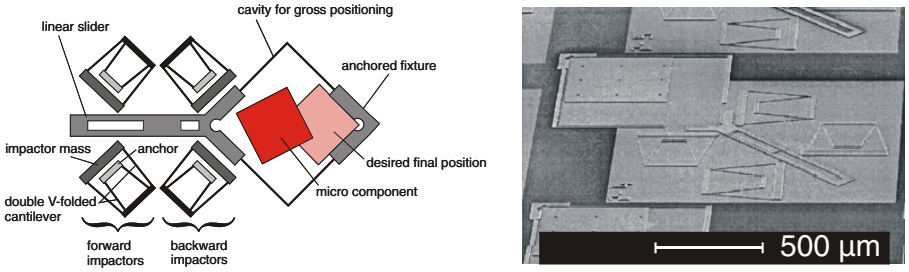

Figure 2.6 Schematic top view and SEM image of the externally resonated linear microvibromotor (Saitou *et al.* 2000)

By applying a different predefined vibration frequency, the part could be released again. The design also allowed batch-wise assembly of micro-parts.

An alternative approach was shown by Li *et al.* (2005), who presented an optical fibre platform in which the fibre tip position could be adjusted by selectively laser trimming silicon nitride strings under pretension keeping the fibre holding block in place. Using this principle it was proven that with a sufficiently large number of strings an adequately small resolution could be achieved.

Examples showing product-internal fixation functionality exist as well. Datta *et al.* (2003) have demonstrated a fibre alignment scheme including an integrated thin film heater for solder re-melting in order to be able to improve the fibre position by external active alignment after which the solder will solidify in the improved position. Other examples have been shown *e.g.* by Su and Lin (2005) and Yang *et al.* (2005).

2.4.3 MST-based PIAF-related examples

In addition to the PIAF examples considered above, there are a number of MST-based devices that are closely related and possess high similarity, but which are not considered to fall under the PIAF definition used in this thesis. As explained in the introduction of this section, this is because they either do not perform discrete part manipulation, or because they have a purpose other than assembly. Starting with the first, examples of both types of PIAF-related devices are shown in the present subsection.

Out-of-plane lifted structures

The first category of PIAF-related examples consists of MST-based devices containing integrated elements that are lifted out of the wafer plane to create three-dimensional structures. Using micro hinges, a large variety of flip-up microstructures has been designed and fabricated, mainly intended for micro-optical components such as mirrors, lenses, and gratings (Wu 1997). Coupling these structures with actuators has allowed the fabrication of systems such as scanning micromirrors, rotating micromirrors, and moving microlenses. Examples are shown by Daneman *et al.* (1996), Reid *et al.* (1998), Ebefors *et al.* (1998), Syms (1999), and McCarthy *et al.* (2003).

Lin *et al.* (1997) have shown a microactuated *xyz* stage for a free-space micro-optical bench, in which 3-D beam steering for optical alignment was achieved by moving two manually folded out-of-plane micromirrors and an upright Fresnel microlens using integrated scratch drive actuators (SDAs), in which a kind of stepping motion is electrostatically induced, allowing for large strokes and small resolutions, see Figure 2.7.

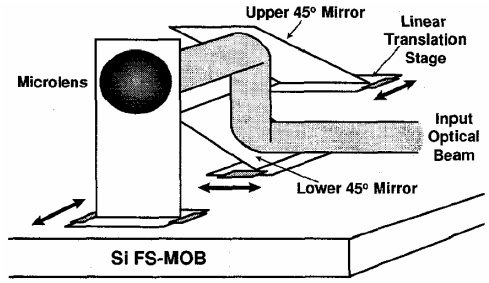

Figure 2.7 Schematic drawing of the microactuated *xyz* stage using integrated scratch drive actuators by Lin *et al.* (1997)

Ishikawa *et al.* (2003) have eliminated the need for manually flipping up, by utilising solder self-alignment for placing the mirror at a 45° angle and using thermal actuation for 2-D tilting, see Figure 2.8.

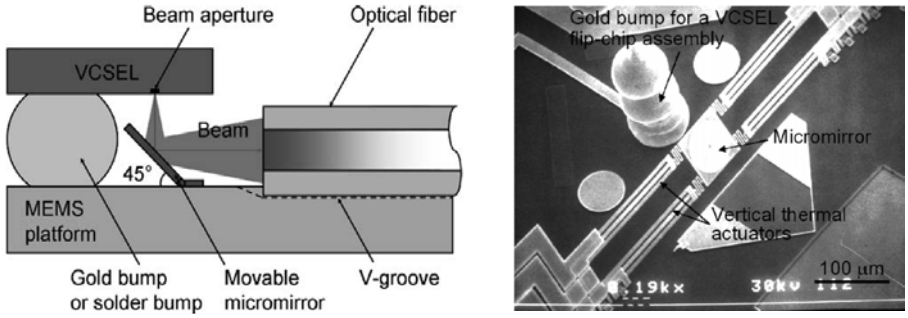

Figure 2.8 Schematic cross-sectional view and close up of electrothermal 2-D tilting VCSEL (*Vertical cavity surface-emitting laser,* see Chapter 3) laser-to-fibre coupling device (Ishikawa *et al.* 2003)

The device by Ishikawa *et al.* is particularly intriguing, because it is a good example of a device of which it is not straightforward whether it may be classified as a PIAF example or not. The purpose of the mirror alignment is steering of an optical beam rather than changing the position of any of the assembled discrete components (the mirror element has been fabricated as part of the substrate); therefore, strictly, it cannot be considered an assembly step. On the other hand, the mirror alignment possibility certainly has *influence* on the assembly accuracy required for the parts that were assembled before the alignment step, and in that sense the alignment functionality should be considered to *support* the assembly process. Taking this into consideration, the example at hand could either be excluded or included as PIAF example.

For optical applications, the beam-steering method described here may be a competitive method to the PIAF concept. However, for the selected case described in Chapter 3, the beam steering approach cannot be used due to the very short distance between the laser diode and the fibre. This makes it impossible to include an integrated beam steering element into the optical path.

Manipulation systems for other than assembly purposes

The second group of PIAF-related device examples is more straightforward. It is comprised of systems that, like PIAF devices, are involved with discrete component manipulation, however in this case for purposes other than assembly or final alignment. Examples in literature also almost exclusively deal with optical applications, and most device examples contain 1-D translation functionality. MST-based optical device examples are optical switches, *e.g.* by Field *et al.* (1996) and Hoffmann *et al.* (2003a, 2003b); variable optical attenuators (VOAs), *e.g.* by Grade *et al.* (2005) and Unamuno and Uttamchandani (2006); a tunable wavelength filter by Pichonat-Gallois *et al.* (2004); a 1-D latching micro optical positioning stage (Syms *et al.* 2004a); an *xy* high-speed scanner for a miniature colour display (Hoshino *et al.* 2003), and a vertical electrostatic lens positioning actuator for use in an MST-based optical pickup unit by Kim *et al.* (2003).

The only non-optical examples in this category were shown by Horsley *et al.* (1997) and Hirano *et al.* (1998), who presented translational and angular electrostatic positioning actuators for magnetic hard disk drives, respectively.

In conclusion, although a limited number of MST-based PIAF and PIAF-related examples were found, as shown in the previous subsections, the technical feasibility of the PIAF method to date has never been systematically investigated in a structured approach. Generally only partial solutions are presented; none of the researches has implemented the complete method in an integral manner. Together with the uncertainty about its economic viability, this has led to the start of the research project, of which the present thesis is the principal result.

3

Case description and specification

The purpose of this chapter is to present the first design choices regarding the configuration of the laser diode device that is selected as product case for the investigation, as well as to define an overview of the requirements for the product-internal assembly functionality for this device.

In Section 3.1, relevant information is provided about the case domain, being optical communications, followed by a description of the selected laser diode device and a discussion of initial design decisions regarding its configuration in Section 3.2. Finally, the PIAF requirements for this device are discussed in Section 3.3, combined into a requirements overview at the end of this chapter.

3.1 Case domain: optical communications

The use of glass fibre to carry communication signals has increased drastically over the last few decades. Its enormous data transmission capacity compared to electrical cable has allowed revolutionary changes in telecommunications of which the widespread proliferation of the Internet is the most outstanding example. Its use has been enabled by development of fibres and devices for optical communications since the early 1960s, which still continues to date, strongly stimulated by an investment boom in the 1990s, instigated by the Internet hype in the last years before the millennium change. Unfortunately, this was followed by a downturn in the early 2000s, causing a shake-down of companies involved in fibre-optic deployment. At present, the industry seems to have recovered from the heaviest

blows and investments in fibre optics are slowly increasing again to the pre-bust level.

The use of optical fibre for communication has a number of well-known advantages over copper cable (Dutton 1998):

- immensely large data transmission capacity;
- small and lightweight;
- less noise (no electromagnetic interference);
- safer to people;
- better security of optical data transmission.

Multiple wavelengths can be combined - called *multiplexing* - with each wavelength having data modulation rates up to 10 Gb/s. The newest technology pushes the rate up to 40 Gb/s, while even higher bit rates are being tested. *Dense wavelength division multiplexing* (DWDM) systems have become standard in long haul high-capacity telecommunication networks having dozens of signals at closely spaced wavelength intervals that can be selectively added and dropped from the line whenever desired.

For access networks to private homes and offices, copper cable is still mostly used for the simple reason of availability. In most cases the bandwidth is still acceptable, which does not justify investments for replacing them by optical fibre. Nonetheless, internationally more and more newly built and existing commercial and living districts are being provided with such fibre-to-the-home (FTTH) and fibre-to-the office connections.

The basic components of an optical communication system are schematically shown in Figure 3.1. First, a serial bit stream in electrical form is presented to a modulator, which encodes the data for fibre transmission. A light source - either a laser or a light emitting diode (LED) - is driven by the modulator and the light is focused into the fibre. The light travels down the fibre, and at the receiver end the light is fed to a detector and converted to electrical form, after which it is reconstructed to the original bit stream, which may then be fed to a using device.[1]

The most difficult and expensive step in achieving optical transmissions is embedded in the accurate coupling of light from a laser diode into a single-mode optical fibre. This requirement is based on specific characteristics of the transport of light through optical fibres and of the laser generating the light.

[1] The sequence described here is deliberately simplified; many additional steps, such as add/drop multiplexing and amplification, may be involved in transporting and routing of the signal, but the general principle remains unchanged.

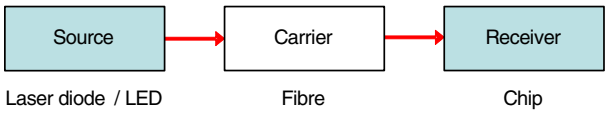

Figure 3.1 Basic components of an optical communication system

Optical fibre characteristics

An optical fibre is a very thin strand of silica glass usually with a diameter of 125 µm. It consists of two parts: the core and the cladding, which is a tubular jacket surrounding the core (see Figure 3.2). The core is doped with impurity atoms, causing it to have a slightly higher refractive index than the cladding. This ensures that light entering at one end of the core may travel, confined within the core, until it leaves the fibre at the other end. As long as the bends do not become too tight, the light will be guided around corners with very little light loss when travelling along the core.

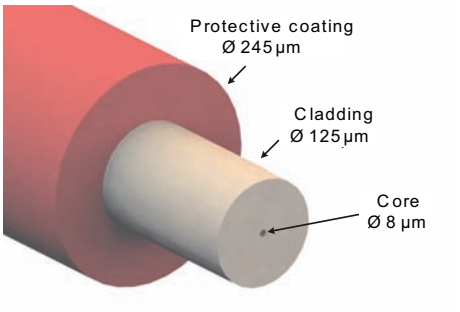

Figure 3.2 Schematic build up of a typical single-mode optical fibre (relative dimensions to scale)

Two critical aspects for long distance data transport are *attenuation* and *dispersion*. Attenuation is the weakening of the optical signal as it travels through the fibre. Pure silica is used as it has the lowest absorption of light of any available material. Only infrared light in certain wavelength bands is used for communication applications, based on its lowest attenuation in these bands. Dispersion is the widening of a light pulse during transmission through the fibre. A pulse becomes longer and may ultimately merge with adjacent pulses, making recovery of the original bit stream impossible.

The dominant types of dispersion are *chromatic dispersion*, and *modal dispersion*. Chromatic dispersion is due to the fact that the fibre has different refractive index characteristics at different wavelengths, causing all wavelengths to travel at different speeds through the fibre. Modal dispersion takes place when the light is able to take different paths as it travels within the fibre. Such a path is commonly referred to as a 'mode', and a fibre allow-

ing the light to travel along multiple paths is called a multimode fibre. The distance travelled by light in each mode is different, so a pulse that has fallen into multiple modes will have components that arrive before others. The effects of both kinds of dispersion increase as the travelled distance gets greater. As bit rates continue to increase, the sensitivity to dispersion becomes higher and stricter measures need to be taken to avoid signals becoming unrecoverable.

In order to decrease dispersion and attenuation, communications systems are operated in appropriate wavelength bands, and so-called *single-mode fibre* and light sources with minimal spectral widths are used. By making the fibre core thin enough - in practice around 8-9 μm for telecommunication wavelengths - the light will have only one possible path: straight down the middle. This single-mode fibre is nowadays used for all medium to long-distance connections, and has as additional advantage that attenuation is lower than in multimode fibre because lower levels of dopant are used.

Chromatic dispersion can of course be reduced by minimizing the spectral width of the light source. A narrow spectral width is also beneficial in DWDM systems, in which it is desirable to pack the channels as closely together as possible in order to maximize the number of channels.

Laser diodes

The spectral width of lasers is smaller than for LEDs, therefore long distance fibre networks are always operated using lasers. Lasers also typically have faster response and better directionality, allowing for higher bit rates and enabling more light to be coupled into a single-mode fibre. In communication systems generally semiconductor lasers are used, which are also commonly referred to as *laser diodes* (LDs). Laser diodes are very small, typically around 300×300×100 μm ($l \times w \times h$), and require little power. Several wavelengths are available and they can also be built into arrays. Compared to other lasers, the output beam of a laser diode is quite divergent and requires refocusing due to its short cavity length and its small output dimensions in the sub-μm to μm range.

Both edge-emitting laser diodes exist, which emit light from the side, and so-called *vertical cavity surface-emitting lasers* (VCSELs), emitting perpendicular to the surface of the chip. For reasons of performance most single-mode laser devices are based on edge-emitting diodes. Special edge-emitting laser diodes have been developed that have extremely narrow spectral widths, such as *Distributed Feedback* (DFB) and *Distributed Bragg Reflector* (DBR) lasers, which makes them pre-eminently suitable for high-bandwidth, long distance optical data transport.

The most commonly applied laser diode material for telecommunication wavelengths is indium gallium arsenide phosphide (InGaAsP), which can be made to operate between 0.9 and 1.7 μm wavelength (Dutton 1997, p. 106). The wavelength band around 1310 nm, which was attractive for its zero fibre dispersion on single-mode fibre, came into use in the mid 1980s, and it is the band in which the majority of long distance communications systems still operate today. From the late 1990s, the band around 1550 nm is used for almost all new long distance communication systems, since it has the lowest attenuation available on current optical fibre (about 0.2-0.3 dB/km). Moreover, in this band *erbium doped fibre amplifiers* (EDFAs) can be used. These are devices that amplify the optical signal directly without having to convert it to electricity, which is naturally very attractive. Special single-mode fibre is used with dispersion optimized around this wavelength band.

Fibre coupled laser diode configurations

Various fibre coupled laser diode configurations exist - also referred to as *pigtailed* laser diodes - depending on application and requirements. Usually, a length of fibre of around one metre is aligned with the laser diode inside a housing, and the opposite side of the fibre is fitted with a standard fibre connector, which allows for relatively easy connection to another connectorized fibre at acceptably low loss values.

The simplest alignment method is by placing the fibre with its cleaved end opposite the chip without touching to prevent damage to the components or their anti-reflection coatings. This is called *butt-coupling* and is widely employed for lower-end devices; the alignment tolerances are not very strict, but the coupling efficiency is not very high, since the optical modes of the laser diode and the fibre do not match very well. The laser beam divergence is too large for confining most of the light within the fibre core.

Only very little design freedom is available for making changes to laser diodes without affecting their performance. Therefore, mode matching to achieve higher single-mode coupling efficiency is usually performed by applying lenses, either in the form of *discrete lens elements*, or a *lensed optical fibre*. Using a lensed optical fibre, generally fewer components are required and the attainable coupling efficiency is higher. However, this is at the price of tighter alignment tolerances compared to the use of discrete lens elements.

High performance laser diode products, such as EDFA pump lasers and DWDM signal lasers are commonly packaged individually in leaded packages such as the 14-pin butterfly-type package schematically shown in Figure 3.3. This type of packages are usually hermetically sealed and may, next to the laser diode, hold a large number of other components such as a mon-

itor diode, a separate modulator, an optical isolator, a temperature sensor, a thermoelectric cooler (TEC), a fibre pigtail, and an assortment of lenses, as well as a control electronics.

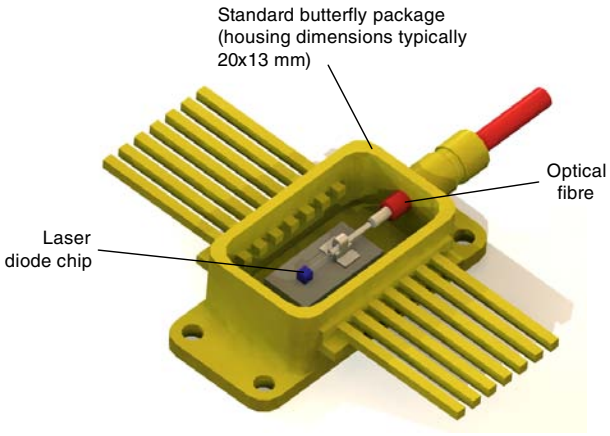

Figure 3.3 Schematic view of a butterfly-type fibre coupled laser diode package (without sealing lid)

High end laser devices generally require temperature and output control to maintain a stable laser output. For example, the operating temperature of a laser in a DWDM module must be kept constant to within 1°C or better, which is performed by use of a TEC, control electronics, and a thermistor for measuring the device temperature.

Except in the case of EDFA pump lasers, which provide continuous output, the light is modulated, either by modulating the laser directly or by separate modulators, which may be discrete components or integrated with the laser diode. Optical isolators may be required to reduce light reflecting back into the laser cavity, which should be avoided since this can harm the laser. Both discrete optical isolators and external in-line fibre optic isolators are available, of which the latter may be used in combination with a lensed optical fibre to reduce the number of components requiring optical alignment.

Optical alignment challenge

A good quality coupling between the laser output and single-mode fibre core is very important, because the optical power that can be generated using laser diodes is limited. The challenge of aligning a laser diode to a single-mode fibre with high coupling efficiency is embedded in the small dimensions and the sensitivity to misalignments of the components. The core of the fibre is 8-9 μm in diameter, while the rectangular output facet of a laser diode is typically around 0.5 by 2 to 4 μm in size. High loss is already

experienced when moved only a small distance away from the optimal position. This is particularly the case in the lateral directions, in which it is generally desired to control the position with μm to sub-μm accuracy. Hyperbolic or wedge-shaped optical fibres can offer very high coupling efficiencies, but at the price of even further reduced alignment tolerances.

These accuracies cannot simply be achieved by hand in a reliable way. Generally, laser diode manufacturers are very reluctant in disclosing their exact methods for achieving the desired coupling quality. The packaging cost of optical fibre interconnects constitutes a considerable portion of the total product cost - sometimes up to 50-80% - therefore proprietary expertise providing a competitive advantage is commercially very important and is protected with care.

Expensive equipment or machines are employed for the alignment and fixation steps, which last typically in the order of minutes. Current methods use expensive and bulky vibration isolated micro-positioning equipment incorporating high-precision mechanical translation stages and piezoelectric actuators. The systems are package and device specific; they generally require dedicated and expensive fixtures and tooling to precisely hold the package and to position and fix the coupled fibre.

The alignment is commonly performed while measuring the coupled optical power. In optics, this is referred to as *active alignment*. The laser is switched on while at the connectorized fibre end the optical power is measured, and alignment is carried out until an optimal coupling efficiency between fibre and laser is found. Although this is an expensive and time-consuming procedure, it is usually required since the strict alignment tolerances cannot be achieved using any other method. For example, the position tolerance of the fibre core relative to the cladding due to fabrication is approximately ± 1.5 μm, depending on the manufacturing specifications. Machine vision cannot be used, because it is impossible to locate the core position inside the cladding with sufficient accuracy, and the same holds for the laser output window location. Usually, the fibre is placed to within a few microns using a microscope or machine vision, after which the final coupling is performed using active alignment, followed by fixation in the achieved position.

Fibre fixation methods

Fixation of the fibre usually takes place by means of laser welding or soldering. Adhesives are also sometimes used, but are often avoided, because during product life they may outgas, producing small quantities of contaminants that may pose a threat to the long-term reliability of the laser.

Soldering or welding requires that the fibre is metallised prior to the assembly process, increasing cost. Solidification and cooling of the solder can shift the relative position between fibre and component. To minimize this, the initial alignment position needs to be tightly controlled based on a full understanding of the solder, including shrinkage versus temperature. Solder-based alignment and attachment yields with single-mode fibre can be relatively low and may require significant rework on individual joints, increasing overall process cost.

Laser welding is the fixation method producing the highest level of accuracy and reliability. A standard approach involves soldering a metallised fibre section in a cylindrical metal ferrule, which is then laser welded via a metal clip to the substrate. Any variation in coupling efficiency resulting from post-weld cooling - also referred to as *post-weld shift* (PWS) - can be corrected by deforming the structure, which can be done mechanically or by laser adjustment. As with soldering, a thorough understanding of the material and process properties are critical to success.

3.2 Laser diode device description and configuration

In this section, the specific laser diode device which is selected for the PIAF investigation is introduced, and a number of initial design decisions regarding its configuration are discussed.

3.2.1 Device selection for PIAF investigation

The extreme difficulties and significant cost involved in aligning high performance laser diodes for long-distance optical data transmission to single-mode fibres makes this type of devices highly interesting for exploring the feasibility of substituting the current assembly methods by the PIAF method.

A representative laser diode layout was chosen with a butterfly type housing having typical inside dimensions l×w×h of 20×13×7 mm. Since the exact laser diode type is not of great influence for the requirements, a generalized edge-emitting single-mode fibre coupled DWDM signal laser diode was taken for the investigation; the output wavelength was assumed to be 1550 nm, the fibre core diameter was 8 μm and the cladding diameter 125 μm.

To keep the number of components limited, a configuration without discrete free-space intermediate optics between the laser diode and the fibre tip

was chosen. This way, a smaller number of different configurations is possible, allowing the emphasis to be on the actual development of product-internal positioning and fixation functionality. A lensed fibre tip was selected for mode matching between the laser and the fibre, enabling the highest possible coupling efficiency, but having tight tolerances and thus requiring accurate positioning and stable fixation to ensure high quality coupling over the complete lifetime of the product.

Conventional starting layout

A schematic cross section of the selected conventional laser diode layout prior to starting the PIAF design is shown in Figure 3.4.

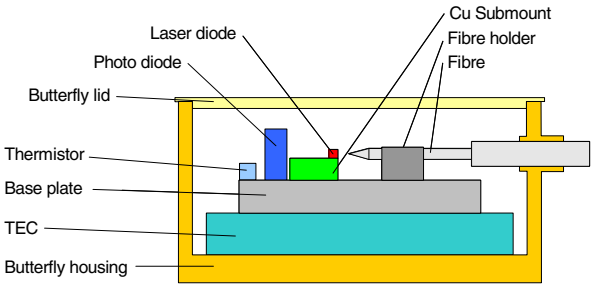

Figure 3.4 Cross section conventional starting layout selected laser diode package

In the housing, the laser diode chip along with all support components take up an estimated 30-40% of the space. It is provided with a thermoelectric cooler (TEC) and a thermistor for temperature control, and a photo diode at the laser diode's back facet for output power control. The laser diode is not directly mounted on the TEC element. Laser diodes are very sensitive to temperature differences and mechanical stress, therefore generally one or more intermediate components are included to spread the heat from the laser and to bridge the thermal mismatch between the dissimilar TEC and laser materials. Although the absolute quantities of heat being produced in the laser are not very large - typically in the mW range - due to the small dimensions the heat flux can be quite significant, locally up to several kW/cm^2. To prevent overheating, commonly metals or ceramics with high thermal conductivities are used for these intermediate components, such as copper alloys, gold, aluminium nitride, silicon carbide or silicon. As low thermal impedance die-attach material normally low-stress solders are used such as indium or gold-tin. Generally solder is used to connect the other components to the TEC. For the selection of the specific combination of intermediate components and solder types many considerations come into play. A common configuration with a separate optical base plate and a laser diode submount was selected and is shown in Figure 3.4.

Conventional assembly sequence

The process of assembling the laser diode module conventionally begins by fixing the TEC element in place by means of soldering at the bottom of the empty 14-pins metal butterfly package. Usually outside of the package an optical subassembly is prepared, consisting of the optical base plate containing laser diode submount, laser diode chip, photodiode, thermistor and other components necessary for the laser diode operation. This subassembly is attached on top of the TEC. The components are electrically interconnected to each other and to the package pins using a combination of patterned metallization surfaces and wire bonds.

The actual fibre pigtailing usually takes place in the next step. Due to the demanded sub-μm accuracy, it is by far the most expensive and time-consuming of all involved assembly steps. Depending on the configuration and the specific fibre fixation method, one or more preparatory steps are required, such as metallization or encapsulation in a metallic fibre ferrule, as described previously.

The laser diode package is typically loaded into a dedicated fixture that holds the package securely in place and also provides electrical pin contact to enable active alignment. Following, the fibre is inserted into the package, usually via an opening in the side of the housing. In the automated fibre pigtailing procedure described by Mobarhan *et al.* (2000), in which laser welding is employed for the fibre attachment, a ferrule with fibre is gripped by a pair of pneumatically actuated tweezers and the fibre loader probe is retracted out of the butterfly package, see Figure 3.5. Next, a metallic weld clip is placed over the ferrule and by using vision the fibre tip is moved close to the laser diode facet location. Subsequently, the laser light and the external photo detector connected to the opposite fibre end are switched on and active alignment is performed by positioning the ferrule in front of the laser facet until optimal coupling is achieved. At this point, the clip is welded to the metallic base at six spots using two Nd:YAG laser beams incident from two directions, followed by spot welding of the ferrule to the clip. The pulse duration and energy are optimized to achieve optimum weld quality while trying to minimize the weld shift induced by the shrinkage upon solidification. However, post-weld shift due to shrinkage typically in the order of several micrometers remains, which can be reduced to sub-μm level by laser adjustment or applying force to the ferrule-clip assembly using the tip of the pneumatic tweezers.

After achieving the desired coupling efficiency, usually some temperature cycling is performed to help settling of the components to ensure stable, long-term operation. Finally, the butterfly package is hermetically sealed in a nitrogen environment using a commercially available seam welder or soldering machine.

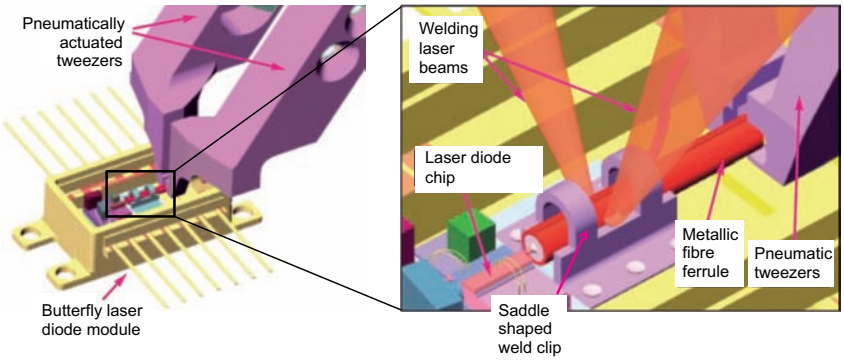

Figure 3.5 Conventional fibre pigtailing configuration using laser welding (Mobarhan *et al.* 2000)

The fibre pigtailing process described by Mobarhan *et al.* from loading the butterfly package including optical subassembly up to post-weld metrology and device unloading was claimed to take between 7 and 11 minutes, see Figure 3.6. This is the only known estimate of the duration for this critical process sequence available from literature. Commonly, manufacturers are reluctant in providing specific information on commercially applied processes. However, it is confirmed that fibre pigtailing is tedious and troublesome and normally lasts in the order of several minutes per pigtail (J. Mink[1], personal communication, April 7, 2005).

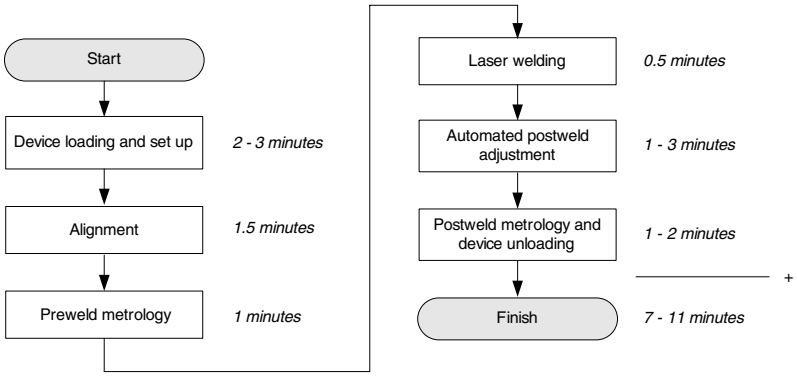

Figure 3.6 Schematic conventional fibre assembly sequence using laser welding, including typical durations for each step (adapted from Mobarhan *et al.* (2000))

[1] Former employee of Philips Optoelectronics in The Netherlands, which later became part of the US-based optoelectronic component manufacturing company JDS Uniphase.

3.2.2 Configuration decisions

As a start in the design process, the following initial choices were made regarding the overall build up of the internal positioning functionality:

- the fibre was selected as the part to be internally fine positioned;
- silicon was chosen as base material for realization of the positioning functionality;
- an adaptation to the laser diode configuration was defined.

Fibre selected to be fine positioned Based on the extreme sensitivity of laser diodes to temperature variations and also to mechanical stress, the optical fibre was selected as the part to be fine positioned using product-internal functionality. The produced laser heat should be removed in a highly controlled manner, which would be significantly complicated with an actuation structure between the laser and the TEC, or between TEC and housing. Although fine positioning of the fibre also involves challenges - particularly related to its large overall length, as is further discussed in the subsection on required actuation forces - it is a passive component, posing less strict demands on the positioning functionality.

Silicon as base material Monocrystalline silicon was selected as base material for the positioning device. It is the dominant substrate material for MST-based devices and it is the only semiconductor material in which devices are being realized at DIMES, at which facilities demonstrators are processed. Silicon is very strong and stiff with a limited thermal expansion, making it a generally suitable material for creating mechanical structures. Compared to other possible substrate materials the available processing technologies are quite extensive and well established, thus providing the best possibilities and the largest flexibility for designing the required functional structures. Finally, the fact that the same set of technologies are used as for creation of integrated circuitry, potentially allows for monolithic integration of control logic on the same substrate (in the case of CMOS compatible processing).

Adapted laser diode configuration An adapted laser diode configuration was defined for the parts that constitute the physical link between the optical features to be aligned, from fibre tip core to the laser diode output window. From assembly perspective, it is attractive to have as few components as possible between the laser and the fibre: the fewer parts the smaller the tolerance build up and also the smaller the required actuation range of the positioning functionality. In a conventional approach using laser welding several parts between laser and fibre are present due to functional reasons. However, in the PIAF approach laser welding is not employed, allowing for a reduction of the number of intermediate components.

Although it is the safest to alter as little as necessary to the primary device build up in order to limit the impact on its functionality, it is interesting to consider the option of replacing all intermediate components by a single silicon positioning component. Silicon is a suitable substrate material for laser diode placement, due to its low thermal expansion coefficient close to that of the laser diode material; good thermal conductivity and its possibility to create electrical leads and accurate geometric features by means of photolithography such as alignment marks and soldering pads. In Chapter 2, a number of examples were shown using silicon as substrate material for laser diodes. As in the initial design stage no information was available on the exact layout of the internal assembly functionality and the involved processing steps, it could not be predicted whether all functionality to position the fibre and to support the laser diode accurately opposite the fibre tip could be integrated into a single component. Therefore, the preliminary choice was made to develop the base part and the positioning subsystem as separate building blocks onto which respectively the laser diode and the fibre would be placed. Based on its attractive properties, silicon was also selected as material for the discrete base part. The resulting schematic laser diode configuration is shown in Figure 3.7. In the figure, the positioning device is drawn as horizontally oriented, so parallel to the bottom surface of the butterfly housing. A comparison between this in-plane configuration and a through-plane build up, with the fibre protruding through the positioning chip, is presented in Section 5.2.

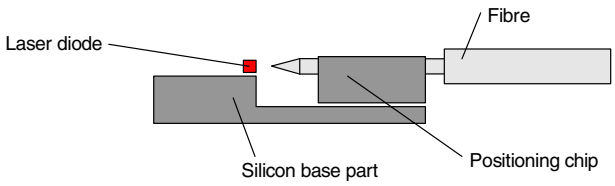

Figure 3.7 Adapted LD-fibre configuration including two silicon parts between LD and fibre

3.3 PIAF requirements

In the present section, the PIAF requirements intended for the selected laser diode product case are discussed. These are combined into a requirements overview at the end of the section.

3.3.1 Optical coupling requirements

For efficient transfer of optical energy from one optical component to another, their respective mode fields should overlap as much as possible.

Counter to intuition, in single-mode light transfer, the losses are bidirectionally equal, meaning that the same amount of light is lost when coupling from a small to a large mode field diameter and vice versa. Typical divergence angles of a laser beam are 10-30° (half angle) in the horizontal plane and 30-50° vertically (Heikkinen 2004, p. 57). As a result, simply butt coupling an optical fibre almost against a laser diode allows for only about a 10-20% coupling efficiency, or a 7- to 10-dB coupling loss (Mickelson *et al.* 1997, p. 51). Figure 3.8 shows a schematic representation of the mismatch between the laser and fibre modes in a butt coupling configuration.

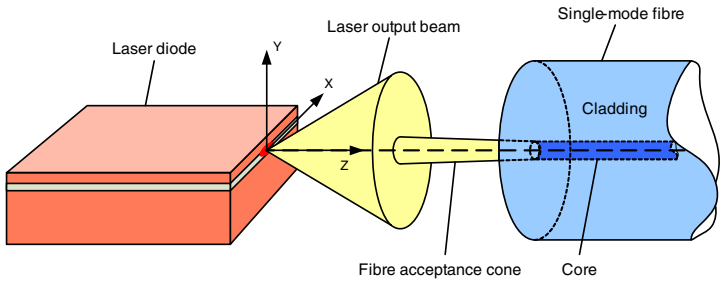

Figure 3.8 Schematic mismatch between LD and fibre mode in a butt coupling configuration

The sign convention, as used throughout the report, is also defined in this figure. It is related to the fibre, the laser diode and all other package components. The origin is defined to be in the centre of the laser diode output window with the positive *z*-axis pointing out towards the fibre; the *x*-axis is in the horizontal plane and the *y*-axis points vertically upwards.

The selected approach of using a lensed fibre is one of the most popular methods to reduce coupling losses due to mode field mismatch in laser-to-fibre coupling. The lens may be formed on the fibre for example by photolithography, chemical etching, heating by a flame or electric arc or laser, dipping into molten glass and fusing, or mechanically grinding and polishing (Heikkinen 2004). The lenses have to be manufactured at sub-µm accuracy in order to fully realise the coupling enhancement, which makes them relatively costly. Due to the short working distance, additional care must be taken so that no contact occurs between the laser and fibre during the assembly process, and extra attention must be paid to minimising backward reflected light from the lensed fibre end face that may result in instability of the laser. For the latter reason lensed fibre ends are usually fitted with appropriate anti-reflection coating.

Many different lensed fibre types exist, see for an overview Heikkinen (2004, p. 62-66). Depending on the laser mode field ellipticity, fibres with rotation-symmetric or non rotation-symmetric fibre ends are able to provide good

coupling results. High coupling efficiencies of around 80-90% have been achieved with hyperbolically lensed fibres (*e.g.* Edwards *et al.* 1993) as well as with fibres having non rotation-symmetric wedge-shaped fibre ends (*e.g.* Modavis and Webb 1995). Generally the higher the coupling efficiency, the more sensitive the coupling is to displacements, as was for example shown by Edwards and Presby (1993), who presented a coupling sensitivity comparison of hemispheric and hyperbolic lensed fibres. With a hyperbolic lens, there was less sensitivity to tilt as in the hemispheric case, for which a much lower coupling efficiency was achieved, but the sensitivity to transverse offsets and longitudinal translation was much higher. For the hyperbolic lens, a 0.45 μm lateral translation or a 2 μm longitudinal displacement away from the optimum position resulted in a 1-dB decrease in coupling efficiency (a decrease of 20%), respectively, whereas the tilt sensitivity for this specific hyperbolically lensed fibre was as much as 15° for the same 1-dB efficiency drop.

Coupling efficiencies as function of misalignments between Gaussian beams have been extensively investigated before, and analytical expressions were provided *e.g.* by Joyce and DeLoach (1984). It is perhaps needless to say that the translational and tilt sensitivities are strongly dependent on the exact laser mode field and fibre lens geometry. For example, Zhang *et al.* (2001), who used wedged fibres for the laser coupling, reported a 15% transverse tolerance of 0.25 μm, and a 15% horizontal and vertical angular tolerance of 4.5° and 3.5°, respectively. The 15% roll tolerance for this fibre - the angular misalignment in the axial direction of the optical axis - was found to be approximately 15°. In a related investigation by Tang *et al.* (2001), 1-dB loss in wedge-shaped fibre to elliptical laser diode coupling was caused by a vertical misalignment of 0.3 μm, a pitch misalignment of 2.5°, or by a yaw misalignment of 4°, respectively.

For the selected coupling case detailed laser facet and fibre lens dimensions were not selected. Instead, based on the findings from literature and expert discussions, generalized requirements were determined for optical alignment between the laser diode output window and the fibre core in all translational and angular orientations. These requirements are shown in Table 3.1.

Degree of freedom	x	y	z	θ_x	θ_y	θ_z
Tolerance	± 0.1 μm	± 0.1 μm	± 0.5 μm	± 1.5°	± 1.5°	± 10°

Table 3.1 Alignment requirements between the laser diode output window and the fibre core for the selected laser diode product case

Minimal coupling losses (< 1 dB) due to misalignments are aimed for. Therefore the allowed alignment offset in the lateral directions *x* and *y* was selected to be 0.1 μm, and the allowable longitudinal misalignment *z* was set to ± 0.5 μm.

Fibre tilt was found to cause a large spread in the coupling loss results, however small horizontal or vertical angular misalignments up to ± 1.5° generally show little effect on the optical coupling (J.H.C. van Zantvoort[1], personal communication, April 7, 2005). Consequently this value was taken as upper level for the fibre tilt.

Little information is available about influences of angular misalignment in the axial direction of the fibre. The wedged-fibre result described by Zhang *et al.* is expected to be realistic for non rotation-symmetric fibres. Therefore, with some safety margin, the maximum angular misalignment in the rotational direction of the fibre was set to ± 10°. In the case of rotation-symmetric fibres the angular rotation around its optical axis is naturally of no concern.

3.3.2 Internally positioned fibre directions

After determining the alignment requirements in all degrees of freedom for the selected coupling case, the directions to be positioned product-internally were selected. As discussed in Chapter 2, realizing complex microsystems - such as multi-degree-of-freedom positioning devices - using MST-based processing is very challenging. This is confirmed by the general lack of examples in literature of MST-based positioning devices having more than 3-D positioning capabilities. Therefore, developing a positioning device able to control all six degrees of freedom was not considered realistic, and attention was focused on positioning of the most critical degrees of freedom instead.

Among the required tolerances in all degrees of freedom for the laser-to-fibre coupling shown in Table 3.1, the translations in *x* and *y* are by far the most critical. It is expected that the three angular rotations can be controlled with sufficient accuracy using relatively low-cost product-external assembly functionality.

The position tolerance in the longitudinal direction - the distance between laser output window and fibre tip - is also quite strict, however not as strict as the lateral tolerances. Moreover, the complexity would be increased significantly if this direction would also require internal actuation, not in the least due to the fact that most likely the fibre is fixed at a given distance from

[1] Packaging expert at the Eindhoven University of Technology, The Netherlands

the tip, expectedly leading to reaction forces that are axially transmitted through the fibre to the positioning device.

For these reasons it was decided that, at least as a start, a limitation was made to product-internal positioning concepts actuating the fibre tip in the two lateral degrees of freedom, perpendicular to the axial direction. Proposed methods for achieving the required position accuracies in the remaining four degrees of freedom and supporting the internal fine positioning step are discussed in more detail in Chapter 5.

3.3.3 Required positioning ranges

The required positioning ranges in x and y can be determined from a careful consideration of the tolerance build up in these directions during the coarse assembly of the components in the physical link between the laser diode output window and the core of the fibre tip. Since the overall cost of the assembly should preferably be lower than the conventional assembly cost of the product, it is tried to lower the accuracy requirements for the coarse assembly process as much as possible. At the same time the required internal positioning ranges in x and y should be kept within limits, since larger ranges demand larger MST-based positioning structures, which are more expensive based on their larger required chip area.

To relax the coarse assembly requirements, the use of accurately fabricated joining features that reduce misalignment was investigated. Grooves, notches and solder self-alignment pads are considered and discussed in more detail in Chapter 5. Based on the results, a coarse assembly procedure is presented, from which the required internal positioning ranges in x and y are finally established.

In the present subsection, for an initial approximation of the required fine-positioning ranges in x and y, preliminary estimates of the assembly and fabrication inaccuracies, contributing to the overall misalignment in these directions, are presented. The overall misalignment resulting after the coarse assembly process is a summation of the position inaccuracies of:

- laser diode on base plate;
- positioning device on base plate;
- fibre on positioning device;
- fibre core inside fibre;
- diode window inside laser diode chip.

A first approximation of the inaccuracies in x and y, presumably achievable by aid of joining features, are provided in Table 3.2. As a result, the overall,

maximal, misalignment in lateral directions was estimated to be in the range of 10 μm. Therefore the required internal positioning range was initially defined at 10-15 μm in both x and y. A detailed coarse assembly design with an improved estimation of the tolerance stack between laser output window and fibre core based on data from literature is presented in Chapter 5.

Part relation	**Estimated inaccuracy in *x* and *y***	**Comments**
LD-base plate	± 1 μm	
Positioning chip-base plate	± 1 μm	With use of lithographically defined joining features
Fibre-positioning chip	± 1 μm	
Fibre core-cladding	± 1.5 μm	Typical geometric single-mode fibre specifications, *e.g.* diameter accuracy and core-cladding concentricity (Draka 2008)
LD window-LD surface	± 0.5 μm	Expected lithographic processing accuracy

Table 3.2 Initial approximation of coarse positioning inaccuracies in *x* and *y*, based on estimates of assembly and fabrication tolerances

3.3.4 Required actuation force

All forces required for positioning the fibre should be delivered by the actuators built in the positioning device. The actuation load is related to:

- displacement (deformation) of the fibre;
- internal deformation of the positioning mechanism;
- friction between the actuator and the fibre;
- adhesive forces between actuator and other parts;
- fibre weight.

To determine the force required for displacement of a fibre, the fibre was assumed to be a single-side clamped beam. The deflection force can then be calculated by Equation 3.1:

$$F = \frac{3EI}{L^3}\delta \tag{3.1}$$

The fibre length was chosen quite arbitrarily. It should not be too short compared to its thickness since in that case high bending forces would be required, and moreover this would result in unacceptably large parasitic angular misalignments. Considering the space available in the package, a cantilever length of 2000-3000 μm was regarded appropriate. For a 10-μm tip displacement of a fibre of these lengths the required deflection forces are in the range of 1-3 mN, with corresponding fibre stiffness in the order of 100-300 N/m. Some MST-based actuators are known to be able to deliver external forces up to several mN (see Chapter 4 for additional information), therefore fibre cantilever lengths in the discussed range are considered realistic.

Forces required to deform the mechanism itself are strongly dependent on the design of the structure and were not considered in the initial estimation. The same holds for friction forces and adhesive forces between parts of the mechanism or between actuator and fibre as they are difficult to determine. Given the expected dimensions, which are quite considerable for microsystems, adhesive forces most likely play only a minor role compared to other force mechanisms involved. At this stage friction and adhesion were also not taken into account, though some additional reserve in actuation force should be taken to overcome these. Fibre weight can be neglected: a 3000-μm long fibre weighs around 0.1 mg, which is approximately equivalent to a force of 1 μN, three orders of magnitude lower than the bending-induced forces.

3.3.5 Industry standards

Commercial optical telecommunication devices generally have to comply with very strict industry standards. Various standards are available, which are all applicable for specific types of applications, provided by for example Telcordia (previously called Bellcore), the International Telecommunications Union (ITU-T), or the US military service (MIL). They deal with mechanical integrity, such as durability against mechanical shocks, vibration and fibre pull, and endurance capabilities, like the resistibility against accelerated aging, high and low temperature storage, temperature cycling and cyclic moisture resistance. The most important standard for laser diode packages is the Telcordia testing standard GR-468-CORE Generic Reliability Assurance Requirements for Optoelectronic Devices Used in Telecommunications Equipment[1], describing an extensive set of tests which the device should comply with.

[1] Issue 2, September 2004, for sale online (Telcordia 2008).

A selection of tests with matching conditions is:

- Temperature cycling -40 to +70 / 85°C, 20 cycles
- Accelerated aging 85°C, active power 2000 hrs
- Damp heat 50°C / 85-95% relative humidity, 3500 hrs
- Fibre pull 1.0 kg, 3 times, 5 seconds
- Mechanical shock 500 / 1500 g, 5 times/axis
- Non-operational vibration 20 g, range 20-2000 Hz, 3 times/axis

Typically these tests should be performed on more than ten samples. Performing all required testing is very time consuming and expensive. It involves dedicated equipment and trained operators, and is therefore normally performed in specialized companies.

When dealing with research demonstrators, attaining these reliability requirements are generally not the primary concern. The main focus in the development of product-internal assembly functionality is to explore its technical feasibility, for which achieving a working proof of concept is already a valuable result. On the other hand, in order to make the investigation realistic, it is relevant to consider, whenever possible, the main issues concerning overall robustness and reliability required for the specific application.

In the requirements overview presented in the following section, a general reference to the standard GR-468-CORE is included, since translating the very specific tests for the complete package into requirements for the product-internal assembly subsystem is not easily performed.

3.3.6 Summarizing requirements overview

In Table 3.3 an overview is presented of the demands (D) and wishes (W) for the conceptual design of the product-internal assembly functionality including coarse assembly adjustments. It is the result of the analysis and information presented earlier in the chapter.

This case study does not have a clear and complete list of requirements. To limit the investigation, not all components of the laser diode package were fully defined. However, sufficient information was available for a realistic case description and to make a start with the conceptual design phase.

Main headings of a checklist for drawing up a requirements list are: *geometry*, *kinematics*, *forces*, *energy*, *material*, *signals*, *safety*, *ergonomics*, *production*, *quality control*, *assembly*, *transport*, *operation*, *maintenance*, *costs* and *schedules* (Pahl and Beitz 1996, p. 54). The relevant demands and wishes are

Category	D/W	Comments
Geometry	D	Must fit inside butterfly package + may not physically interfere with already present components
	W	Small footprint (range 5 × 5 mm)
	W	Mechanism width preferably < 250 μm (possibility of use in fibre array)
Kinematics	D	Product-integrated actuators
	D	2 lateral degrees of freedom to be controlled: *x* and *y*
	D	Positioning resolution < 0.1 μm
	D	Displacement range > 10 μm in *x* and *y*
	W	Positioning speed preferably below 1 s
Forces	D	Sufficient force for fibre manipulation (range 1-3 mN)
Energy	W	Electricity preferred as energy supply
	W	Low number of electrical connections (low pin count)
Material	W	Base material: monocrystalline silicon
	W	IC-processing compatible materials
Production	W	Positioning functionality: MST-based fabrication
	W	Compatible with MST fabrication possibilities at DIMES
Assembly	D	Coarse assembly design must facilitate product internal assembly process to reach required tolerances
	W	Relaxed assembly requirements, simple pick-and-place of components preferred (range ± 20 μm)
	W	Geometrical features aiding coarse assembly steps
Operation	D	No or acceptably low adverse interference with primary functionality
	D	Long term position stability < 0.1 μm (range 10-15 years)
	W	Fixation: no power required
	W	Straightforward control
	W	Reliable and robust regarding external influences, such as temperature changes, vibrations and mechanical shocks (compatibility with standard GR-468-CORE)
Maintenance	D	No need for maintenance during service life
Costs	W	Overall production & assembly cost per laser diode < conventional assembly cost

Table 3.3 Specification overview for the design of the product-internal assembly functionality including coarse assembly adjustments

listed under the corresponding headings in the table. Demands are defined as requirements which must be met under all circumstances. Wishes are requirements that should be taken into consideration whenever possible.

4

Selecting and exploring MST-based actuators for fibre positioning

The purpose of this chapter is to discuss the selection of an MST-based actuation principle for the fibre tip positioning in the chosen product case, and to present test results of embodiments for this actuation principle. To this end, in Section 4.1 an overview is presented of MST-based actuation principles, from which a selection is made in Section 4.2. Thermal expansion is selected as actuation principle for the fibre-chip alignment case, of which possible embodiments are discussed in Section 4.3. Following, in Section 4.4, the results are presented of the first series of in-plane U-beam and V-beam thermal actuators developed and fabricated as part of this project.

4.1 MST-based actuation for fine part positioning

In this section, an overview is presented of MST-based actuation principles which may be used for fine part positioning for the purpose of micro-assembly. In the overview, they are compared according to aspects relevant for this application.

Actuators are devices that perform useful work on the environment in response to a command or a control signal. Comprehensive overviews of microactuators are provided *e.g.* by Fujita (1998) and Tabib-Azar (2000), of which MST-based actuators are an important subcategory.

A common classification of actuators is by the primary type of energy that is converted into mechanical work. In theory, all energy domains can be converted into mechanical work: radiation, electrical, thermal, magnetic,

chemical, but also mechanical energy, *e.g.* supplied in the form of vibrations (Tabib-Azar 2000).

4.1.1 Actuation principles and embodiments

In accordance with the distinction between *physical principle* and *embodiment* of solution principles for given sub-functions made by Pahl and Beitz (1996, p. 26-29), actuators can be seen as a combination of an *actuation principle* and an *actuator embodiment*.[1] The actuator embodiment may contain deformable parts and mechanical links. Its main function is to provide a mechanism for the actuation principle to produce useful work.

Actuation principles

Common actuation principles in the micro domain are different to those in the macro domain, since either unfavourable or favourable scaling occurs and moreover, when moving towards smaller dimensions, fabrication limitations have to be considered. Whereas in the macro domain electromagnetic, hydraulic, and pneumatic actuation are the most commonly applied actuation principles, in the micro domain other methods dominate, such as electrostatic, piezoelectric, and thermal actuation.

In MST-based actuation, the energy form that is to be converted into mechanical work is preferably generated by means of electricity. Devices that allow an electrical input are very attractive, since electrical power is widely available and voltage and current are easily controlled. Methods for fabricating electrical contacts with small dimensions are well-established, allowing for electricity transfer to highly localized points of use.

It is here decided to consider only those actuation principles that can be considered as proven technology both for their functionality and for their manufacturing process. In this project the focus lies on evaluation and integration of existing actuation and manufacturing technology and less on the development of new technology.

Actuators within some domains can not be considered proven technology (*e.g.* chemical actuators). Some actuator types deliver insufficient work, *e.g.* actuators based on radiation. Mechanical energy, such as vibration or fluidic energy, needs to be generated from one of the other energy types before it can be converted into useful work. Therefore, only the following three physical domains were chosen to be investigated in more detail: the *electri-*

[1] Different terms could also be used, such as *build up* or *construction*. Tabib-Azar (2000) uses a*ctuator shell* for this, whereas he uses *actuation means* or *method* to denote what in this thesis is referred to as actuation principle.

cal, *magnetic*, and *thermal domain*. In addition, a number of actuation principles belonging to these domains were not considered: electrostriction and magnetostriction[1], which are rarely applied principles in the micro domain, and phase-change actuation, which is discarded for its considerable fabrication complexity and its limited possibility for application in multiple degrees of freedom.

Actuation principles that appear most promising for the purpose of internal part positioning are:

- Electrostatic: the use of attraction between dissimilar electrical charges.
- Piezoelectric: the use of dimensional change of piezoelectric materials when a voltage is applied across them.
- Electromagnetic: the use of attraction between opposing magnetic poles.
- Thermal expansion: the use of dimensional change of a material when it is heated.
- Shape memory alloy (SMA): the use of large dimensional change of a shape memory alloy due to a change in solid state upon heating.

The choice for silicon as base material and MST-based fabrication has as a consequence that *e.g.* bulk piezo and bulk shape memory alloy actuator solutions, although principally capable of delivering high workloads, are not considered. Also hybrid solutions, comprising of silicon structures with assembled components for actuation, such as discrete magnets, wound copper wire coils, and piezoceramic or SMA plates or blocks, are not regarded as good alternatives, because additional preparation and assembly steps should be avoided to reduce the cost as much as possible.

Actuator embodiments

Many different actuator embodiments exist. From the viewpoint of their attainable actuation directions, usually a distinction is made with respect to the direction of the actuation *relative to the substrate*. Using this approach, microactuators can be divided into in-plane and out-of-plane actuators.

Commonly applied actuator embodiments are for example:

- Electrostatic comb drive: two arrays of interdigitated fingers, leaving a lateral and axial air gap. Due to Coulomb force attraction the two

[1] Electrostriction is a property of all electrical non-conductors, or dielectrics, that causes them to change their shape under the application of an electric field. Magnetostriction is a property of ferromagnetic materials that causes them to change their shape when subjected to a magnetic field.

arrays move towards each other. This mechanism is mostly used for in-plane actuation, but sometimes also for out-of-plane actuation.

- Thermal straight beam: simple straight beam lengthening upon actuation.
- Thermal V-beam: bent beam that is anchored at both ends. Lengthening upon actuation results in an in-plane outward displacement of the bent angle.
- Thermal U-beam: two beams (mostly one narrow, one wide), interconnected at one end and anchored at the other end. Upon actuation, one beam lengthens more than the other. Because the beams are connected to each other at their free end, the difference in lengthening results in an in-plane deflection in the direction of the wider beam.
- Unimorph or bimorph cantilever (piezoelectric / thermal / SMA): layered cantilever with one (unimorph) or two active layers (bimorph), with different lengthening upon actuation, causing internal stress and - generally out-of-plane - deflection.
- Stepper (electrostatic / piezoelectric / thermal): incremental stepping motions converting small actuator displacements into a large overall / part displacement. This type of mechanism is generally capable to perform 1 or 2-D in-plane translations, and potentially also rotations around the axis normal to the surface.

In the following, a number of important considerations are discussed related to the development and manufacturing of different types of MST-based actuator embodiments for fine part positioning.

Monolithic structures For the type of motions required for PIAF, monolithic, flexible structures are very suitable. An important design consideration in micromechanical engineering is to avoid sliding contacts, if possible. Typically, bearing design in the micro domain is rather troublesome due to the relatively large play (compared to the device's feature dimensions), and friction and wear between micromachined surfaces are difficult to predict. Monolithic structures, *i.e.* structures consisting of one single element, use parallel beam mechanisms, flexible hinges, torsion beams and blade hinges to realize translations and rotations and therefore require no bearings and no (internal) sliding of parts. Disadvantages are energy loss and the building up of internal stress due to deformations inside the structure. Monolithic structures allow for small deformations only, which is not expected to be a problem considering the small required actuation ranges in comparison with the allowable overall structure dimensions.

Serial or parallel configuration Multi-degree of freedom solutions can either be achieved by constructing the actuators themselves in different

directions, or by using intermediate mechanisms to convert the actuator motion into an output motion in the desired direction. Two main basic build ups can be distinguished: *serial* and *parallel*. In a serial build up, there is one kinematic chain of links and joints between the end effecter and base. In a parallel build up, multiple independent kinematic chains exist parallel to each other between the end effecter and the base. The overall stiffness of a parallel construction can be substantially higher than the stiffness of a serial construction. Another disadvantage of a serial set-up, especially in microsystems, is that routing of the electrical connections to the actuators not directly attached to the base is complicated. Only the actuator connected to the base is stationary; actuators further away are movable and are usually connected to the stationary structure by means of flexible elements, which should be relatively narrow to obtain sufficient compliance in the actuation direction. Electrical leads in microsystems are relatively large and may be too wide to be routed across these flexible elements. For these reasons, in most cases a parallel configuration is considered favourable.

Combined in- and out-of-plane positioning Some combinations of positioning directions are more difficult to accomplish than others. In particular combinations of in-plane and out-of-plane translations are difficult to achieve. Due to the planar nature of MST-based fabrication processes, design flexibility is chiefly limited to the directions parallel to the wafer plane. Out-of-plane actuation is possible, for example by using bimorph cantilevers, but their fabrication is not easily combined with in-plane actuators that generally require different materials and processing steps. On the other hand, constructing a mechanism to convert in-plane to out-of-plane motion is not straightforward either (see Brouwer (2007, p. 67) for a more detailed discussion).[1]

Stepping actuator configurations Various stepping actuator configurations exist, which are mostly composed of multiple actuators of one of the other types, for example bimorph cantilevers for conveyor-type actuation or in-plane thermal actuators for long-stroke 1-D linear actuation, see *e.g.* Maloney *et al.* (2004). Consequently, they are generally more complex with the main advantage that larger actuator ranges can be achieved, which is not specifically required for the fine part positioning. Stepping principles are therefore not treated separately, except for scratch drive actuators (SDAs), which are based on a distinctly different principle, and by which 3-D translational micro-positioning stages have been created, see *e.g.* Lin *et al.* (1994).

[1] Of the opposite possibility - conversion of out-of-plane actuator motion into in-plane end effecter movement - no examples are known from literature. The only actuation principle perhaps acting in a comparable way is the scratch drive actuator mentioned before, which transforms small out-of-plane electrostatic parallel-plate attraction into incremental sub-μm in-plane stepping motions.

4.1.2 Actuator overview

Table 4.1 shows an overview of the selected MST-based actuation principles, compared according to the aspects listed below. In addition, a brief explanation of the main characteristics of the individual actuation principles is provided.

Aspects for actuator comparison

In order to make a comparison between the various possible actuation principles, a number of aspects here listed are used as criteria.

The actuators are compared according to the following important aspects:

- actuation range;
- force;
- typical dimensions;
- work density;
- robustness;
- control & output: stability, accuracy, hysteresis, drift;
- construction: processing techniques, materials;
- design flexibility: in- / out-of-plane actuation, potential of combining into multi-degree of freedom positioning.

Actuation range and force, together forming mechanical work, are based on an actuator having certain dimensions. Therefore, *work density* is also included as parameter to compare the different actuators. In most cases, typical dimensions can be changed to reach a desired force or displacement.

By *robustness* is meant the ability to withstand external disturbances without damage or loss of functionality. This includes a certain load bearing capacity, but also the ability to withstand external component placement forces.

Electrostatic actuators

Many different electrostatic actuation configurations exist, for both in-plane and out-of-plane actuation. The most common in-plane electrostatic actuators are comb drives, which are also the most widely used actuators in the MST domain. The main advantage is their simple construction. They can be fabricated with rather standard processing techniques and conventional materials. For in-plane actuators deep reactive ion etching (DRIE) can be used (Robert Bosch 1994), allowing for the construction of robust structures.

Energy domain	Actuation principle	Embodiment	Actuation range [µm]	Force [µN]	Typical / example footprint [µm]	Work density [J/m^3][(1)]	Robustness	Actuation direction	Comments (control, construction, design flexibility)
Electrical	Electrostatic	Lateral comb drive	10^1-10^2	10^0-10^2	>500x500	10^2-10^5	+	In-plane	High voltages up to > 100 V. Standard processing techniques and materials. Robustness depending on structure height and suspension dimensions. Few examples of out-of-plane actuation.
		Parallel plate	10^0-10^1 / ~10 deg[(2)]	10^0-10^2	100x100	10^3	+/-	In- / out-of-plane	Nonlinear control, high voltages. Out-of-plane: surface micromachined -> low robustness. More suitable for on-off switching than incremental positioning.
		Scratch drive (SDA)	10^1-10^2	10^0-10^2	100x100		-	In-plane	Conversion of out-of-plane into in-plane motion. Surface micromachined -> low robustness.
	Piezoelectric	Unimorph	10^1	10^4	100x500	10^2-10^5	+/-	Out-of-plane	Voltages may remain low, significant hysteresis and drift. Multiple electrode layers required. Non-standard materials, mostly PZT or ZnO. Generally poling required by strong electric field prior to use.
Magnetic	Electromagnetic	General	-10^3	-10^5	Mm range	10^3-10^5	+/-	In- / out-of-plane	Increasingly less attractive at smaller scales. Problematic construction: difficult to produce small coils and magnetic circuits on-chip. Deposited magnetic materials require magnetization, potential risk of crosstalk.
Thermal	Thermal expansion	V-beam	10^1	10^3-10^4	100x1000	10^5	+	In-plane	Moderate voltages. Standard processing techniques and materials. Low robustness in case of surface micromachining. Locally high temperatures, potential risk of crosstalk. Relatively slow response.
		U-beam	10^1	10^2-10^3	100x1000	10^4	+	In-plane	
		Bimorph	10^1-10^2	10^0-10^3	100x500	10^5	+/-	Out-of-plane	Moderate voltages and temperatures. Significant initial curvature with considerable variation for thin cantilevers. Potential crosstalk.
	Shape memory alloy	Unimorph	10^1-10^2	10^4	200x1000	10^6-10^8	+/-	Out-of-plane	Low voltages, modest temperatures. Large hysteresis and nonlinearity. Non-standard materials, generally NiTi. Film thickness ~5 µm. One-way SMA actuation requires bias force; two-way requires training steps.

Table 4.1 Overview of MST-based actuation principles and accompanying characteristics

(1) Motamedi (2005), Tabib-Azar 2000)
(2) Texas Instruments (2008)

The energy density of electrostatic actuators is relatively low. In order to generate acceptable forces using the comb drive principle, large numbers of fingers are required. Typically, μN-range forces and displacements of several tens of microns can be achieved. Electrostatic actuators are easy to control, but a main disadvantage is that often high voltages are involved, sometimes up to a few hundred volts.

For out-of-plane actuation mostly parallel plate actuation is employed. Depending on the specific configuration, small linear displacements or angular rotations can be achieved. A well-known example is the Digital Light Processor (DLP) chip developed by Texas Instruments containing over a million electrostatically switchable micromirrors for optical beam steering (Texas Instruments 2008). Generally, these actuators consist of surface micromachined structures, and are therefore most likely insufficiently robust to carry realistic external loads. For example, although the mass of a micro component is very small, a suspended polysilicon microstructure fabricated by sacrificial surface micromachining could very well collapse onto the substrate under the weight of such a component. This is due to its small structural height and substrate clearance, which are typically both a few microns (Syms *et al.* 2004a). Therefore, a stronger construction with a larger structural height is generally required. This is also considered true for most electrostatic in-plane stepper actuators, such as scratch drive actuators, which, too, consist of thin surface micromachined structures. Most electrostatic 3-D micropositioning stages presented in literature are based on electrostatic linear stepper actuators, and therefore have the same limitation.

Piezoelectric actuators

Bulk piezoelectric actuators are very versatile and many different actuator types are available. However, they are not considered for the PIAF application, because they are incompatible with silicon microfabrication processes. Techniques have been developed to deposit thin piezoelectric films on substrates like silicon and glass, and to subsequently pattern these films. Various techniques, such as sputtering, evaporation, chemical vapour deposition, and sol-gel deposition have been applied to deposit a number of piezoelectric materials like zinc oxide (ZnO) and lead zirconate titanate (PZT). PZT is the material type possessing the largest piezoelectric coefficients, allowing for the largest work densities. Typically, the integration in MST processing is difficult, and much expertise is required to deposit these special materials and to control their material characteristics.

Out-of-plane bending cantilevers are the most commonly used actuators based on these films, because they require relatively easy fabrication processes, and they can be used to amplify the small deformations into reasona-

bly large displacements (~ 10 μm). This is at the expense of a decreased output force (typically a few tens of μN, depending on the thickness and Young's modulus of the layers) and work density, since the input energy is for a large part internally stored as a stress-strain combination inside the actuator.

The required voltages decrease proportionally to size. In micro-actuators, the thickness of piezoelectric layers can be a few micrometers or less, for which a few volts are sufficient to reach the required field strengths. Piezoelectric actuators have the drawback that piezoelectric materials exhibit hysteresis (defined as the difference in the actuator output Y when Y is reached from two opposite directions) and drift, making control somewhat more difficult. A last disadvantage is that most piezoelectric materials need to be poled by a strong external electric field prior to use.

Electromagnetic actuators

Electromagnetic actuators, although theoretically capable of achieving large forces and displacements, do not perform very well at the micro scale due to construction problems. The magnetic field is usually either generated by a current-carrying coil, or a permanent magnet. Micromachining techniques have been developed to produce coils and magnetic circuits on-chip, but these are generally flat, and for example coils produced with these 2-D processing techniques do not possess the compactness and efficiency of wound coils used in large motors. To compensate for the reduction of the flux density, the coils become relatively larger when scaled down. Significant effort and skills are required to deposit and subsequently pattern magnetic materials in thick layers (> 10 μm) and to obtain good material characteristics.

The lack of 3-D processing possibilities complicates the construction of compact MST-based electromagnetic actuators with multi degree of freedom (DOF) actuation capability. Another difficulty could lie in possible unavoidable magnetic cross coupling between adjacent actuators when aiming to activate them individually. Lastly, deposited permanent magnets need to be magnetized in-situ, meaning that only one magnetization direction is possible, which could be a further restriction when attempting to implement multi DOF actuation.

Thermal actuators

Electrothermal actuators have received wide interest as they can produce a large displacement, large force, generally have a simple construction, and can be fabricated with standard processing techniques and conventional materials. Attainable forces can reach up to several millinewtons and displacements up to over a hundred microns. Depending on the materials

used, local temperatures can be high, *e.g.* 500-600°C in the case of the commonly used heater material polysilicon. Usually, the actuation voltages can be kept to moderate values, which is preferred for practical applicability.

In literature, thin surface micromachined thermal actuators are presented as well as actuators having a larger structural thickness, possessing significantly higher robustness against disturbances. As indicated earlier, both in-plane and out-of-plane thermal actuators exist, of which the latter generally are of the bimorph type and which typically require different processing. A benefit of the use of silicon as structural material is its high thermal conductivity, enabling the rapid removal of heat from the actuator, resulting in highly localized heated areas. This potentially allows for the design of closely spaced heated microstructures without observable cross-talk.

Shape memory alloy actuators

As for piezoelectric and electromagnetic materials, techniques have also been developed to deposit shape memory alloy films on silicon, such as TiNi and TiNiCu. Based on this, out-of-plane bending cantilevers have been constructed capable of achieving large displacements of several tens of microns and large forces in the range of tens of millinewtons. Typically, shape memory alloys are very difficult to control due to their large hysteresis and non-linearity. Compared to thermal expansion actuators, generally much lower temperatures are used.

Two basic methods are employed using SMA actuators, each imposing different requirements: so-called *one-way actuation*, for which a bias force on the SMA structure is needed, and *two-way actuation*, requiring preparatory training steps, see *e.g.* Motamedi (2005, p. 153).

The only shape memory alloy actuators based on integrated thin film deposition presented in literature are of the out-of-plane type, as for thin film piezoelectric actuators. The design flexibility to create multiple DOF actuation functionality using this type of actuators is therefore limited.

Evaluation MST-based actuation principles for PIAF

Based on the presented overview, it can be concluded that none of the discussed actuation principles are easily implemented for internal fine part positioning. Particularly achieving multi DOF positioning in a monolithic structure is highly challenging, especially in combination with the demand of a relatively high load bearing capability. This practically excludes the possibility to use surface micromachined actuation structures.

All shown actuation principles are capable of providing displacements over 10 μm and μN forces in individual degrees of freedom. Electrostatic and

thermal actuation appear to be the most promising based on their relatively simple construction and they do not require special materials. They are capable of achieving both in- and out-of-plane actuation, although these generally require dissimilar processing, and most out-of-plane electrostatic actuators lack robustness. Piezoelectric, electromagnetic and shape memory materials are not routinely implemented but can be deposited in thin layers on a substrate. For piezoelectric and SMA actuation this results in a general limitation to out-of-plane bending. Electromagnetic actuation suffers from constructive problems in creating structures for generating the required magnetic fields. Although principally possible, the combination of different actuation principles - such as piezoelectric and thermal actuation - integrated in a single device to realize multi-degree of freedom positioning functionality could not be found in literature, most likely because this would bring about even larger challenges in process integration than described above.

4.2 Actuation principle selection for positioning the fibre

Based on the overview presented in the previous section, an MST-based actuation principle is selected for the fibre tip positioning in the optical coupling product case. The most important requirements for the positioning functionality are briefly repeated here:

- Positioning capability in DOF perpendicular to optical fibre axis: x and y;
- Displacement range > 10 μm;
- Minimum position resolution 0.1 μm;
- Sufficient force for fibre manipulation ~ 1-3 mN;
- Sufficient robustness;
- Small dimensions, ideally less than a few mm long and 250 μm wide including fibre diameter of 125 μm.

From the overview, actuation by thermal expansion is the most promising one for this application. It is capable of generating the required forces, whereas for electrostatic actuation this would be very challenging, if not impossible. Furthermore, it generally consists of simple structures that can be made using proven processing techniques with conventional materials, rendering a high degree of design flexibility. However, thermal loading might present unwanted complications, and thus special care should be taken during the design of thermal actuators to limit the thermal influence on neighbouring actuators and other surrounding structures. The fact that

fixation after positioning was chosen, makes this issue less critical, since it only needs to be employed once in its lifetime during assembly. General characteristics of thermal actuators are their low efficiency and low response speed, which are both of minor importance for the considered application.

4.3 Thermal expansion actuator embodiments

In this section, the most commonly applied thermal expansion actuation embodiments are discussed in more detail. To this end, first the fundamentals of thermal expansion are briefly presented, including heat generation, principles of heat transfer, and the conversion from heat to mechanical work.

Thermal expansion actuators deliver mechanical work when heated. The most commonly applied method to generate heat by means of electricity is by passing a current I through a resistor with resistance R, referred to as resistive heating or Joule heating. The heat generated per unit of time is equal to $P=I^2R$.

Once the heat is generated, it dissipates to colder regions by means of three possible heat transfer mechanisms: *conduction*, *convection* and *radiation*.

- *Conduction* is heat transfer across a stationary medium that occurs when there is a temperature gradient inside the medium;
- *Convection* is heat transfer between a surface (solid or fluid) and a moving medium (fluid or gas) caused by a temperature gradient;
- *Radiation* is heat transfer in the form of electromagnetic waves from a surface of a specific temperature.

For silicon devices, usually conduction through the solid material accounts for the largest amount of heat transfer, due to its high thermal conduction coefficient. However, when aiming to model the thermal behaviour accurately, generally one or more other heat transfer mechanisms should also be included. For example, conduction through air may be significant in structures with dissimilar temperatures separated by a small air gap (in the order of a few microns). Alternatively, when air gaps are larger, in the order of several tens of microns or more, the effect of convective heat dissipation may become substantial. Conduction and convection are linear functions of the temperature difference, whereas radiation has a fourth power dependency on temperature. For most cases, heat loss by radiation is negligible because the temperatures in silicon thermal actuators usually do not exceed 600°C. For more general information on the subject of heat transfer the reader is referred to *e.g.* Mills (1999).

In a thermal actuator, the heat is converted to mechanical work by utilizing the thermal expansion of the material. For a straight beam of length L, cross-sectional area A, Young's modulus E, and thermal expansion coefficient α the elongation, caused by an average temperature rise ΔT_{av}, is given by Equation 4.1:

$$\Delta L = \alpha L \Delta T_{av} \tag{4.1}$$

The maximal force (force generated when the elongation of the beam is blocked) is, assuming linear spring behaviour (Hooke's Law), given by Equation 4.2:

$$F_{bl} = cu = \frac{EA}{L}\Delta L \tag{4.2}$$

where c is the actuator stiffness. The maximum possible output work is equal to:

$$W_{max} = \frac{1}{2}cu = \frac{1}{2}F_{bl}u = \frac{1}{2}\frac{EA}{L}\Delta L^2 \tag{4.3}$$

Expansion of a straight beam renders rather small displacements. Therefore, generally transmission ratios of various sorts are used to increase the displacement output of thermal actuators. The common thermal expansion microactuator types *bimorph cantilevers*, *U-beams*, and *V-beams* are each based on a different principle, and are each briefly discussed hereafter.

4.3.1 Bimorph actuators

Thermal bimorph or multimorph actuators are based on the difference of the thermal expansion coefficients of two or more dissimilar layers. They generally consist of a cantilever with two or more layers, of which one is used as a heating resistor. When current is passed through the heating resistor layer, a thermal stress is generated between the layers, causing the cantilever to bend. See for a typical bimorph actuator Figure 4.1. This so-called bi-metal effect was already described by Timoshenko (1925), but the first to show such a cantilever-type micromachined silicon actuator were Riethmüller and Benecke (1988), who fabricated bimorph actuators consisting of epitaxial silicon and electroplated gold heated by an integrated polysilicon heater. Since then, several examples of bimorph and multimorph cantilevers were demonstrated, mostly consisting of a polysilicon or single crystal silicon layer and a metal layer, such as aluminium or nickel. The metal layer is deposited by evaporation, sputtering or electroplating, which are all planar deposition processes. This planar layer arrangement generally allows actuation normal to the wafer plane only, however Sehr *et al.* (2001) also showed examples of in-plane moving thermal bimorph actuators.

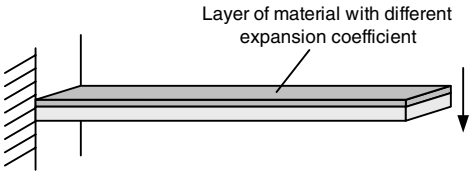

Figure 4.1 Typical bimorph actuator

Typical layer thicknesses are a few to several microns, based on the relative difficulty of creating a layer of substantial thickness (10-20 μm) on top of the silicon cantilever and the apparent lack of need for use in high-force applications. These bimorph cantilever sizes are generally 300-500 μm long and 100 μm wide, and for example the 500 μm long cantilevers with 4 μm and 2.5 μm thick silicon and gold layers by Riethmüller and Benecke showed over 75 μm out-of-plane deflections. A similarly sized actuator by Read *et al.* (1995), which was estimated to be half as thick, was reported to be capable of delivering a blocking force of 0.15 mN, whereas it could still produce 5 μm deflection under a 0.05 mN load. For both examples of relatively thin cantilevers, initial curvature due to residual stress from the device fabrication was observed, with considerable variation in curvature radius.

MST-based bimorph actuators with larger layer thicknesses were also found in literature. Greitmann and Buser (1996) showed an assembled microgripper system of a 1.5 mm long bimorph cantilever together with an opposing force sensing finger. The bimorph finger was built up from 10 μm thick silicon and 6 μm thick aluminium; it could deflect approximately 140 μm, and a maximum gripping force of over 0.25 mN was measured. A thermally actuated cantilever having comparable layer thicknesses (7 μm silicon and 6 μm aluminium) for atomic force microscopy purposes was shown by Akiyama *et al.* (2002). Haake *et al.* (1998) proposed a three axis thermal micro positioning stage for fibre tip manipulation (also described in Chapter 2), in which the out-of-plane positioning was performed using a bimorph actuator consisting of bulk silicon and electroplated nickel fabricated by means of the expensive X-ray LIGA technique. Displacements over 120 μm were obtained, however the exact layer thicknesses and attainable forces were not stated.

4.3.2 U-beam actuators

U-beam thermal actuators generally consist of two suspended parallel adjacent arms connected to each other at the tip and to the substrate at the anchors. Although several variations exist (such as by Hoffmann *et al.* (2003b) and Pichonat-Gallois *et al.* (2004), see Chapter 2, and Pan and Hsu (1997), who presented a microactuator based on different lengths of the two

adjacent beams), most designs are based on a difference in width of the arms, resulting in asymmetrical heating causing the structure to deflect laterally. A typical U-beam actuator geometry is shown in Figure 4.2. The thin arm has a higher electrical resistance than the wide arm, and consequently gets heated and elongates more than the wide arm. The greater compliance of the structure in bending as compared to the axial direction then results in an amplification of the relatively small difference in axial thermal expansion into a large lateral motion, with the narrow section of the cold arm acting as an elastic hinge.

Figure 4.2 Typical U-beam actuator

The first to show this type of in-plane actuators were Guckel *et al.* (1992), who used electroplated nickel and X-ray LIGA, followed by Comtois *et al.* (1995), who fabricated and tested 2 μm thick freestanding surface micromachined polysilicon U-beam actuators made using the established Multi-User MEMS Process (MUMPs)[1]. Field *et al.* (1996) presented a 1×2 optical fibre switch having two 1.5 mm long U-beam actuators consisting of 50 μm thick electroplated nickel, capable of estimated displacements of over 180 μm and forces at zero displacement of around 3.5 mN. Using electroplating, considerable thicknesses can be attained, but since this is limited to metals, a disadvantage is that generally very high currents are needed. More recently, others, such as Syms (2002) have used DRIE for constructing U-beam actuators in silicon-on-insulator (SOI) wafers, allowing for larger device thicknesses using silicon as the structural layer. In the device by Syms, the silicon thickness was 100 μm and the structure was metallised with thin chrome and gold layers that functioned as heaters.

Interestingly, the described U-beam actuator is known under various names, such as *pseudo-bimorph thermal actuator*, *heat-drive actuator* or *heatuator* (Comtois *et al.* 1995), *electro-thermal-compliant* (ETC) actuator (Mankame and Ananthasuresh 2001), and *hot-leg/cold-leg* actuator. Throughout this thesis, this actuator type is denounced as *U-beam* thermal actuator, partly for distinguishing it clearly from the other frequently used

[1] MUMPs is a commercial programme that started in 1992 offering customers standardized processing knowledge to enable them to develop MST-based devices. It is one of the few MST fabrication standardization programmes available, and now being offered by the US-based company MEMSCAP (2008).

in-plane thermal V-beam actuator, and also to be consistent in their naming.

4.3.3 V-beam actuators

The other common class of in-plane electrothermal actuators is based on linear thermal expansion, like the simple straight beam discussed earlier. In the case of V-beam actuators, however, the electrical current is passed through a bent beam anchored at both ends, and thermal expansion caused by the produced heat pushes the angle tip outward. As end effecter of the beam, displacement of this tip is used for actuation. Instead of having the actuation displacement in the same direction as the length of the beam, which is the dominant direction of expansion, the actuation is now at an angle to this direction, allowing for significant displacement amplification. Figure 4.3 shows a typical V-beam actuator geometry. Like the U-beam actuator, it is also known under different names, such as *bent-beam* actuator, *buckling beam* actuator, and *chevron* actuator. The fabrication requirements are similar to those of U-beam actuators, therefore they are also found in literature in the commonly used structural materials polysilicon, nickel, and single crystalline silicon. In the same fibre micropositioning device containing the out-of-plane thermal bimorph actuator, Haake *et al.* (1998) have shown electroplated nickel V-beam actuators fabricated using X-ray LIGA, capable of delivering over 30 μm displacement and forces up to several tens of mN. As for the bimorph actuator, the nickel layer thickness was not stated. Relatively thin V-beam actuators on the order of 2-4 μm in polysilicon, highly doped silicon, and electroplated nickel were investigated by Que *et al.* (1999, 2001), and in polysilicon by Sinclair (2000), who placed several actuators in parallel, thereby enabling an increased output force. Chu and Gianchandani (2003) presented a 2-D in-plane positioning stage containing two 65 μm thick silicon V-beams constructed in the low resistivity top layer of custom SOI wafers. The 3000 μm long and 36 μm wide actuators were each capable of 19 μm displacements and had a designed blocking force of 72.5 mN. Unamuno *et al.* (2005) showed 1-D in-plane fibre alignment using a thermal V-beam array having ten parallel beams providing 24 μm fibre tip displacement, with a calculated opposing fibre force of 1.83 mN.

Recently, polymeric electrothermal actuators have received attention as they are capable of producing large displacements at lower power consumptions and operating temperatures than silicon thermal actuators due to the larger thermal expansion coefficient of polymers. For example, Chronis and Lee (2005) have presented a polymer microgripper for cell manipulation in liquids consisting of two U-beam actuators with a 20 μm thick layer of the popular SU-8 as structural material and thin chrome and gold layers serving

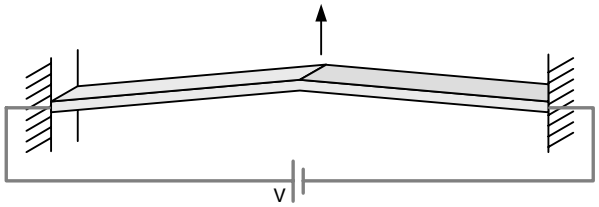

Figure 4.3 Typical V-beam actuator

as heating elements. With an overall length of 650 μm, gripper openings of at least 12 μm were achieved at modest temperatures of 80°C and low voltages of 1-2 V. Achievable forces are generally much smaller, based on the considerably smaller Young's modulus of SU-8 compared to the other commonly used actuator materials.

Other interesting recent polymeric thermal actuator layouts were shown by Lau (2007), who used meandering silicon segments with in-between confined polymer material for increased thermal expansion to realize thermal actuators aimed at having large tip motions and reasonable forces at low temperatures and power consumption. Although the initial results were promising, fabrication was still challenging and therefore this type of actuators was not considered for the fibre alignment case.

4.4 The first thermal actuator demonstrator series[1]

In this section, the design considerations, fabrication process, and the experimental results of the first thermal actuator demonstrator series developed in the PIAF project are presented.

4.4.1 Design and processing

The main purpose of this series was to obtain the first working thermal actuators, and to acquire improved insight into attainable positioning ranges and forces by using these actuator types. The aim was to develop thermal actuators capable of achieving displacements approximately in the 10-μm range, which was the lower limit specified in the requirements overview in Table 3.3 in the previous chapter. To reduce the processing complexity a limitation was made to in-plane actuation structures only (U- and

[1] With some alterations, Section 4.4 has previously been published as Henneken *et al.* (2006) in the Journal of Micromechanics and Microengineering.

V-beam actuators). Compared to thermal bimorph actuators with thick layers, their fabrication is less challenging, and more examples are available of devices capable of achieving the required high forces. Moreover, they have been extensively modelled, see for example Huang and Lee (1999), Mankame and Ananthasuresh (2001), Lott *et al.* (2002), Hickey *et al.* (2003), and Geisberger *et al.* (2003), which is beneficial for the potential of successful applicability.

For the device manufacturing, bulk micromachining was employed since this rendered the possibility to fabricate sufficiently stiff and robust structures for the considered application. A considerable amount of out-of-plane stiffness was achieved through the use of a sufficiently large layer thickness, obtained by DRIE using the Bosch-process (Robert Bosch 1994). This fabrication method provides well-defined structures having straight sidewalls perpendicular to the wafer surface with high aspect ratios and a large design freedom in the wafer plane. With feature sizes down to 20 μm, the device layer thickness was safely set to 100-120 μm.

We used conventional silicon wafers in order to keep the recurring costs low. Of course, the use of more costly SOI wafers can be considered as this simplifies the process. The backside was thinned using a timed anisotropic wet etch, allowing for flexibility in achieving device thickness variations.

Heating was chosen to take place by current flow in a thin doped polysilicon layer on the top surface. This was selected as it is a common material for thermal actuation, and it can be used up to high temperatures (500-600°C) (Ehmann *et al.* 2001, Lee *et al.* 2006), which are required to achieve sufficient deformations due to the small thermal expansion coefficient of silicon. Moreover, its electrical resistivity can be tuned in a wide range to obtain convenient voltage and current levels. Diffusion of phosphorous was used to dope the polysilicon layer. This was selected to obtain relatively low sheet resistance values (approximately 30O/square) in order to achieve sufficient power dissipation at moderate voltage levels. Little, if any, parasitic out-of-plane bending was expected, based on the small difference in thermal expansion coefficient with the single crystal silicon of the substrate and the high temperature uniformity across the cross-section of the structures due to the high thermal conductivity of silicon. This was verified by thermal modelling using the commercial finite element modelling software ANSYS^{TM} and also by analytically determining the Biot number for the cross-section of the structures. It was much smaller than unity, indicating that the internal cross-sectional temperature gradients were small and the required time for the heat to penetrate from the top of the cross-section to the bottom was short compared to the time required to transport the heat to the anchors (Hickey *et al.* 2003). For thermal calculations this has the

advantage that the model can be simplified because only the temperature distribution along the beam length needs to be considered.

A chip design was made containing various U- and V-beam variants. Here only one of each is discussed. A schematic overview of the main fabrication steps is shown in Figure 4.4. See Appendix A for a more elaborate process flow description.

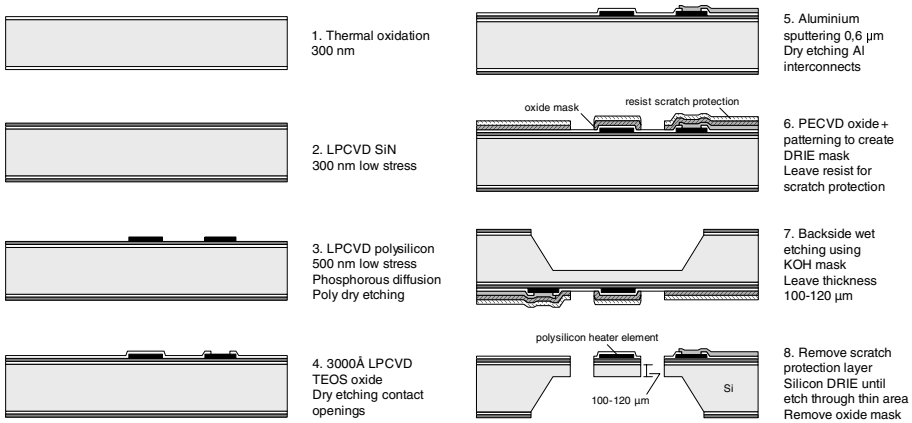

Figure 4.4 Process sequence in-plane actuation structures

The starting substrate was a standard 525 µm silicon wafer onto which a 300 nm oxide layer was thermally grown, followed by low-pressure chemical vapour deposition (LPCVD) of 300 nm low-stress silicon nitride (steps 1 and 2). A 500 nm low-stress polysilicon layer was deposited using LPCVD, and subsequently doped with phosphorous by diffusion, and patterned using a resist mask by means of dry etching (step 3). After this, a 300 nm tetraethoxysilane (TEOS) oxide layer was deposited using LPCVD, which was similarly patterned using dry etching to form the openings for contacting the underlying poly layer (step 4). Subsequently, aluminium was sputtered and patterned to form the electrical leads to the heaters (step 5), and the DRIE mask was created by plasma etching a PECVD oxide layer. This mask was used at the end of the flow to create the fibre grooves and actuators. The resist mask was left for scratch protection (step 6). On the backside openings were created in the nitride-oxide layer, after which wet anisotropic etching was employed to form cavities until a substrate thickness of 100-120 µm remained (step 7). Finally, the resist scratch protect layer was removed, and DRIE was used to create the actuator structures and fibre grooves, after which the oxide mask layer was removed (step 8).

The specific U- and V-beam actuators discussed in this section are shown in Figure 4.5, together with their respective overall geometrical dimensions.

These dimensions were determined using finite element modelling, which is briefly discussed in the following subsection. The polysilicon layer, which is omitted here for clarity, was taken 4 μm narrower on both sides than the structural beams to ensure that the polysilicon layer was fully covered (also on its sides) by the silicon dioxide insulation layer to prevent the potential presence of undesired current paths.

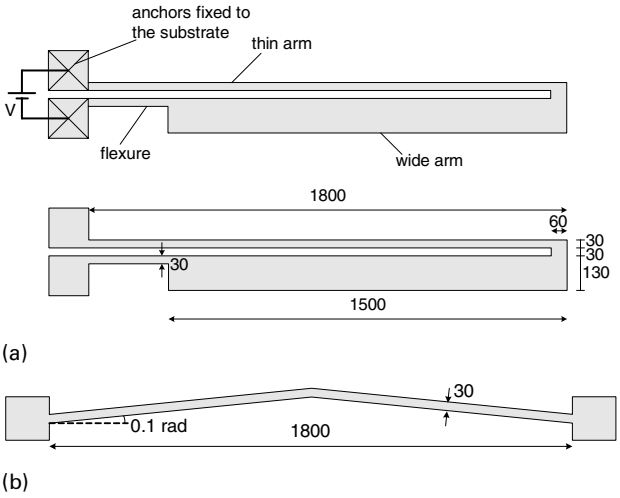

Figure 4.5 Schematic representation of (a) the U-beam and (b) the V-beam thermal actuation structure. The polysilicon layer followed the same geometry, only was 4 μm narrower on each side.

4.4.2 Modelling

Based on finite element modelling using ANSYS, the expected free deflection at a 40 V load was just under 15 μm and a little over 10 μm for the U-beam and the V-beam actuator, respectively (see Figure 4.6). When including a fibre these values were estimated to drop to around 10 μm (the V-beam structure was significantly stiffer than the U-beam, hence the difference in deflection decrease). The modelled power needed for these deflections was 0.42 W for the U-beam and 0.64 W for the V-beam structure, producing approximate peak temperatures locally of up to 500°C and 600°C, respectively. Figure 4.7 provides numerical results of deflection and maximum temperature versus voltage for the range from 0 to 45 V, for both the U- and V-beam thermal actuators.

The finite element modelling presented here was intended as virtual prototyping tool. The goal was to determine the overall dimensions needed for achieving the desired output performance. The model only required to be sufficiently accurate for this purpose, instead of being as accurate as possi-

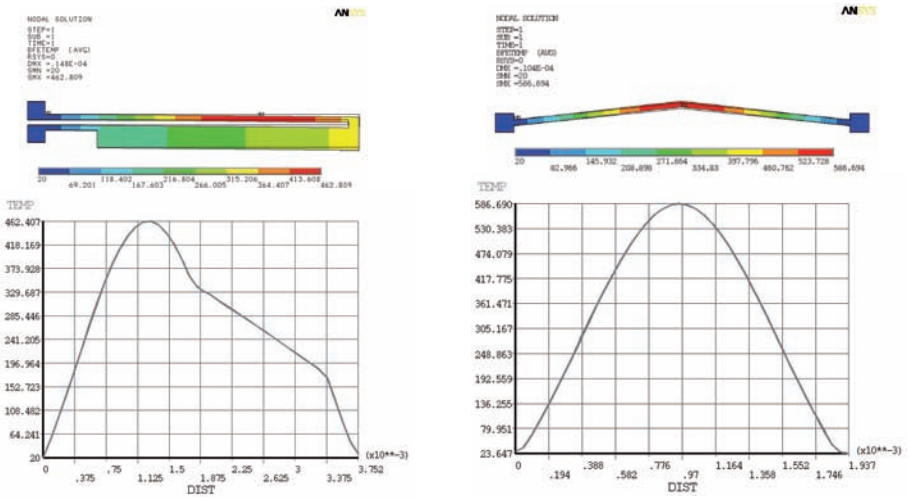

(a) (b)

Figure 4.6 (a): Finite element model of the U-beam actuator at 40 V load including matching temperature profile along the beams, starting from the anchor on the hot arm side (in °C). (b): Model of the V-beam actuator at 40 V and matching temperature profile along the beam.

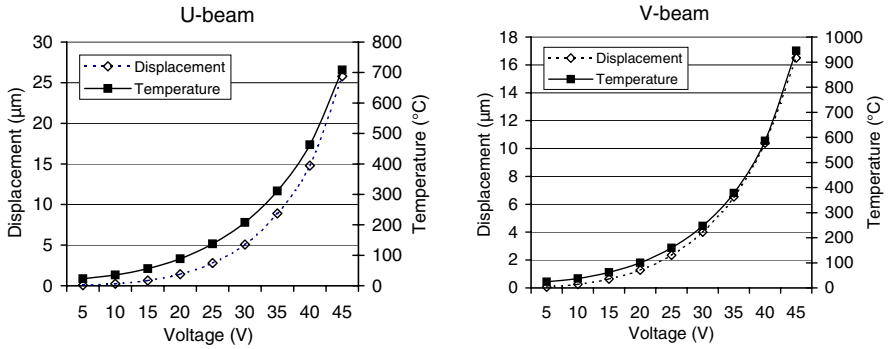

(a) (b)

Figure 4.7 Modelled displacements and maximum temperatures at a voltage range from 0 to 45 V, (a) for the U-beam and (b) for the V-beam thermal actuation structure, respectively

ble. Purely conductive heat transfer was assumed, and convection, radiation and conduction through air were not taken into account. The thin polysilicon resistor layer - as well as the other thin deposited layers on top of the beams - was not included in the models. Modelling was performed with an equivalent electrical resistivity inside the bulk of the beams. Besides thermally, mechanically this had also very little influence, in the order of the

thickness ratio between these layers and the overall beam thickness (~ 1%). The Young's modulus, the thermal expansion coefficient and the thermal conductivity were inserted into the models as temperature dependent properties.

4.4.3 Fabrication results and experiments

The fabrication results are shown in Figure 4.8. In Figure 4.8(a) an overview image is provided of two individual U-beam actuators and one V-beam actuator after final release. Figure 4.8(b) shows a close up of the end connection of the right U-beam actuator. Both images were taken from a 45° viewing angle. It can be seen that the fabrication had rendered very smooth straight sidewalls without observable under etch. The in-plane dimensions very accurately matched the designed values. The cold actuator arm was provided with an extra wide part at the top end so that the fibre had a well-defined contact area with the actuator structure. (The thin light-coloured aluminium lines visible on top of the U-beam actuator were included for temperature measurement purposes.)

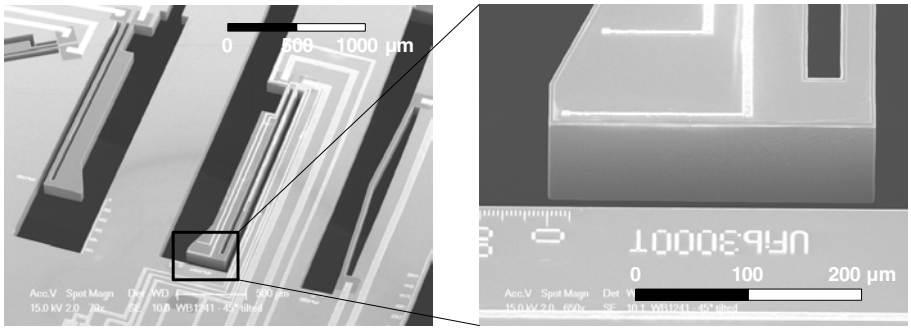

(a) (b)

Figure 4.8 SEM images of fabricated in-plane actuators at a 45° viewing angle: (a) overview of two U-beam actuators (left) and one V-beam actuator; (b) close up of a U-beam actuator tip

The actuator thickness was measured to be 130 µm, which was more than the 120 µm originally aimed for due to the fact that the wafer thickness of 525 ± 25 µm had not been measured before processing. Although this gave somewhat different actuation behaviour, this thickness variation was not critical and even though the KOH backside etching was a timed process the thickness could have been controlled much more accurately if desired.

In order to be able to perform experiments both with and without fibre, a groove for holding a fibre was devised extending from the actuator down-

wards. This fibre groove was designed to be 126 μm wide, just 1 μm wider than the nominal fibre diameter. Between the actuator-fibre contact area and the narrow fibre groove the fibre was sideways unsupported, see Figure 4.9. This free length, which is denoted as L_{free} in the figure, was clearly defined and can be considered as the free length of a fibre clamped at the groove extremity. Both actuator structures were fabricated with two different free fibre lengths (2000 and 3000 μm), since this has a significant effect on the stiffness to be overcome by the actuator (for 3000 μm only around one third of that for 2000 μm). The groove was provided with a taper on the outside for guiding the fibre when inserted from the side.

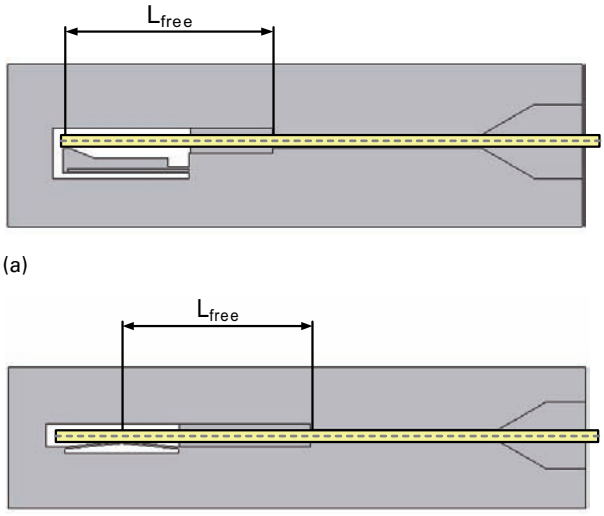

Figure 4.9 Schematic overall geometry of a U-beam (a) and of a V-beam actuator (b), both including fibre holding groove. Indicated is the free length across which the fibre is unsupported between groove and actuator contact area.

The actuator-fibre contact area and the fibre holding groove were placed exactly in line with each other, so in-off state the fibre was nominally positioned just against the actuator. In reality the fibre ends were not always perfectly straight, and since an opposing passive spring was omitted in the design it was possible that the fibre was not in direct contact with the actuator at 0 V. Therefore, for all measurements including fibre it was ensured that the fibre at least made contact with the actuator. In practice this meant that at the start the fibre most of the times exerted a slight pressure onto the actuator.

Inserting a fibre in either of the in-plane structures did not render unexpected difficulties. The manual handling operation was delicate, but no noticeable damage to the fibre or to the actuation structure was observed. It was particularly easy to insert a fibre from the side into the fibre groove, although it could also be inserted from the top. When inserting from the side, no fibre buckling or obstructions due to friction effects were observed. Figure 4.10 for a top view of a U-beam structure with a fibre directly positioned against the actuator.

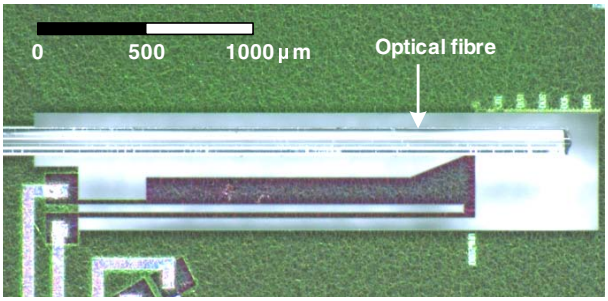

Figure 4.10 U-beam structure including optical fibre

A first performance inspection of an 1800 µm long U-beam actuator without fibre loading proved acceptable accordance of the measurement results to the modelled values. A linear increase in voltage from 0 to 40 V yielded an estimated maximum free end effecter displacement of over 10 µm. A colour change was observed at approximately two-third of the thin arm length from its anchor due to the temperature increase.

Subsequently, it was determined to which voltage level the actuators could be powered. For this purpose, a U-beam actuator was subjected to linear voltage ramps from 0 V to increasingly high end voltages. During this, the resistance value of the actuator was measured and plotted against the corresponding voltage level. The result of this test is presented in Figure 4.11.

For each cycle it could be observed that initially the resistance increased with increasing voltage. This is a known phenomenon for heavily doped polysilicon and silicon heated structures, which is caused by decreasing carrier mobility due to increased electron-phonon scattering in the silicon (Sernelius 1990). Also it could be seen that the first three cycles (subsequently with maximum voltages of 20, 40 and 50 V) for their common part closely corresponded. Only the graph for the fourth linear increase (to 60 V) noticeably started to deviate from the previous three graphs. This could only be explained from a change that had occurred in the previous cycle up to 50 V. In fact, when completing the linear increase to 60 V, the resistance reached a certain maximum value, after which it started to

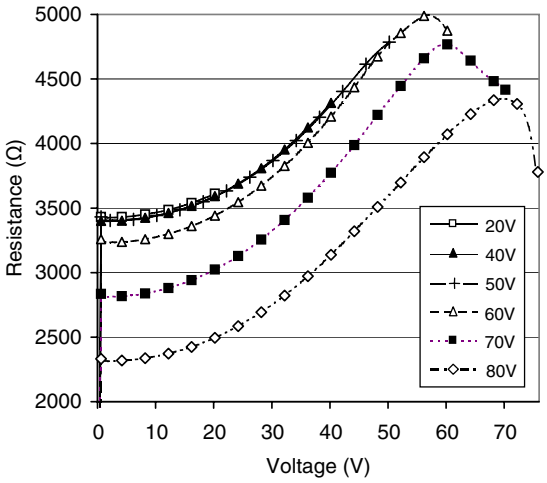

Figure 4.11 Measured voltage-resistance behaviour of the U-beam actuator at successive linear voltage ramps from 0 V to increasing end values up to 80 V

decrease when proceeding to higher voltages. This is a known behaviour for semiconductor materials, which is caused by an increase of the intrinsic carrier concentration with temperature (Chui *et al.* 1999). At increasing temperatures, more and more electrons are excited into the conduction band of the silicon. At a certain temperature, denoted as the intrinsic temperature T_{int}, the intrinsic carrier concentration increases to such an extent that it exceeds the external doping concentration, leading to a decrease in electrical resistivity[1], which in turn allows more current to flow. This generates more resistive heating, leading to a further drop in resistance. This positive feedback cycle may cause instability in case of voltage control in which the temperature of the heater region suddenly rises in an uncontrolled manner, also referred to as thermal runaway, eventually leading to abrupt failure of the device.

For the following linear voltage ramp even a further decrease of resistance was observed, indicating progressing change of the actuator structure. It could be seen that the top of the resistance curve had decreased to approximately the end resistance level of the previous curve. When attempting to increase the voltage in the subsequent cycle to 80 V, the resistance level indeed ultimately dropped very rapidly, accompanied by an uncontrolled

[1] Note: the maximum resistance in the actuator is dependent on the temperature profile, determined by the geometry, and may therefore not occur precisely at the intrinsic temperature. Furthermore, the intrinsic temperature is higher at higher dopant concentrations.

current increase, followed by a safety stop of the measurement equipment at approximately 75 V. Just before reaching this value the actuation structure started emitting visible light at the thin arm, where the temperature reached the highest level. After this test, although the current path had been damaged significantly, it was not interrupted and the mechanical integrity of the overall structure was still intact.

Changes in room temperature resistance of doped polysilicon heater elements after high-temperature loading were also reported by Ehmann *et al.* (2002) and Chu *et al.* (2006). However, this phenomenon is not yet fully understood. It was found to be strongly depending on cooling rate, and it was even shown to be possible to reversibly switch between different room temperature resistances by applying appropriate cooling rates (Ehmann *et al.* 2002). Slow cooling enabled the polysilicon to relax to a low temperature state with higher resistance, whereas at fast cooling the lower resistance value seemed to be frozen. Though the exact cause was unclear, this was suggested to be related to a redistribution of doping atoms between grains and grain boundaries at high temperatures.

Many more temperature-dependent effects were shown to occur, such as polysilicon recrystallization above approximately 870 K and plastic deformation above ~ 930 K (Deladi *et al.* 2004). However, it was proven possible to operate the devices above 870 K for more than six hours without failure (Ehmann *et al.* 2001). Although the changes were not inherently detrimental - in many cases the actuator performance was improved over time (Chu *et al.* 2006) - this was not investigated further, and temperatures above this value were avoided for safety. For the V-beam structure similar behaviour was found, and a maximum voltage for both actuation structures for the remaining tests was set to 45 V.

Deflection measurements were performed both without fibre, and with a fibre fixed respectively at 2000 μm and 3000 μm from the actuator tip. In Figure 4.12(a) and Figure 4.12(b) the deflection behaviour is shown of the U-beam as function of applied voltage and of dissipated power, respectively. In Figure 4.13(a) and Figure 4.13(b) the same is shown for the V-beam actuator. The deflection measurements were performed by means of software recognition using the in-plane measurement functionality of a Polytec MSA-400 laser Doppler vibrometer (Polytec 2008, see also Appendix D), and were estimated to be approximately 50 nm accurate. For the U-beam actuator, a significant difference in deflection with and without fibre was present, and also with the fibre at different cantilever lengths. This can be attributed to the comparable stiffness of the U-beam actuator and the fibre. At 2000 μm cantilever length the fibre stiffness was close to the actuator stiffness, whereas at 3000 μm length the fibre stiffness was only around one third of this value. Theoretically, the power-deflection behaviour was

expected to be linear (Hickey *et al.* 2003), but due to the considerable increase in electrical resistance with increasing temperatures, the deviation from linear was significant.

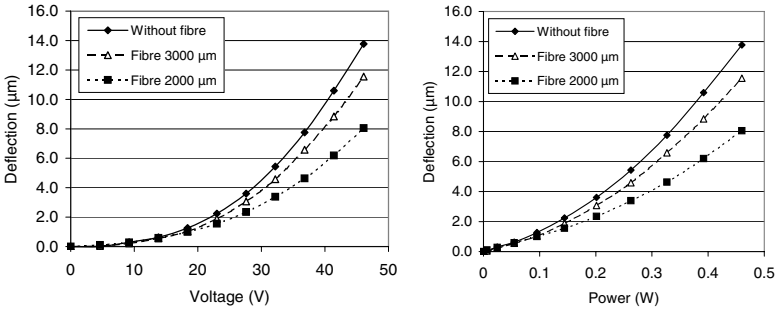

(a) (b)

Figure 4.12 Deflection curve U-beam actuator as function of voltage (a), and power (b), with and without fibre loading at two different cantilever lengths

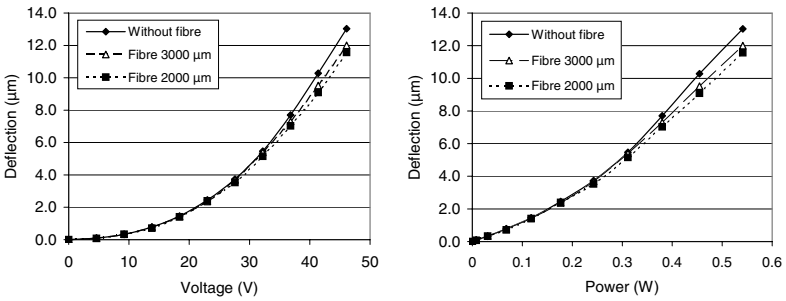

(a) (b)

Figure 4.13 Deflection curve V-beam actuator as function of voltage (a), and power (b), with and without fibre loading at two different cantilever lengths

The V-beam actuator had a considerably higher stiffness than the U-beam actuator, and therefore the decrease in deflection due to the fibre loading was much smaller. Although the achievable deflection without fibre was lower for the V-beam than for the U-beam actuator, when the fibre was cantilevered at 3000 µm the deflection was comparable, and at 2000 µm the situation was reversed.

Finally, also using the Polytec laser vibrometer system the dynamic step responses of both the U- and V-beam actuators were measured, again without and with fibre loading at 2000 µm and 3000 µm cantilever lengths. These are shown in Figure 4.14(a) and Figure 4.14(b) respectively. At time

$t = 0$ s a voltage step signal of 45 V was applied to the actuation structure, after which the time-deflection behaviour was recorded. Both the U-beam and the V-beam actuator were tested twice on different devices without fibre. As can be seen from the plotted graphs the results closely matched each other, indicating that the behaviour is reproducible.

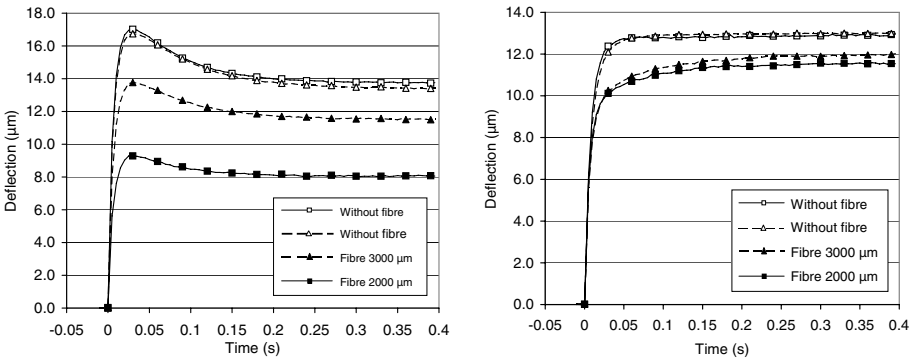

(a) (b)

Figure 4.14 Step response U-beam (a) and V-beam structure (b) with and without fibre loading (both tests were performed twice without fibre)

For the U-beam actuator a significant overshoot was observed, which decreased at increasing fibre load. The V-beam on the contrary exhibited no overshoot, but instead a gradual movement to its end position. Including fibre load, the V-beam actuator was slower in reaching its end position, due to the significant thermal influence of the fibre onto the actuator. The contact between actuator and fibre was at the hottest actuator location, therefore initially a large temperature difference was present between actuator and fibre. The slower transient behaviour can be explained by the lower thermal diffusivity α of glass compared to silicon. The thermal diffusivity of a material is a parameter that provides an indication of its ability to adjust its temperature to that of its surroundings, and it is calculated by taking the ratio of thermal conductivity k to volumetric heat capacity ρC_p of the material. Glass has approximately a 20 times lower thermal diffusivity than silicon, therefore the combined actuator-fibre system is much slower in reaching its steady-state situation than the actuator alone. For the U-beam actuator the presence of the fibre had less effect on its transient behaviour, because the actuator temperature at the fibre-actuator contact area was significantly lower than for the V-beam actuator.

For both actuators after approximately 0.3 s the end position was reached to within ± 0.1 µm. Also shown is the cooling down behaviour, which, perhaps against intuition, was found to be even faster than the heating behaviour;

typically within 0.2 s cooling down is achieved with a position stability of better than ± 0.1 μm (see Figure 4.15).

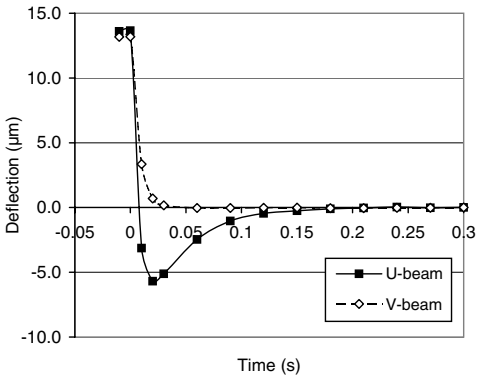

Figure 4.15 Cooling step response U- and V-beam structures

The experimental results were in acceptable agreement with the modelled values. Overall, the deflections were lower than originally modelled, which may be due to the increased electrical resistivity of the heater elements at elevated temperatures and to the fact that convection, radiation and conduction through air were not included in the models. The exact peak temperatures in the U- and V-beam actuators could not be determined, because no equipment was available for this. Since the power levels during the experiments were lower than calculated using the models, the maximum temperatures were also lower. Therefore, it was estimated that at 45 V the maximum temperatures during the experiments have remained below 600°C.

The uniform deformation of the overall beam structure without observable torsion or out-of-plane curling indicates that the temperature gradient over the vertical cross section of the actuators is indeed relatively small and may be neglected, as was predicted.

4.5 Discussion

From the overview presented in Section 4.1, it may be concluded that the most promising MST-based actuation principles for internal fine part positioning are electrostatic and electrothermal actuation, based on their simple construction requiring no special materials, and their relatively large design flexibility. Nevertheless, in general both the attainable number of degrees of freedom that can be actively controlled as well as the attainable actuation ranges using MST-based functionality are rather limited; for example

achieving useful actuation in more than two degrees of freedom with translations of over 10 μm is considered very challenging.

For the fibre alignment case electrothermal actuation was selected, since this principle is able to provide the high work loads required for this application. In-plane U-beam and V-beam thermal actuators were fabricated and tested in order to obtain improved insight into the capabilities of these actuator types. Using 1800 μm long U- and V-beam thermal actuators, free end effecter displacements of around 13-14 μm were achieved at a voltage level of 45 V. When including a fibre the displacements reduced to 11-12 μm, except for the U-beam at 2000 μm cantilever length, for which the deflection decreased to 8 μm. The power consumption for these deflections was approximately 0.45-0.55 W, with a typical heating time of around 0.3 s. The attained travel ranges and position stability are promising for the fibre-chip coupling application, and also the control of the actuators can be acceptably fast. The V-beam is considered the most attractive actuation structure of the two, based on its high stiffness, resulting in smaller displacement reductions at comparable loads. It occupies less area than an equivalent U-beam actuator, particularly for applications requiring relatively high actuation forces. Additionally, V-beam actuators can be placed in parallel to increase output force with no coupling penalty, whereas for U-beams placed in an array, the connecting beams reduce the achievable displacement by consuming much of the energy in bending them (Sinclair 2000).

Using the insights gained in this chapter, the PIAF design is continued in Chapter 5 by first studying the coarse assembly process that should precede the final fine positioning of the fibre. This results in sharper requirements on the fine positioning ranges in x and y, which are then used as inputs for the development of the 2-D fibre fine positioning concept presented in Chapter 6. Electrothermal actuation will be used for this concept, as determined in the present chapter.

5
Coarse assembly process

In this chapter a design is proposed for the coarse assembly process that should precede the final fine positioning of the fibre. This design is validated on the basis of a tolerance analysis using data from literature. Based on a realistic estimation of the tolerance stack between laser output window and fibre core in the directions perpendicular to the fibre axis, the minimum actuation ranges for the internal positioning functionality in these directions are determined. These will function as improved requirements for the continued 2-D fibre positioning concept development, presented in Chapter 6.

An advantageous method to achieve the high required coarse assembly accuracy is using accurately defined features in the parts to be mated. Available methods to achieve accurate part positioning are discussed in Section 5.1. Following, the proposed coarse assembly design of the crucial components in the laser diode device is discussed in Section 5.2, whenever possible aided by MST-based alignment features to reduce the coarse placement accuracy requirements. Finally, a detailed analysis of the tolerance build up between the optical components is presented in Section 5.3.

5.1 Methods for achieving position accuracy

The purpose of the so-called 'coarse' assembly process is to place the part 'roughly' within the actuation ranges for the degrees of freedom that are subsequently fine positioned, and to obtain sufficient positioning accuracy in the remaining directions. Since the overall assembly cost should be com-

petitive with conventional assembly methods, attention should be paid to the related additional cost.

Generally, the lower the required positioning accuracies, the faster and less expensive the assembly steps can be. For example, for assembling optoelectronic components at ± 1 μm placement accuracy, generally specialized machines are required having typical throughputs in the range of 30 to 100 placements per hour (Schwab *et al.* 2004). In contrast, commercially available pick-and-place machines are quite routinely able to place thousands of components per hour at 20 μm in-plane positioning accuracies at relatively low cost.

To avoid time consuming and costly coarse assembly steps, the internal assembly functionality would ideally take care of fine positioning in all critical directions, allowing the coarse assembly to be very straightforward and cheap to accomplish. However, as we have seen in the previous chapter the attainable number of degrees of freedom that can be actively controlled using MST-based functionality is rather limited. Based on these results, achieving useful actuation in more than two degrees of freedom is expected to be very challenging. This means that in cases needing accurate positioning in more than two degrees of freedom, in one or more of these directions this accuracy needs to be achieved by external assembly functionality, which increases cost.

To prevent this situation, an attractive alternative solution for achieving the required coarse assembly accuracy is using accurately defined features in the parts to be mated. This is schematically depicted in Figure 5.1, showing basic alternatives for achieving positioning accuracy.

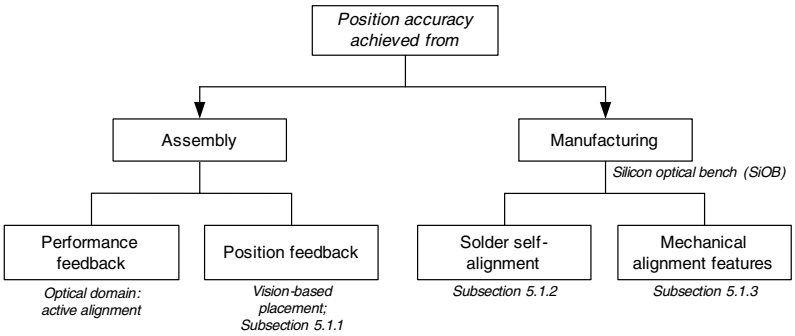

Figure 5.1 Alternative possibilities for achieving part positioning accuracy

As shown in the overview, the two main methods of achieving position accuracy from assembly are by *performance feedback* and by *position feedback*. The earlier discussed active alignment is a common example of

employing performance feedback for optical applications. It is not considered in this chapter, since it is a very expensive solution, and thus not regarded fit for coarse assembly in combination with PIAF. The most commonly used method of using position feedback is by means of vision. This method applied to laser diode placement is briefly discussed in Subsection 5.1.1.

Besides achieving the part position accuracy from the assembly by means of performance or position feedback, there are two main methods relying on manufactured features in the parts to be mated:

- the use of solder self-alignment;
- the use of mechanical alignment features.

Using these methods, it is possible to obtain a self-positioning effect of the parts, which would allow the use of simple pick-and-place functionality at much lower cost. The fact that MST-based fabrication was chosen for the positioning actuators is very attractive in this respect, since it pre-eminently allows for fabricating this type of very accurate features by means of photolithography.

In literature, many examples are available of the use of lithographically fabricated features in silicon to aid in the accurate positioning of parts. The silicon base part in these examples is usually referred to as *silicon optical bench* (SiOB) or *silicon waferboard*. Generally, the purpose is to develop low-cost optoelectronic devices by replacing active alignment by passive alignment, by means of mounting all components on an accurately microstructured silicon carrier (Mickelson *et al.* 1997). By careful design and combining techniques, relative positioning accuracies in the μm range have been shown. This is sufficient for low-cost optoelectronic devices, and is also promising for the coarse assembly of the components in the case investigated in this project. Seen in this view, the PIAF concept could be regarded as an extension to the silicon optical bench approach, in which additionally active assembly functionality is integrated with the product for enhanced positioning accuracy in selected degrees of freedom. Solder self-alignment and the use of mechanical alignment features are discussed based on examples from literature in Subsections 5.1.2 and 5.1.3, respectively.

5.1.1 Vision-based placement

Examples of accurate laser diode assembly using vision-based positioning are given by Cohen *et al.* (1991), Kurata *et al.* (1996), Yamauchi *et al.* (2000), Owen (2000), Breedis (2001), Goodrich (2001), Dautartas *et al.* (2002), and Rho and Lim (2007). In this method, alignment marks - also called *fiducials* - are patterned on the laser diode (LD) and on the silicon surface by means

of photolithography. The LD is positioned by detecting each alignment mark, and subsequently attached using solder. This method is also commonly referred to as *index alignment*.

Commercial systems are nowadays available that can perform component placement with sub-μm post-bonding accuracy, *e.g.* the TRIAD 05 AP flip-chip bonder by the French company S.E.T.[1] can obtain a ± 0.5 μm post-bond accuracy in all three orthogonal directions (3 sigma) and achieve a maximum throughput of up to 200 units per hour, see also Rho and Lim (2007). Similar post-bonding accuracies were also presented by Kurata *et al.* (1996) and Dautartas *et al.* (2002). Alternatively, instead of purposely made fiducials, Nakagawa *et al.* (1998) used already present features on the LD and the silicon optical bench for the alignment. For the LD chip, the mesa structure at the active laser region and the front edge of the chip were used. The measured in-plane positioning accuracy was better than 1 μm and the rotation around the vertical axis was within 0.4°.

5.1.2 Solder self-alignment

The self-centring effect in solder bonding for optoelectronic component alignment was first used by Wale and Edge (1990). They used eutectic lead-tin (PbSn) solder bumps for self-aligning an integrated optical device chip to single mode optical fibres on a silicon V-groove array, thereby allowing for a lower initial placement accuracy. A self-alignment accuracy of approximately 1 μm was reported.

An early overview of solder self-alignment examples in literature was provided by Tan and Lee (1996). In general, these examples showed self-alignment accuracies of better than 2 μm, both with and without use of mechanical stops or spacers, also called *pedestals* and *standoffs*, respectively. The self-alignment effect is based on the surface tension of molten solder, as is shown in Figure 5.2.

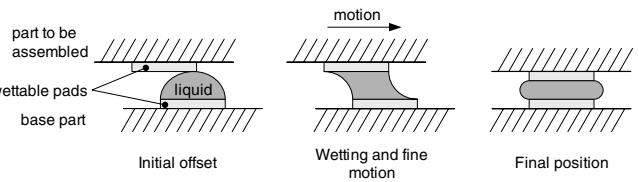

Figure 5.2 Self-alignment based on surface tension

[1] Previously manufactured by SUSS MicroTec, but since 2007 by S.E.T. SAS (2008).

The in-plane restoring force, which is responsible for final alignment, becomes vanishingly small at the final stages of alignment, practically limiting the attainable alignment accuracy using this method. Efforts were made to overcome this by aid of mechanical alignment features, *e.g.* by Jackson *et al.* (1992), which also allowed less precise solder volume control. An increased restoring force was obtained by deliberately offsetting the solder pads of the chip with respect to the substrate to ensure contact between the aligning surfaces. Using mechanical alignment structures defined in an already present layer in which optical waveguides were created (see Figure 5.3), alignment of better than 2 μm after an initial misalignment of 25 μm was reported.

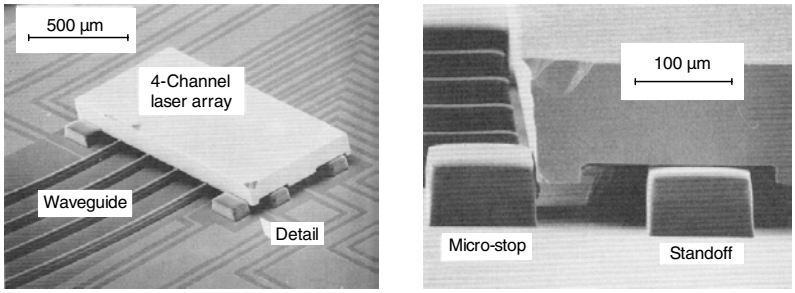

(a) (b)

Figure 5.3 Flip-chip solder bump attachment for a four-channel laser array using solder self-alignment combined with mechanical alignment features; (a) overview image, and (b) close up of corner (Jackson *et al.* 1992)

A general challenge of using mechanical alignment features is formed by the interfacial frictional forces that must be overcome. The restoring forces must be large enough to move the component to the final position once the stops make first contact. More recently, concepts using this approach were also presented by Rehm *et al.* (2000) and Hutter *et al.* (2004), the first of which reported an achieved 1.4 μm final offset between laser and fibre after placement of the laser chip with an initial tolerance of approximately 10 μm. Hutter *et al.* clearly showed that the alignment features between the components were in direct contact, indicating that the achievable alignment accuracy was solely determined by the fabrication accuracy of the components. Both used eutectic gold-tin (AuSn) as the solder material, which is the solder material of choice for laser diodes and other optical chips requiring accurate alignment. Its high stability and - unlike most other solder materials - absence of creep behaviour make it the preferred choice. In addition, soldering can be fluxless, which is beneficial, because the use of liquid flux may contaminate the optically active surface by organic residue.

Another approach for improved in-plane positioning accuracy using solder self-assembly was presented by Humpston (1997). In this method, pairs of wettable metal pads were deliberately misaligned so that the equilibrium position was a balance of opposing forces. Using this approach, in-plane alignment accuracies of better than ± 0.25 μm could be achieved. However no additional literature was found to support this claim.

As mentioned before, a small solder height is desired to achieve small bump height variations. However, according to Sasaki *et al.* (2001), to achieve good self-alignment with spherical bumps, the aspect ratio of bond height over pad diameter of a solder bump should be above a lower limit, which was found to be around 0.75 for AuSn. To reduce the bump height, smaller bumps should be formed, thus increasing the required initial chip placement accuracy. To overcome these difficulties, they presented a solution with stripe-type solder bumps capable of achieving ± 1 μm bonding accuracy in both in- and out-of-plane directions, see Itoh *et al.* (1996) and Sasaki *et al.* (2001). These solder bumps were created by means of punching preforms from AuSn ribbon and directly pressing them onto stripe-shaped pads on the substrate, and subsequently melting to reflow the solder. The stripes were oriented orthogonally with respect to each other, each set working in a perpendicular direction (laterally with respect to the stripe length). The best results were obtained with stripe-type solder bumps of 25 μm wide × 140 μm long × 18 μm high, which were shown to self-align with maximum initial misalignments of up to ± 20 μm at a high reliability. This approach was tested for various chip sizes, and according to modelling results presented in Sasaki *et al.* (2001), the heat resistance had increased somewhat compared to a full film solder layer between optical chip and substrate. However, this increase was considered acceptable for low-power optical transmitters with continuous heat generation in the order of 20 mW. Similar results were presented by Lindgren *et al.* (1997), who reported an estimated achievable misalignment of ± 1 μm in the plane perpendicular to the fibre axis with an initial laser chip positioning inaccuracy of approximately ± 20 μm.

5.1.3 Mechanical alignment features

Instead of being used in combination with index alignment or solder self-alignment, mechanical alignment features can also be used as stand-alone technique to aid the assembly equipment in achieving accurate positioning of parts. This approach was already used in 1986 for the accurate positioning of a waveguide chip to a single mode fibre array by help of reactive ion etched alignment ribs and silicon V-grooves by Kaufmann *et al.* (1986). The two most common methods of using MST-based mechanical alignment features are by stops in the form of ridges or pedestals, and by anisotropi-

cally wet etched cavities such as the well-known fibre V-grooves, see Figure 5.4.

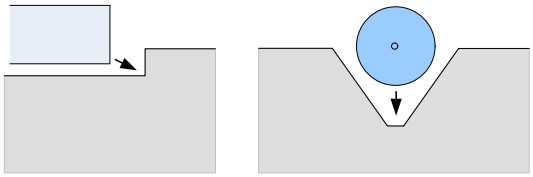

Figure 5.4 Two common approaches of using MST-based mechanical alignment features: (a) moving a planar component against a vertical shallow ridge; (b) inserting a component into an anisotropically wet etched cavity

Ridges and pedestals are usually relatively shallow and are therefore mostly used for planar components having flat surfaces with sharp edges. Examples are shown by Armiento *et al.* (1992) and Boudreau *et al.* (1998), who both used pedestals and standoffs to define the position of a laser bar during robotic placement. The mechanical micro features were etched with a tolerance of less than 0.5 μm, permitting the placement of the laser array to an accuracy of ± 1 μm, of course similar to the position accuracies observed for the combined use of solder self-alignment and mechanical alignment features. Armiento *et al.* reported an applied force of 10 mN to ensure that the laser was brought in contact with the alignment pedestals and held in contact during the solder reflow process. According to Boudreau *et al.* the whole processing cycle, including pick up, alignment and die bonding was performed within 15 s, which they claimed to be much faster than typically achieved using expensive vision-system piezo-electric based bonders. More recent papers, *e.g.* by Mitze *et al.* (2006), reported similar results.

Besides the well-known V-grooves for positioning optical fibres, the use of anisotropically wet etched cavities has also been shown for ball lenses, *e.g.* by Huang *et al.* (1998), and LDs. In Hunziker *et al.* (1995) a laser array is aligned to KOH etched side walls on the silicon substrate by means of vertical alignment trenches in the laser that are accurately defined with respect to the active laser area. The guidance by the silicon side walls during the insertion results in a self-positioning effect. The V-grooves for the fibre were defined in the same step, allowing for larger tolerances in the sidewall fabrication, since process-related variations have effect on both the vertical laser and fibre positions, causing - within limits - the optical alignment to be maintained. In their approach, the initial misalignment tolerance for the placement tool was relaxed to approximately 10 μm.

In Choi *et al.* (1999), similar anisotropically etched silicon sidewalls were used on the substrate for the laser and fibre positioning. Only in this case, instead of using etched vertical trenches inside the laser chip, the outer edges were used for aligning the chip, which were accurately defined using anisotropic wet etching (see Figure 5.5). Conventionally, side-emitting laser die are cleaved at the front and rear faces along crystallographic planes to obtain optically smooth surfaces, and along the sides they are generally separated by means of dicing. Normally, the locations of these cleaved and diced faces are only controlled in the range of several microns. Therefore, Choi *et al.* lithographically etched small grooves along all sides of the chips to ensure breaking to occur at these specified locations. In this way, the size of the laser diode chips and the distance between the sides of the chip to the active region could be controlled to ± 0.5 μm. The overall alignment accuracy from laser to fibre was estimated to be ± 3 μm based on output measurements.

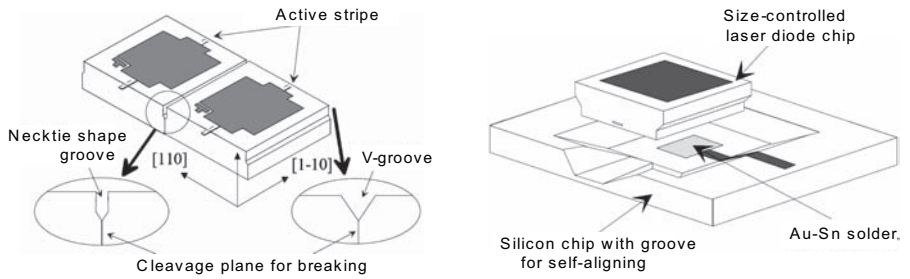

Figure 5.5 Self-alignment of size-controlled LD in cavity of silicon base part: (a) bottom view of two laser die before cleaving; (b) LD and Si base part prior to positioning (Choi *et al.* 1999)

The anisotropic cavity width can be controlled to within ± 0.5 μm if the etch mask is carefully aligned to the in-plane crystallographic orientation of the silicon substrate. The wafer flat, which indicates the crystallographic orientation, is typically specified to a tolerance of ± 0.5°, which, if taken as reference, could result in larger cavity width variations in the range of ± 1 μm. By testing each wafer individually, the actual crystal orientation can be determined to better than ± 0.2°, which upon proper alignment results in a width variation within ± 0.5 μm (Goodrich 2001). As can be understood, mask undercut resulting from a misalignment between etch mask and crystallographic orientation mainly contributes to a misalignment in the vertical direction (Breedis 2001).

A general disadvantage of the use of mechanical alignment features is their added fabrication cost and complexity. Fibre V-grooves are easily fabricated and commonly used, but for example trenches in the silicon substrate for laser chips may require patterning of metallization layers on the bottom and side walls for solder bonding and electrical connections. This typically involves non-standard processing steps that should be carefully fitted into the processing sequence.

5.2 Proposed coarse assembly design fibre-chip coupling case

In this section, a coarse assembly design is proposed for the important components of the fibre coupling case considered in this investigation, whenever possible aided by MST-based alignment features to reduce the initial coarse placement accuracy requirements, aiming to decrease the coarse assembly cost.

First, in Subsections 5.2.1 and 5.2.2, supplementary information is provided on relevant issues concerning the laser diode and fibre assembly, after which the actual proposed coarse assembly design is presented in Subsection 5.2.3.

5.2.1 Additional measures for improved laser diode alignment

The placement accuracy of the die on the silicon substrate is only one of the aspects contributing to the position tolerance of the active laser region with respect to the fibre core. Therefore, a number of additional issues need to be taken into account for improved alignment of the laser diode.

Preventing mask overlay errors If the alignment marks are defined in different layers than the structures that must be aligned, mask overlay errors can result in inaccuracies in the range of 0.5 μm. Therefore, if possible, the fiducials on the LD are created in the same mask as the active laser region, and on the silicon submount in the same mask as for defining the fibre groove, see *e.g.* Goodrich (2001).

Distance control between output window and fibre tip As mentioned, the LD front facet is usually created by mechanical cleaving, resulting in tolerances on the distance in z-direction between the cleaved front facet and the fiducials on the LD up to approximately 10 μm. In case the fibre end is placed at a fixed location, for example against a mechanical stop, and the distance between laser output window and fibre should be controlled, then

this variability may be compensated by measuring and shifting the LD over this distance, such as shown by Yamauchi *et al.* (2000). Alternatively, the fibre end face position could be altered to compensate for this variability.

Solder height and output window position control For *vertical* control of the output window position, two main parameters are important: solder height and output window position inside the laser die. As indicated by Dautartas *et al.* (2002), the thickness of the solder is difficult to control very precisely - typically the thickness variation is 5-10% of the total metal thickness, which could add up to 0.8 μm for a common layer thickness of 8 μm. This inaccuracy may be reduced by using the die bonder to hold the chip at the desired height during solidification of the solder (*e.g.* Kurata *et al.* 1996). An alternative option is shown by Dautartas *et al.*, in which the solder metallization is deposited in a specially made recess, which is smaller than the laser, such that the laser die makes direct contact with the silicon surface during bonding. This approach is similar to the fabrication of standoffs to control the vertical position of the laser, as discussed in Subsection 5.1.3, only with the benefit that this method does not introduce additional vertical tolerances due to fabrication of the alignment features.

The active area of the laser is generally located a few microns from the LD top surface. In most cases the laser die is placed upside down (commonly referred to as *active side down*, *junction down*, or *epi-down*), because the tolerance in vertical direction from the top surface can be controlled to sub-μm level, in contrast to the distance from the bottom, since the chip thickness usually is not precisely controlled during manufacture. An exception is shown by Owen (2000), who placed the laser epi-up for improved thermal performance. In this approach, the LD fiducials were observed from the top in the same focal plane as the alignment marks on the silicon, and the vertical LD position was measured using an interferometer and corrected during bonding. Using this approach, an average alignment error of 0.2 μm was obtained, with a standard deviation of 1.0 μm.

5.2.2 Fibre fixation inside a V-groove

The fibre is usually fixed inside a V-groove by means of adhesive[1] (*e.g.* Joo *et al.* 2000, Lo *et al.* 2004, Priyadarshi *et al.* 2006), and sometimes by solder (*e.g.* Rassaian and Beranek 1999, Beranek *et al.* 2000, Ou *et al.* 2004), but mechanical clamping is also shown (Strandman and Bäcklund 1997, Bostock *et al.* 1998).

[1] As mentioned in Chapter 3, many practitioners do not allow adhesives or any other kind of organics inside a hermetic package, but this is most likely too strict in many cases. If applied at sufficient distance, properly selected low-outgassing adhesives may be used without contaminating the laser facets.

In most papers dealing with V-grooves for fibre alignment, no or very little attention is paid to the adhesive or solder attachment of the fibre inside the V-groove and possible position variations resulting from this. Generally, it is assumed that *e.g.* for adhesive joining, the fibre remains in contact with the V-groove walls. This can indeed be achieved by applying high pressure throughout the curing process. Another approach was shown by Lo *et al.* 2004, who used low-viscosity epoxy dispensed in a reservoir connected to the fibre V-groove. The epoxy filled the V-groove below the fibre due to the capillary effect and was able to pull the fibre in place, similar to the solder self-alignment in combination with mechanical stops as discussed in the previous subsection. However, as with solder, the stresses in the adhesive material and in the component interfaces increase with a decreasing spacing between fibre and substrate, potentially resulting in delamination and cracks (Rassaian and Beranek 1999, Priyadarshi *et al.* 2006). Typically, due to the fixation of the fibre inside the V-groove, an additional position tolerance of around 0.5 μm in the directions perpendicular to the fibre axis can be expected when it is not checked whether the fibre makes direct contact with both V-groove surfaces.

For solder attachment, the fibre and the V-groove need to be metallised, which makes it more costly than adhesive joining, so usually it is only applied when high bond strength and stability are extremely important. The rather exotic option of mechanically clamping or pressing the fibre into the groove renders the connection adjustable, which could potentially be attractive for the PIAF concept. In the fibre-chip coupling case, for example, the fine positioning step may perhaps benefit from a fibre that can slide in axial direction during fine alignment. A disadvantage however, is the added complexity and cost of the extra process steps required for creating the clamps, as for the previously mentioned use of mechanical alignment features in general.

5.2.3 Coarse assembly design fibre coupling case

Based on the above information obtained from literature, a design was proposed for the coarse assembly procedure of the crucial components in the laser diode device that should precede the final fibre fine positioning. As starting point, the preliminary overall configuration with a separate silicon optical base part and positioning chip was taken that was defined in Chapter 3, shown in Figure 5.6. As much as possible, the assembly procedure was aided by MST-based alignment features to reduce the initial coarse placement accuracy requirements.

So far no final choice was made between an in-plane configuration, as shown in Figure 5.6, and a through-plane build up, consisting of an

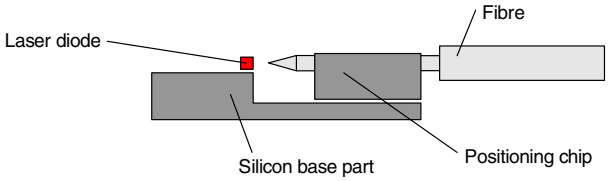

Figure 5.6 Selected schematic LD-fibre configuration including two silicon parts between LD and fibre (repetition of Figure 3.7)

arrangement in which the fibre would protrude through the positioning chip, which in turn would be placed orthogonal to the laser diode. This latter option has the advantage of simpler actuator creation, since it only requires in-plane actuators for positioning the fibre tip in the plane perpendicular to its optical axis[1]. However, this configuration was not considered for further investigation, due to its more complicated assembly and its lower potential for achieving an acceptably small tolerance build up, requiring the fine positioning travel ranges to be very large. Moreover, a planar build up remains closest to the conventional build up, which is also preferred.

The following coarse assembly design was proposed. Solder self-alignment without additional mechanical alignment features was selected both for the LD and for the positioning chip assembly on the silicon base part. This way, relatively inaccurate placement using standard pick-and-place equipment was allowed, while still achieving relatively low in- and out-of-plane tolerances of ± 1 μm. The LD was proposed to be assembled active side down in order to accurately locate the emitting region in the vertical direction, and AuSn was selected as solder material for both chips, which could be reflown simultaneously without the use of flux to prevent deposition of organic material on the laser facets. Addition of the metallisation layers on the silicon parts for solder attachment is relatively straightforward and is not expected to give problems in combination with other anticipated processing steps.

A V-groove was selected for the fibre placement, since this is the easiest and most commonly applied way of accurate definition of the fibre position and orientation. Although individual wafer alignment for improved V-groove control is a possibility, it was assumed that orienting the wafer using its primary flat would be sufficient, delivering a ± 1 μm tolerance in vertical direction. The fibre was proposed to be fixed using UV curing adhesive inside the V-groove.

[1] One particular 2-D through-plane concept was developed in the same process run as the first V-beam and U-beam actuators presented in Chapter 4. See Appendix C for additional details and some brief test results.

Based on its specific geometric characteristics, it was possible to constrain the position of the optical fibre in only four degrees of freedom (x, y, θ_x and θ_y). The lensed fibre tip was not allowed to touch the LD or any other component to prevent it - and the output facet of the LD - from damaging. Practically, it is very difficult to create high accuracy alignment features in any other part of the fibre. For example, tolerances on the fabrication of the tapered section around the fibre tip generally are so large that mechanical stops cannot be used for achieving the desired positioning accuracy in the longitudinal direction.

Therefore, unfortunately, for achieving the ± 0.5 μm positioning accuracy in z-direction of the fibre tip relative to the laser diode facet, still an accurate positioning step was required, assisted by visual feedback. After this final coarse assembly step, the alignment of the fibre tip in x and y-direction could be performed actively using the product-internal positioning functionality.

5.3 Tolerance analysis

In this section, the tolerance stacks in all six individual degrees of freedom between laser output window and fibre core are discussed. As is clear from the previous section, the z-direction did not have to be included in the tolerance analysis since the final accuracy in this direction is achieved by positioning the fibre tip directly relative to the laser diode facet. All values stated are indicative. They are mostly based on results obtained from literature, and as such actual values may differ. They are intended to give a good estimate of the tolerance stack in order to be able to determine realistic travel requirements for the fine positioning functionality in x and y.

For the tolerance stack calculation, a worst case approximation was taken to ensure that under all circumstances the fine positioning functionality would have sufficient actuation range. The total tolerance build up was calculated by summation of all tolerances of the relevant part dimensions and intermediate bond inaccuracies from laser facet to fibre core. This is the most conservative approach[1], giving the largest tolerance range. Worst case

[1] In literature, the overall tolerance chain is sometimes also calculated using the so-called *root sum of squares* (RSS) method, in which the *chance* that certain independent contributions to the overall tolerance have a given value and are of the same sign is taken into consideration. This is calculated by first squaring the errors, then adding them together, and finally taking the square root of the sum, hence its name. This method results in smaller tolerance ranges than the worst case method. Examples of its application for tolerance analysis in optoelectronic packaging can be found in Kurata *et al.* (1996), Dautartas *et al.* (2002), and Schwab *et al.* (2004).

analysis is generally appropriate when typical, rather than guaranteed values, are known, so when detailed information about the values of the individual contributions is not available.

Tolerance in *x*-direction

The overall tolerance stacks in both *x* and *y* were calculated by combining all tolerances of the relevant part dimensions and intermediate bond inaccuracies from laser facet to fibre core. Schematically, all relations contributing to the overall tolerance build up between LD facet and fibre tip in *x* and *y* are shown in Figure 5.7.

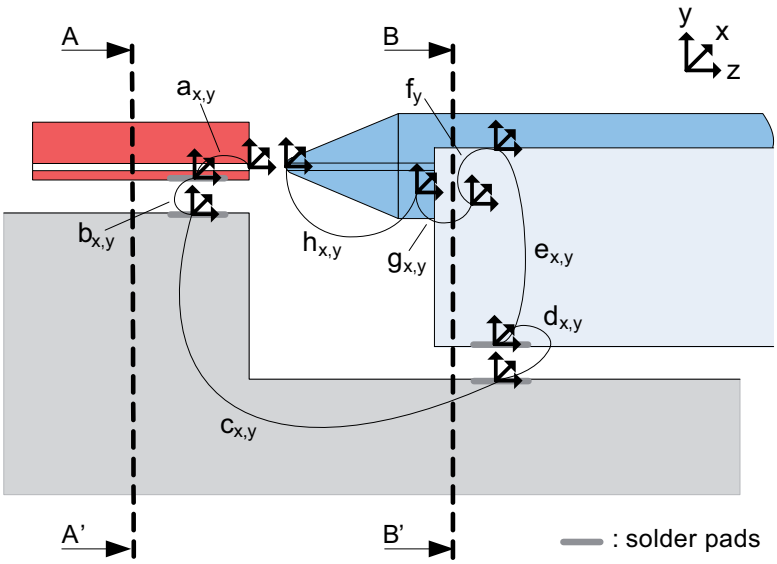

(a)

Figure 5.7 Schematic overview of all relations contributing to the overall tolerance build up between LD facet and fibre tip in *x* and *y*; (a) side view, and (b) cross sections A-A' and B-B'

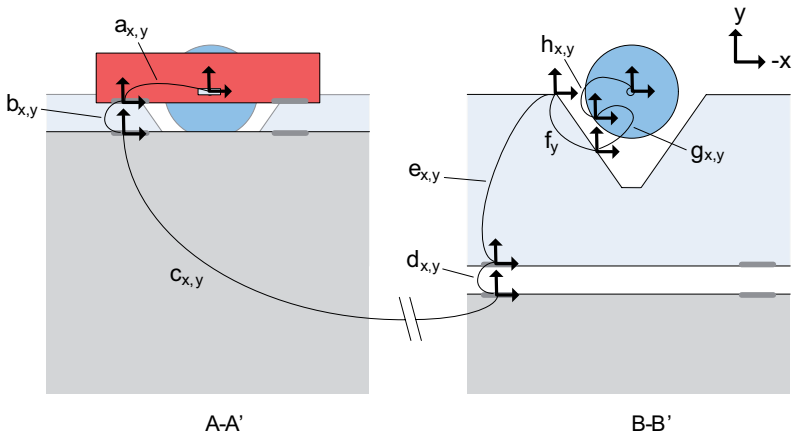

(b)

Figure 5.7 Schematic overview of all relations contributing to the overall tolerance build up between LD facet and fibre tip in *x* and *y*; (a) side view, and (b) cross sections A-A' and B-B' (continued)

For determining the tolerance stack in *x*-direction, it was assumed that, unlike for fiducials, as was shown by Goodrich (2001), the solder pads on the LD could not be defined in the same lithographic step as the active region. Therefore, an in-plane mask overlay tolerance of ± 0.5 µm was included (a_x). The opposite was assumed for the solder pads on the silicon base part at the bottom of the recess and on the top surface, for mounting the positioning chip and the LD, respectively (c_x). In this case however, due to the large height difference, a variation of ± 1 µm was assumed. For the positioning chip, back-to-front alignment was required for defining the V-groove at the front relative to the bond pads at the back (e_x), with an achievable tolerance of ± 1 µm (EV Group 2008a). V-groove width variations were only expected to contribute to vertical variations, so not to in-plane misalignments (f_x). The fibre core location could vary as much as ± 1.5 µm with respect to its cladding due to core-cladding eccentricity, cladding diameter variations and cladding ellipticity (h_x). An overview of all dimensional variations in *x*-direction is shown in Table 5.1.

The resulting overall *x*-direction tolerance build up was ± 6.5 µm, and therefore the travel requirement in *x* for the fine position functionality at least 13 µm.

Tolerance in *y*-direction

For determining the tolerance stack in *y*-direction, the depth variation of the recess in the silicon base to accommodate the positioning chip was estimated to be ± 1 µm, since it required a timed etch over a significant height

	Contributing aspect in *x*-direction	**Tolerance**
a_x	Active region LD position variation	± 0.5 µm
b_x	Solder self-alignment LD - silicon base part	± 1 µm
c_x	Solder pads silicon base part top surface - recess	± 1 µm
d_x	Solder self-alignment silicon base part - positioning chip	± 1 µm
e_x	Positioning chip back-to-front alignment	± 1 µm
f_x	V-groove position variation (not applicable)	-
g_x	Fibre attachment variation	± 0.5 µm
h_x	Fibre core variation	± 1.5 µm
	Overall *x*-direction tolerance	**± 6.5 µm**

Table 5.1 Dimensional tolerance build up from LD facet to fibre core in *x*-direction (the parameters in the first column refer to the same parameters in Figure 5.7)

(c_y). The out-of-plane misalignment due to V-groove height variation was also estimated to be ± 1 µm (f_y). An overview of all estimated dimensional variations contributing to the overall tolerance stack in the *y*-direction is listed in Table 5.2.

	Contributing aspect in *y*-direction	**Tolerance**
a_y	Active region LD height variation (mounted active side down)	± 0.5 µm
b_y	Solder thickness variation LD - silicon base part	± 1 µm
c_y	Recess silicon base part depth variation	± 1 µm
d_y	Solder thickness variation silicon base part - positioning chip	± 1 µm
e_y	Positioning chip thickness variation	± 2 µm
f_y	V-groove height variation	± 1 µm
g_y	Fibre attachment variation	± 0.5 µm
h_y	Fibre core variation	± 1.5 µm
	Overall *y*-direction tolerance	**± 8.5 µm**

Table 5.2 Dimensional tolerance build up from LD facet to fibre core in *y*-direction (the parameters in the first column refer to the same parameters in Figure 5.7)

The resulting estimated overall *y*-direction tolerance build up was ± 8.5 µm. As a consequence, the travel requirement in *y* for the fine position functionality was at least 17 µm, equal to the total distance between the outer tolerance bounds.

Combined, the required fine positioning ranges in *x* and *y*, including 0.5 µm margins, were set to 13.5 µm and 17.5 µm, respectively. These values were used as improved requirements for the continued development of the MST-based fine positioning functionality, which is discussed in the next chapter.

Rotation θ_x (pitch)

The allowed rotational tolerances around *x* and *y* were ± 1.5°, significantly smaller than around the *z*-axis, and therefore all contributing aspects to the overall rotational misalignment were carefully considered. The fibre was assumed as a single-side clamped beam with a cantilever length of 2000-3000 µm. With an estimated tip correction by the product-internal actuators of 15 µm in *x* and *y*, parasitic fibre tip rotations around the *y*- and *x*-axis on the order of 0.4-0.6° are induced, which were also taken into account in calculating the rotational tolerances in θ_x and θ_y. For a worst case estimation these were assumed to act in a single direction only.

Wafers are fabricated very accurately and their top and bottom surfaces are highly parallel. For example, typical total thickness variations (TTV) of 100 mm single side polished silicon wafers are below 10 µm (Silicon Valley Microelectronics 2008). Therefore, wedge angles due to chip thickness variations are negligibly small. The recess in the base part for the positioning chip could have some depth variation, but this was not expected to be more than perhaps one micron over a chip length of several mm, so this was also considered negligible. The same was concluded for the solder thickness variation below the positioning chip. However, in the case of the LD this had much more effect due to its smaller in-plane dimensions. For an estimated maximum solder thickness variation of 0.5 µm and a laser length of 300 µm, the angle variation was calculated to be ± 0.1°, resulting in a combined worst case estimation of the tolerance in θ_x from -0.7° to +0.1°, or vice versa, depending on the direction of actuation. The maximum allowed angle of ± 1.5° was not exceeded.

Rotation θ_y (yaw)

For in-plane rotations (θ_y), the main contributions were also the parasitic fibre tip rotation and the rotational LD misalignment. In this case the LD misalignment was at maximum ± 0.4°, because the solder bump misalign-

ment could reach up to 1 μm. With angles in θ_y from -1.0° to +0.4°, again the maximum angular tolerance was not exceeded.

Rotation θ_z (roll)

The allowed angular rotation in θ_z direction was infinite for circular and rotation symmetric fibres and ± 10° for non-rotational symmetric fibres. Fibre rotation in this direction could not be constrained by alignment features, but achieving this rotational accuracy using assembly equipment could quite easily be accomplished, and chip rotations as a result of variations in solder thickness could be neglected.

5.4 Discussion

In this chapter, methods have been presented to reduce the required initial placement accuracy for the assembly equipment, while still being able to achieve sufficiently accurate coarse positioning of the components to enable fine positioning with acceptably small positioning ranges. These methods rely on obtaining the required positioning accuracy from accurate MST-based alignment features in the parts to be mated that may be fabricated at relatively low cost, since MST is also planned for creating the product-internal assembly functionality.

Using this approach, a design was proposed for the coarse assembly procedure for the components in the optical chain from laser diode to optical fibre in the selected laser diode configuration. In this proposed coarse assembly design, it was possible to relax the initial coarse placement requirements in all necessary directions, except for the *z*-direction. In this the optical fibre could not be constrained at sufficient accuracy without risking to damage its tip or the LD facet. Therefore, in this direction still a relatively accurate positioning step was required, supported by visual feedback.

As can be understood, the preliminary decision to assume two discrete silicon components in the mechanical link between laser diode and optical fibre had significant influence on the overall tolerance build up, and indirectly also on the required actuation range for the fine positioning functionality. For reference, in Table 5.3 and Table 5.4 the reduced tolerance build ups in *x* and *y* are respectively shown in case the silicon base part and the positioning chip could be integrated into a single component.

Contributing aspect in *x*-direction	**Tolerance**
Solder self-alignment LD - positioning chip	± 1 μm
Fibre attachment variation	± 0.5 μm
Fibre core variation	± 1.5 μm
Reduced overall *x*-direction tolerance	**± 3 μm**
Calculated minimum *x*-direction fine positioning travel	**6.5 μm**

Table 5.3 Reduced dimensional tolerance build up in *x*-direction, based on integration of the silicon base part and the positioning chip into a single component

Contributing aspect in *y*-direction	**Tolerance**
Height variation active region LD (mounted active side down)	± 0.5 μm
Solder thickness variation LD - positioning chip	± 1 μm
V-groove height variation	± 1 μm
Fibre attachment variation	± 0.5 μm
Fibre core variation	± 1.5 μm
Reduced overall *y*-direction tolerance	**± 4.5 μm**
Calculated minimum *y*-direction fine positioning travel	**9.5 μm**

Table 5.4 Reduced dimensional tolerance build up in *y*-direction, based on integration of the silicon base part and the positioning chip into a single component

As can be seen, if this would be possible, a significant reduction of the required fine positioning range could be achieved, from 13.5 × 17.5 μm to 6.5 × 9.5 μm, which is almost half the travel. This would be very advantageous, since this would allow a considerably reduced chip size, and consequently significantly reduced manufacturing cost, which is strongly related to chip area. However, without additional information regarding the exact fabrication steps for the fine positioning functionality, assessing whether integration of the silicon base part and the positioning chip into a single component could be achieved was not possible. Therefore, the previously defined fine positioning range of 13.5 × 17.5 μm in *x* and *y* is used as input for the continued development of the MST-based 2-D fibre positioning concept, discussed in the next chapter.

6

MST-based 2-D fibre positioning concept

In this chapter, the design, fabrication and testing of the MST-based functionality for positioning the fibre tip in the two directions perpendicular to the fibre's optical axis are presented. Design choices made and insights obtained in the previous two chapters were employed as basis for the development, *i.e.*:

- the use of thermal actuation (Chapter 4);
- improved requirements on the positioning range (13.5×17.5 μm, Chapter 5).

The conceptual design of the developed thermal 2-D fibre positioning functionality is presented in Section 6.1, and the fabrication and test results are subsequently discussed in Sections 6.2 and 6.3, respectively.

6.1 Design 2-D fibre tip positioning concept[1]

In this section, first the principle layout of the developed 2-D fibre positioning concept is explained, followed by a discussion of the detailed layout.

[1] With some alterations, Sections 6.1 until 6.3 have previously been published in Henneken *et al.* (2008) in the Journal of Microelectromechanical Systems.

6.1.1 Principle layout

As starting point for the design of the 2-D fibre fine positioning concept, the requirements listed at the end of Chapter 3 were taken, except for the required displacement range, which was extended to 13.5 μm × 17.5 μm in *x* and *y*, based on the coarse assembly tolerance stacks determined in Chapter 5. Schematically, the starting point for design of the 2-D fibre tip positioning concept is shown in Figure 6.1.

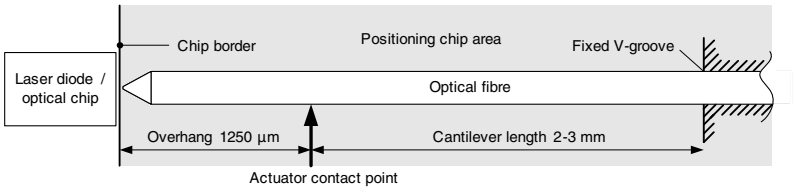

Figure 6.1 Schematic top view of the positioning chip area near the fibre tip including the main boundary conditions for development of the on-chip 2-D fibre positioning functionality

In Chapter 5 it was decided that the fibre would be placed in-plane with the positioning chip in a fixed anisotropically etched V-groove, to facilitate the fibre placement and to achieve a small tolerance build up, so that the fine positioning ranges could be kept acceptably small. In addition, it was decided that for optimal component placement flexibility in front of the fibre tip, the chip would have a straight edge perpendicular to the fibre axis, as close as possible to the fibre tip.

In order to limit the chip size, the distance between fixed fibre groove and tip location being deflected was chosen to be around 2-3 mm, which also resulted in acceptable fibre displacement forces and rotations, as discussed in Subsection 3.3.4. Furthermore, it was verified that the overhang from the fibre support location to the fibre tip can be at least 1250 μm[1], leaving more than 1 mm distance from the chip border for the internal positioning functionality to act on the fibre tip.

A schematic cross section of the developed 2-D fibre positioning concept is shown in Figure 6.2.

Independently controllable positioning mechanisms Ideally, to minimize uncertainties in positioning behaviour, friction is avoided, both inter-

[1] The first resonance peak at this length is above 10 kHz, which is well above frequencies from common environmental noise sources, which generally lie in the range of 1 to a few hundred Hz, and therefore it is expected that the fibre can be treated as a rigid body that 'follows' external vibrations from environmental disturbances.

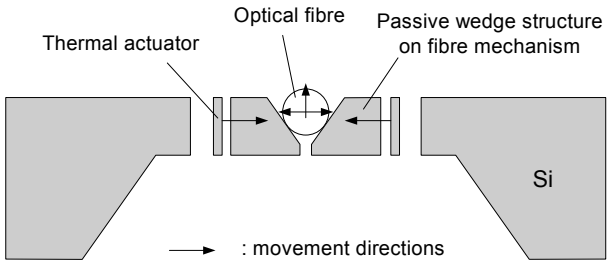

Figure 6.2 Schematic cross-sectional view of the 2-D fibre positioning concept

nally and also between components. This can be achieved by integrating all degrees of freedom into the positioning chip, and by permanently fixing the fibre to the positioning chip, as well as the positioning chip to its surroundings. This implies that inside the positioning chip a structure should be created, having sufficient load-carrying capacity to carry the fibre, and capable to independently control in- and out-of-plane motions for positioning the fibre. In practice, realizing such a support structure in a silicon chip using MST-based fabrication is highly challenging. Therefore it was decided to create two individually controllable actuation mechanisms, each capable of independently deflecting the fibre, and to allow limited sliding between fibre and these positioning elements. The fact that an optical fibre is a long, flexible part is very beneficial for this approach, since it may still be permanently fixed at some distance from its end, while allowing relatively simple actuators including sliding contacts for tip positioning. Any possible consequences of these sliding contacts naturally required investigation at an early stage.

Conversion of in-plane thermal actuation to *xy* fibre motions For the fibre positioning concept, it was decided to use in-plane thermal actuators in combination with a mechanism for converting the in-plane actuator motions into *xy* fibre tip movements, so in- and out-of-plane relative to the chip surface. Technically, the required in- and out-of-plane positioning could be achieved by a combination of in-plane and out-of-plane actuators integrated in the same chip. As shown in Chapter 4, significant processing complexity is involved in combining in-plane thermal actuators with out-of-plane moving thermal bimorph actuators with sufficiently thick layers for fibre displacement. As also indicated in Chapter 4, no examples are known of the opposite option, using out-of-plane actuators with a mechanism for conversion to in-plane motion. In addition, it is considered significantly more difficult to implement, and was therefore not selected.

Decoupling actuator and fibre support The simplest way to achieve out-of-plane motion conversion is by means of sliding along a wedge. By hori-

zontally sliding a wedge under a part, and by simultaneously obstructing its lateral motion, the fibre is lifted up. By placing two wedges opposite each other, and by individually moving them in- or outwards, the fibre can be moved both horizontally and vertically. This approach was used in our concept, with the wedges formed by the <111> planes in the silicon wafer, which are manufactured using anisotropic wet etching. Using these wedges, it is possible to convert the in-plane thermal actuator motions into both in-plane and out-of-plane fibre tip motions, as can be seen in Figure 6.2. The wedges were fabricated on separate fibre support structures, called the *fibre mechanisms*, so that after positioning these fibre mechanisms could be held in place with a relatively low force, and the actuators could return to their initial position without obstruction. This is preferred to constraining the actuators as well, which possess relatively high in-plane stiffness.

6.1.2 Detailed layout

Of the two most common in-plane thermal actuator topologies discussed in Chapter 4, the V-beam design was selected. The only disadvantage for V-beam actuators is their requirement to be anchored at both ends, with the end effecter in the middle. Consequently, if the V-beam size is too large, it cannot act directly on the fibre tip close enough to the chip border to avoid the fibre overhang being significantly larger than 1250 μm. Therefore, it was expected that a transmission mechanism was required between actuator and fibre actuation point. However, this aspect, and also the potential placement of the fine fixation functionality, was not yet considered for the basic 2-D fibre positioning concept, which was primarily intended for evaluating manufacturing and functionality uncertainties. Extension of this concept, taking into account these aspects, was performed in the subsequent step, which is discussed in Chapter 7.

The top view of the basic 2-D fibre positioning concept is shown in Figure 6.3. Finite element modelling was performed to determine the device dimensions and to predict its performance, see also Section 7.5. The basic design consisted of two thermal V-beam actuators with a length L of 4200 μm, thickness t of 45 μm and an initial angle of 0.03 radians. To prevent unwanted asymmetric buckling, the V-beam slenderness t/L was kept below 1/100, according to Wittwer *et al.* (2006). The slender beams of the fibre mechanisms were 2000 μm long and 25 μm wide.

The fixed V-groove for coarse placement of the fibre was located on a lower level in the wafer than the wedges on the fibre mechanisms in order to produce a well-defined pretension on these wedges by the fibre. This configuration allowed easy coarse assembly by simply placing the fibre into the fixed V-groove, thereby pushing the fibre mechanisms sideways by sliding

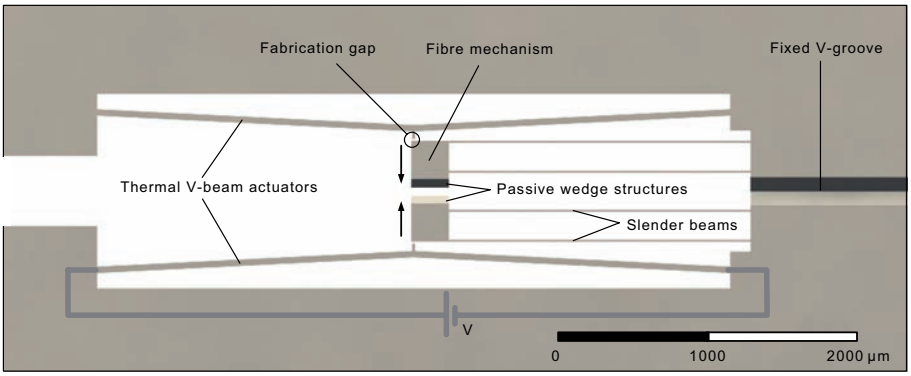

Figure 6.3 Top view 2-D fibre positioning device

along the wedges, see Figure 6.4. The height difference between fixed V-groove and movable wedges on the fibre mechanism was chosen such that the 10 µm wide fabrication gap between the actuator tip and the fibre mechanism was just closed, preventing that part of the actuation range could not be used for positioning.

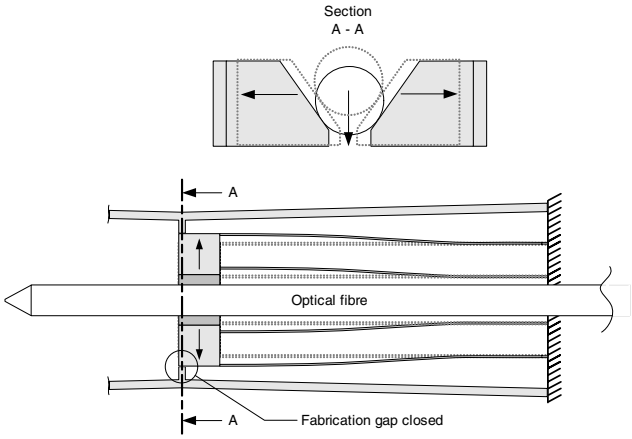

Figure 6.4 Sideways motion of passive wedge structures due to fibre loading (sizes and deformations not to scale)

Once the fibre was pressed onto the mechanisms the positioning could then take place. Theoretically, the window in which the fibre can be positioned is diamond shaped, as shown in Figure 6.5. By independently controlling the voltage levels on the thermal actuators, lateral and vertical motions in the plane orthogonal to the fibre axis could be performed. This allows the fibre tip to be positioned in front of the LD, which was designed to rest in the centre of the alignment area.

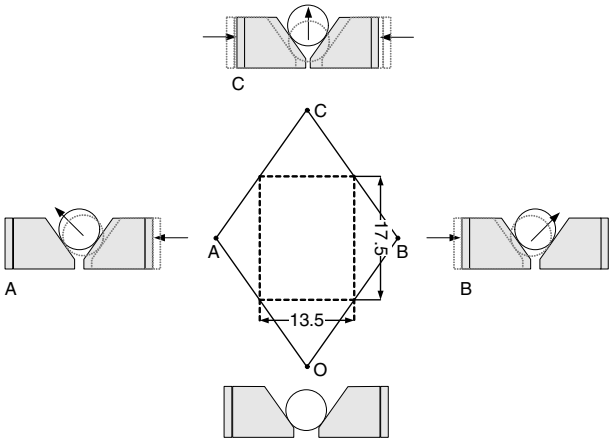

Figure 6.5 Schematic representation of the diamond-shaped positioning window with the three outer actuation positions A-C (dimensions in μm, positioning window not to scale)

The tolerance build up of the coarse assembly process required the diamond-shaped window to enclose a positioning rectangle of 13.5 μm wide and 17.5 μm high, as determined in Chapter 5. Therefore, the size of the enclosing diamond shape based on the 54.73° angle of the <111> plane with the horizontal plane was 27 μm wide and 39 μm high. Consequently, a single actuator needed to move the fibre tip approximately 27 μm while delivering sufficient force to position the fibre. Following from the mechanical gain in deflection due to the overhanging part of the fibre, the actual actuator stroke needed to be smaller; approximately 14 μm for a 1250 μm overhang (Sassen 2007, p. 52). A maximum force of around 10 mN was required based on calculations made on a bent fibre and on assuming a worst case friction coefficient between mechanism and fibre of 0.4 (Deng and Ko 1992). Using this concept, the maximum parasitic fibre bending was approximately 1°, which was acceptable since it introduced negligible additional coupling loss. The reader is referred to Sassen (2007) and Van der Burgh (2007) for more elaborate engineering calculations.

6.2 Fabrication 2-D positioning functionality

The in- and out-of-plane positioning of the optical fibre required large forces and a robust design of the structures, even more than for the 1-D in-plane thermal actuators shown in Chapter 4. For this reason, the mechanical structures were again etched by DRIE inside thick membranes created by anisotropic KOH etching from the backside of a standard 525 μm thick

silicon wafer. To increase the robustness, the membrane thickness was enlarged from nominally 120 μm to 150 μm.

Heating of the thermal actuators again took place by current flow through a thin polysilicon layer on top of the bulk material. The V-grooves on the front side of the wafer were also created using anisotropic wet etching in KOH.

A schematic overview of the process sequence used to fabricate these novel devices is presented in Figure 6.6. A more detailed process flow description is presented in Appendix A.3.

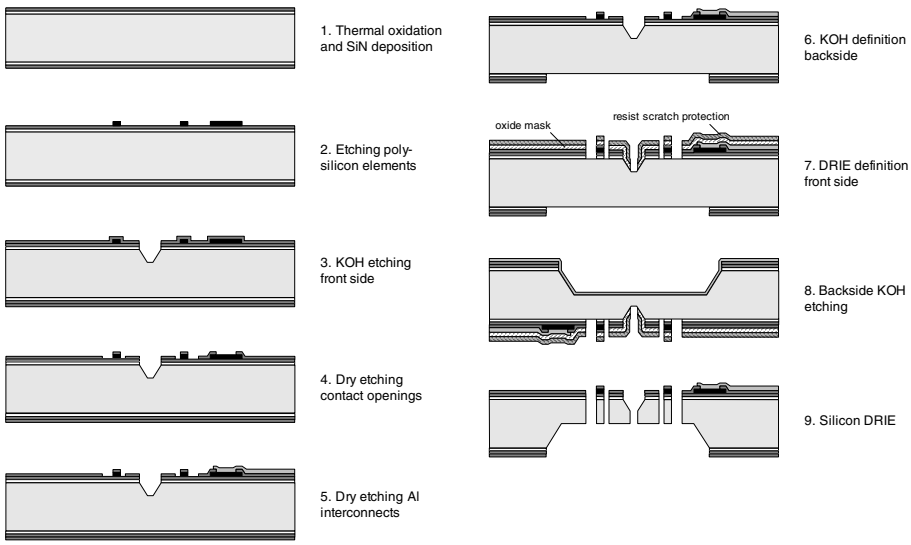

Figure 6.6 Fabrication sequence of the process run including in-plane actuation structures and KOH-etched <111> planes for fibre tip out-of-plane motion conversion

On the silicon substrate, a 300 nm thick oxide layer was thermally grown, followed by a 300 nm thick low stress SiN layer deposited by LPCVD (1). A 500 nm thick low stress polysilicon layer was then deposited by LPCVD. This layer was doped with phosphorous in a diffusion process and patterned using a resist mask and a dry etching step (2).

Next, the V-grooves were created in the front side of the wafer (3). A second layer of SiN was deposited and patterned. The silicon was etched in a 33wt% KOH solution to form the 100 μm deep V-grooves. At this point the contact openings to the polysilicon and the Al metallization were realized. For these two lithography steps, the resist was spray coated to uniformly cover the planar surface as well as the V-grooves side walls and bottom (Pham *et al.* 2004).

Following, the membranes were defined on the backside of the wafer (6) as well as the DRIE structures on the front side of the wafer (7). For the masking layer in the DRIE process a 3.0 μm thick PECVD oxide layer was used. At this point, the wafer presented a high topography surface and the fine structures needed to be patterned at different depths. To achieve this, a newly developed spray coater, EVG 101, at the EV Group in Austria was used (EV Group 2008b). Moreover, the structures were divided in two DRIE masks. The first mask contained only the DRIE openings inside the KOH cavities. Extra time was necessary to expose the resist in the deep cavities. This extra exposure time would alter the dimensions of the small structures present on the planar part of the wafer. A second DRIE mask that contains all DRIE structures was then applied, followed by development and pattern transfer into the oxide and nitride layers by plasma etching (stopped on the silicon).

Before the dry etching step, the membranes were etched from the backside using a KOH etching process until a 150 μm thick silicon membrane remained (8). A 500 nm aluminium stop layer for the DRIE process was then deposited on the backside of the wafer. In the final step, the scratch protection was removed and the DRIE step was executed. Finally, the aluminium stop layer on the backside and the oxide layer on the front side were removed (9). After dicing and wire bonding, the devices were ready to be tested.

The integration of the wet etching process with the partially overlapping dry etching process to realize the movable fibre wedges introduced some complexities. After the DRIE step, a thin silicon frame was left at the edges of the KOH mask openings (see Figure 6.7). This was probably due to a small under etch during the KOH step that caused an unintentional protection of the edge of the pattern during the DRIE process. This frame was mechanically removed from the devices resulting in the fully released structures presented in Figure 6.8. With some minor adaptations of the KOH etching process and a modification of the layout the under etch can be reduced and this problem can be avoided in future fabrication. Additional fabrication results are shown in Appendix E.

The surfaces of the movable wedges were very smooth in appearance. The darker areas at the bottom of the wedges indicated some aluminium residues. This was only a very thin layer on the <111> plane and it did not have a noticeable influence on the fibre positioning.

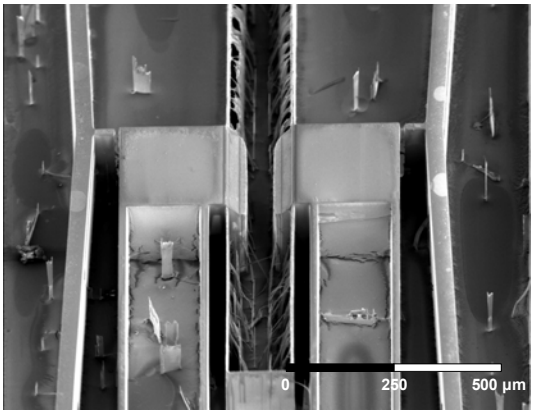

Figure 6.7 SEM detail image (45° tilt) of fibre mechanisms before the backside processing. The remaining vertical frame is clearly visible.

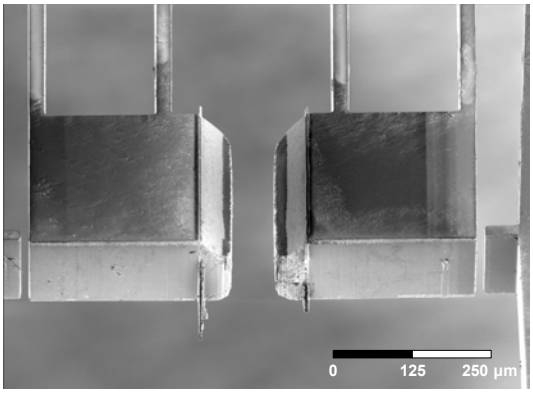

Figure 6.8 SEM close up of <111> plane wedges after full release and with frame removed

6.3 Experiments

Although the functionality was intended for fibre-to-laser alignment, in the experiments a fibre-to-fibre arrangement was used for convenience. Similarly, single mode fibre with a core of 4.3 µm was used because visible red light with a wavelength of 635 nm was easier to handle during the experiments than standard telecommunication fibre having a core of 8 µm to be operated at a wavelength of 1550 nm.

A schematic of the fibre-to-fibre alignment test setup used to measure the size of the actual positioning window is shown in Figure 6.9. In this setup,

two fibre ends were placed opposite to each other and light was coupled from one fibre to the other, continuously measuring the coupled power. One fibre was placed on the positioning chip and the other on a computer controlled Thorlabs *xyz* positioning stage having 5 nm positioning resolution in *x* and *y* (see Figure 6.10). The *x*-*y* fibre tip movement was determined indirectly by successively moving the fibre by the actuators on the positioning chip and aligning the computer controlled positioning stage until maximum optical power was regained, while each time recording the displacement of the positioning stage. Using this method, measurements of the *x*-*y* positioning window of the fabricated 2-D fibre positioning concept and of its achievable positioning resolution were performed.

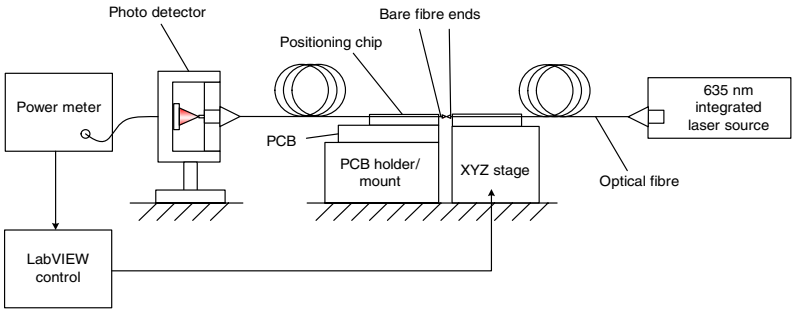

Figure 6.9 Schematic representation of the computer controlled fibre-to-fibre alignment test setup

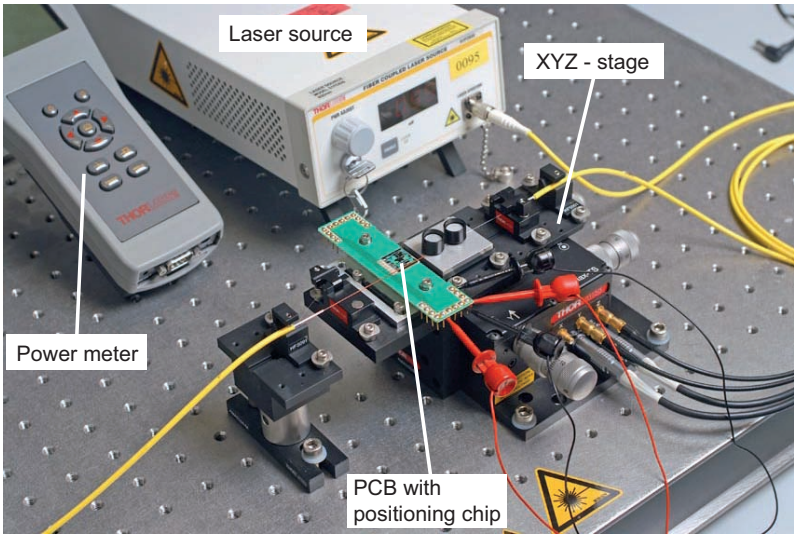

Figure 6.10 Fibre alignment setup including Thorlabs S1FC635 fibre coupled laser source and PM120 handheld power meter connected to sensor (not shown)

During the measurements, different fibre overhang lengths were used when measuring the size of the positioning window of the device. Increasing the overhang length significantly enlarged the size of the positioning window because of the angular pivot with the fixed V-groove. The positioning window measurements are presented in Figure 6.11(a) and Figure 6.11(b). These measurements were performed with approximately 1000 μm fibre overhang.

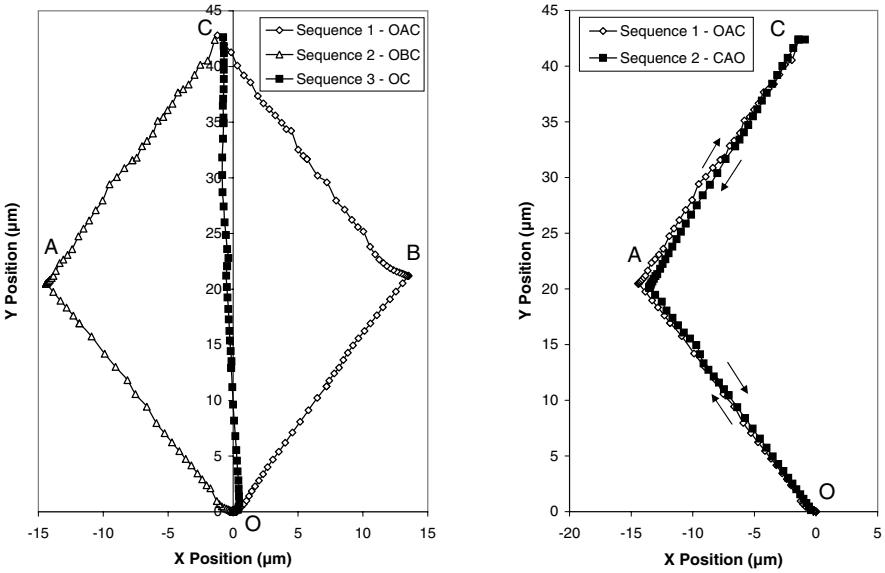

(a) (b)

Figure 6.11 Positioning measurements with 1000 μm fibre overhang: (a) measured 2-D positioning window; (b) upward and downward fibre motion to show hysteresis due to friction between fibre and <111> plane wedges

The results in Figure 6.11(a) show, as expected, a diamond shaped window in which the fibre tip can be positioned. The positioning window is slightly tilted by 1.5°, which can be attributed to a rotational misalignment of the positioning chip along the axis of the fibre in the experimental setup. The left and right lines each show two separate actuator movement sequences. An increasing voltage across the right actuator (see Figure 6.5) results in a displacement from O to A in Figure 6.11(a). Then, holding the right actuator at a constant voltage and applying an increasing voltage across the left actuator results in a displacement from A to C. This completed the trace of the left side boundary of the diamond-shaped positioning window from the bottom vertex (O) to the top vertex (C). By moving both actuators sequentially after each other, the final position of the fibre was approximately 43 μm vertically above the starting position. The right side boundary was

obtained by resetting the actuators to 0 V and then reversing the actuator order. This resulted in the traces from O to B, and then, from B to C. The middle line in Figure 6.11(a) shows the fibre motion when an equal voltage is applied to both actuators at the same time. All three lines ended at the same nominal position. The maximum applied voltage to each separate actuator was 36.5 V, which resulted in a 27 μm wide and 43 μm high positioning window with sides having directions in agreement with the etched <111> planes.

The friction between the fibre end and the <111> plane was expected to cause hysteresis and a stick-slip effect. A hysteresis measurement was performed which is presented in Figure 6.11(b). The first sequence consisted of an upward motion of the fibre with an increasing voltage applied first to the right actuator and then to the left actuator. In the second sequence, the actuator voltages were decreased in reverse order. The results indicate that the hysteresis had a minimal effect in positioning the fibre tip with this device.

To measure the effects of stick-slip, the left actuator was held constant at a voltage of 33.5 V and the right actuator was displaced from 33.5 to 36.5 V using a linear step of 50 mV, which was the minimal stable voltage output of the test setup. At these high voltages, the output sensitivity of the actuator was the highest, resulting in the worst attainable displacement resolution. Figure 6.12 shows the measured *x*-*y* displacement plot with the same 1000 μm fibre overhang, and because there are no large jumps between successive data points, it is assumed that the stick-slip had little effect on the displacement of the actuator. The *x*-direction was also the direction of actuation, therefore, this was used as the reference direction in the measurement to determine the linearity of the *y* data. For comparison, the silicon <111> lattice plane, which would be an ideal reference, has a slope of 1.41 (the square root of 2). The measured slope of *y* with respect to *x* was 1.32. Although there was a difference between the ideal slope and the measured value, this could be attributed to rotational misalignment shown in Figure 6.11(a) and not to stick-slip.

Using a linear least squares approximation, the difference from this and the measured value was less than ± 0.1 μm. However, the difference appeared to have a non-linear component in the signal. Because the data did not show significant effects of stick-slip, the source of this non-linearity may have been due to the non-linear displacement characteristics of the actuator, examples of which were already shown in Chapter 4. However, the difference from ideal and the stick-slip effects were less than the target values and therefore this was not investigated further.

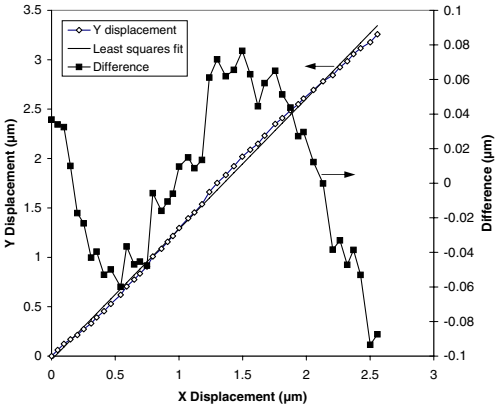

Figure 6.12 Measured *x-y* displacement upon actuator voltage steps of 50 mV from 33.5 to 36.5 V

6.4 Discussion

The measurements confirmed that the presented concept for 2-D fibre positioning using <111> plane wedges successfully meets the positioning requirements for the selected fibre coupling case. The results showed fibre tip displacements in a diamond shaped positioning window of over 25 µm in-plane and more than 40 µm in the out-of-plane direction with only a small visible hysteresis effect. Positioning resolutions smaller than 0.1 µm were measured, and correcting for non-linearity in the actuator may lead to a significant further improvement in displacement resolution.

In order to prevent the remaining frame shown in Figure 6.7, the combination of wet and dry anisotropic etching should be optimized which is expected to be achievable with minor modifications.

Recently, a similar 2-D fibre tip positioning concept as was developed in our project was shown by Morgan *et al.* (2007). Their device also uses wedges to convert in-plane motions from two opposing linear actuators to in- and out-of-plane fibre tip motions, see Figure 6.13. However, their wedges are fabricated using grayscale lithography, which is a rather new technology for creating 3-D silicon structures, currently lacking surface smoothness due to the limited resolution of the lithography mask. SEM inspection resulted in an estimated roughness of 1-3 µm over the majority of the slope, leading to positioning resolutions not much better than 1.25 µm over a 20-by-20-µm actuation area. Significant hysteresis of around 4 µm was also observed, as well as stick-slip for small step sizes, attributed to static friction between the

wedges and fibre. To 'unstick' the fibre, and to reduce hysteresis effects, after each actuation step a 100-ms pulse of (0 V, 0 V) had to be included.

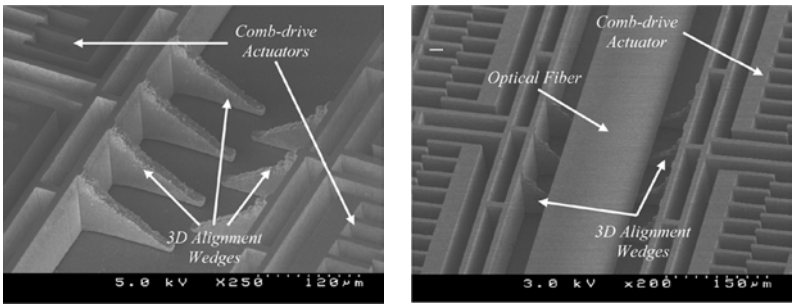

(a) (b)

Figure 6.13 SEM images of grayscale fibre aligner (a) before and (b) after fibre attachment (Morgan *et al.* 2007)

Electrostatic comb-drive actuators were used, only capable of exerting low forces in the range of 100 μN at 100-150 V. Therefore a large fibre cantilever length of approximately 10 mm was needed, resulting in relatively large dimensions. Since the fibre attachment process was entirely manual, it was difficult to consistently ensure that the fibre touched both wedges in its rest state. Finally, fixation of the fibre tip after fine positioning was not incorporated, although plans for including mechanical functionality for locking the wedges after positioning were announced.

Summarizing, the 2-D fibre positioning concept presented in this chapter has significant advantages over the concept by Morgan *et al.*:

- better defined fibre placement, and easier fibre fixation inside V-groove;
- smoother wedge surfaces, resulting in better positioning resolutions, and lower hysteresis and stick-slip;
- thermal actuation, capable of exerting larger forces, allowing for a smaller device area.

In addition, fixation of the fibre in its final position is included, which is topic of the next chapter.

7

Fine fixation and integration with positioning functionality

In this chapter, the selection and design, as well as the fabrication and testing results of the functionality for fine fixation of the fibre tip are presented. Mechanical clamping is selected as fine fixation method. To allow integration of the clamping functionality into the positioning chip, adaptations were made to the 2-D positioning concept presented in the previous chapter. Their joint performance was verified both experimentally and by thermal modelling.

In Section 7.1, the most promising fixation methods for application in a PIAF approach are discussed, after which mechanical clamping is selected for fixation of the fibre in Section 7.2. Next, the design of the mechanical clamping functionality and adaptations made to the positioning functionality are presented in Section 7.3, followed by a discussion of their fabrication and test results in Section 7.4. Thermal modelling was performed to assess the temperature profiles and heat flow inside the structures, which is briefly discussed in Section 7.5. Following, the beneficial consequences of the chosen positioning and clamping embodiment for the coarse assembly process are presented in Section 7.6.

7.1 General methods for fine part fixation

In Figure 7.1, an overview is presented of the main fixation methods that may be applied on the micro scale. See Van Brussel *et al.* (2000) and Cohn *et al.* (1998) for additional information on these fixation methods for micro-assembly.

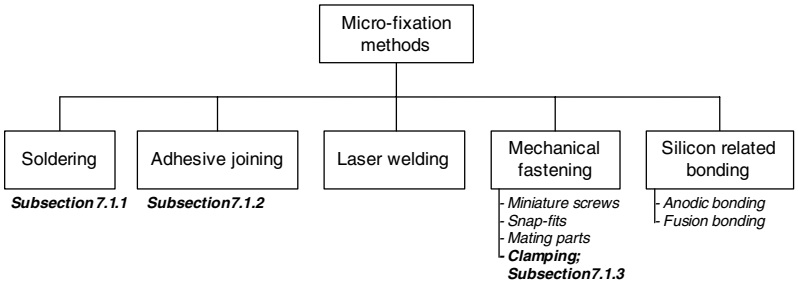

Figure 7.1 Overview of methods applicable for fixation on the micro scale

Only part of these methods is practically applicable for fixation in a PIAF approach. Most important for this purpose is the ability to fix a micro-component at an initially unknown position within the fine positioning range at sub-µm accuracy and high long-term stability in the most critical directions during the device's economic life. Furthermore, the methods should be sufficiently fast and require no or limited, simple preparatory steps, have limited space requirements, low complexity and practical assembly conditions, so that they may be applied at moderate cost.

Laser welding, although very popular for fibre attachment based on its sub-µm accuracy, speed and long-term joint reliability, is not considered a promising method in combination with MST-based internal part positioning due to its difficult controllability and the relatively large deformations produced by individual shots, resulting in loss of position accuracy. Moreover, laser welding requires metal structures, which are not easily combined with the silicon components of the fine positioning functionality.

In addition, many mechanical fastener types found in literature, such as miniature screws, micro-Velcro (Han *et al.* 1992), snap-fits (Prasad *et al.* 1995, Yeh *et al.* 1996), microrivets (Shivkumar and Kim 1997), press fits, and mating parts (González *et al.* 1998) are also not suitable because they cannot be used for achieving sub-µm attachments at varying positions.

Finally, silicon-related bonding techniques cannot be applied since they typically require high temperatures and high electric potentials and/or high bonding pressures for extended durations, rendering these methods highly impractical for use in a PIAF procedure.

The remaining fine fixation methods that are considered most promising for use in combination with product-internal assembly functions are *soldering* and *adhesive bonding* - also discussed in the previous chapter for use as coarse fixation methods - and *mechanical clamping*, which is not commonly applied, but nevertheless considered attractive for fine fixation. These three

fine fixation methods are briefly discussed in the following three subsections, respectively.

7.1.1 Soldering

Soldering for the purpose of accurate die attachment was already quite extensively discussed in Chapter 5. There it was noticed that achieving repeatable sub-μm accuracy bonds by using soldering is very challenging, particularly in the direction of the gap height. Solder solidifies at elevated temperatures, and shrinks upon cooling. Additionally, most solder materials suffer from creep, possibly resulting in increased deformation with time, and solder joints may fail due to delamination and crack formation from internal stresses. Nevertheless, typically reliable, strong joints with relatively high long-term stability can be achieved, with potential applicability for sub-μm accuracies. Especially if the joint is oriented such that the highest deformations act in the least critical directions, *i.e.* with the solder height orthogonal to the fine positioned directions, accurate positioning can be achieved.

The solder process itself can be relatively fast, in the order of seconds to tens of seconds, and the joint fairly compact, depending on the desired bond strength. Optionally, rework can be performed to increase yield, although this is limited as the solder joint integrity may degrade upon repeated reflow.

Melting the solder may be realized by contact heating, localized/on-chip electrical resistance heating (Witham *et al.* 2000, Datta *et al.* 2003), or laser-assisted reflow (*e.g.* Flanagan *et al.* 2003). Care should be taken to minimize adverse effects due to increased temperatures in the region surrounding the solder joint.

An aspect limiting the application of solder on a silicon substrate mainly to out-of-plane orientations with respect to its surface is the fact that selective metallisation for solder wetting must be realized by means of lithography. This would suggest that the highest accuracy may be expected in directions parallel to the wafer plane. However, as shown for example by Flanagan *et al.* (2003), by proper joint design, sub-μm out-of-plane accuracies may also be achieved. They used laser assisted reflow to attach metallised fibres to flat substrates and attained a maximum lateral misalignment of $\pm$ 0.2 μm. Over 60% of the attachments succeeded within the first reflow to achieve 95% retained power, and the total yield using up to 10 reflows was 98%, with an average cycle time of less than 5 minutes. Fibre displacements were less than 0.3 μm through Telcordia GR-468-CORE compliant mechanical shock, vibration, high temperature storage, and temperature cycle testing.

7.1.2 Adhesive bonding

The method which intuitively seems most attractive for fine fixation of miniature parts in variable positions is by applying adhesive, due to its flexibility in use and its capability to fill gaps of various geometries. A wide range of dissimilar materials can be bonded, without the need for additional parts, and it is typically an economic process requiring low equipment investment. Indeed, adhesives are increasingly used in applications requiring high accuracy bonds with high long-term stability.

Unfortunately, adhesives do have some drawbacks for use in this type of applications. Generally adhesives shrink upon curing, have relatively high thermal expansion coefficients compared to most engineering materials, and exhibit creep and aging, affecting long-term stability of the bond. Typically, using adhesive bonding, lower stability is achieved than with solder.

As for soldering, by proper joint design, the effects of adhesive deformations on the part position can be reduced, as well as the build up of internal stress that could cause delamination and crack formation inside the bond. Again, the highest accuracy in a given direction is obtained by letting the adhesive joints act in the plane normal to this direction. Generally the part position and internal stress levels are better controlled by accurately applying a number of small adhesive dots at specific locations rather than filling the entire gap between the parts to be joined with adhesive.[1] An extensive discussion of different configurations for accurate part fixation by means of adhesives is beyond the scope of this thesis. A comparison of common constructions for obtaining accurate adhesive bonds can be found in Vereniging FME-CWM (1999).

In literature on micro-assembly, generally little attention is paid to the joint design in order to reduce adhesive related misalignments. For example for fibre fixation in published PIAF approaches, mostly the fibre tip is simply surrounded by adhesive, and the adhesive is cured after fine positioning. In most cases, the position shift after curing is not specifically stated, see *e.g.* Kikuya *et al.* (1993), Unamuno *et al.* (2005), and Luetzelschwab *et al.* (2005).

In Lin *et al.* (2006), a fibre array and a micro-lens array were actively aligned, and subsequently adhesive was applied to a glass plate, which was attached to both fibre and microlens array, and then cured. Although the adhesive was applied in one of the critical tolerance directions, part of the position shift was compensated, because the adhesive shrinkage in both

[1] Particularly in the engineering domain known as *optomechanics*, significant expertise and best-practices have been developed for applying adhesives for accurate and stable fixations of optical components, such as required in optical space instruments.

joints acted in the same direction. Since the adhesive areas were rather large, the layers had to be at least 75 μm to prevent delamination or cracking. The smallest achieved relative alignment shift at this thickness was calculated to be 0.6 μm.

UV curing adhesives

For application as fine fixation method in the PIAF approach, adhesives that can be cured by exposure to UV light are the most suitable ones. Unlike most other curing mechanisms, the start of the curing process can be exactly controlled - so-called *cure on demand* - and curing generally takes a relatively short time (in the order of a few to a few tens of seconds), allowing for fairly short cycle times. Moreover, UV curing usually can be performed at room temperature, minimizing thermal shrinkage.[1]

UV penetration in relatively thin adhesive layers up to a few hundred micron is generally not a problem. UV curing adhesive types exist that continue curing without further exposure, making them suitable for bonds with shaded areas. Several companies, such as Dymax and Addison Clear Wave (www.dymax.com; www.addisoncw.com), have developed special UV adhesives for optical applications, with low curing shrinkage, a low thermal expansion coefficient (CTE), and low outgassing. These properties are usually obtained by addition of fillers with low CTE, mostly quartz particles. Generally, these fillers increase the adhesive viscosity, affecting the possibility of dosing this type of adhesives in small volumes.

The most flexible methods for applying small quantities of adhesives are needle dispensing and non-contact jetting. By piston-based contact needle dispensing, droplet sizes down to approximately 0.2 mm can be deposited (nanolitre range), whereas using jetting even smaller droplet volumes in the picolitre range can be achieved, depending on the viscosity. By jet dispensing, droplet volume reproducibility is in the range of one to a few percent, but adhesive placement accuracies are usually not specified. It is uncertain whether jetting can be reliably used for angled surfaces, or for applying adhesives in difficult-to-reach areas, such as narrow gaps. Contact needle dispensing may be a better solution for these situations, although this may suffer from variability in the dispensed volume due to enclosure of air bubbles within the dosing unit (Dilthey *et al.* 2001). Gerlach *et al.* (1999) showed that in case of sufficient substrate wetting - necessary for good adhesion of the glue to the substrate - and at moderate adhesive viscosities of around 1500 mPa·s, adhesives can fill narrow gaps with heights of 4-6 μm by capillary action to depths over 1 mm within only a few seconds. Of

[1] UV curing intensities are in the order of 1 to several W/cm^2, so a limited temperature rise of the irradiated region during curing generally does take place.

course, by proper joint design and careful volume control, penetration into regions that should be kept free of adhesive must be prevented.

7.1.3 Mechanical clamping

So far, we have seen that using solder or adhesives for fine fixation, it is challenging to achieve sub-μm accuracy part fixation. A promising alternative approach is by using mechanical means to clamp the part or its support structure in the desired position. Since this method relies upon solid mechanical contact between parts and the stiffness of the clamping structure, high positioning accuracies may be achieved by employing careful clamp design. Besides, it provides the additional benefit of simplified releasability, allowing reapplying the clamp during assembly if required. Drawbacks are the larger space required and uncertain reliability compared to soldering and adhesive joining. Moreover, it may require considerable additional design effort as well as might be complex to apply successfully.

The focus is on internally actuated MST-based clamping solutions, since these are considered most realistic for application in the PIAF concept. Two main categories of clamp designs are *form closure* and *force closure* (also referred to as *friction-based clamping*). Generally, if the part motion is restricted by friction forces, this is called force closure, whereas if the clamp contact itself is sufficient to maintain the part position disregarding the applied forces, this is referred to as form closure.

An example of MST-based form-closed clamping - in this case referred to as *latching* - is shown by Syms *et al.* (2004a). In this example, a 1-D translation stage was demonstrated with thermal V-beam actuation for in-plane positioning of a 5 mm square table fabricated in the 85 μm thick top layer of an SOI wafer and a rack-and-tooth mechanism for latching the table at discrete positions, see Figure 7.2.

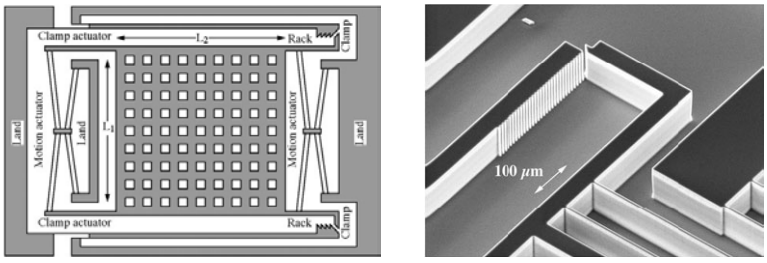

(a) (b)

Figure 7.2 (a) Overall layout of latching translation stage, and (b) detail image of clamp with teeth (Syms *et al.* 2004a)

Unlatching was performed by electrothermal U-beam actuators. The stage travel was over 100 μm and the latching increments were 10 μm, with the clamp force acting in the positioning direction. The tooth separation was determined by the ability of the DRIE process to transfer the rack pattern to the full structural depth, and by the need to maintain clearances during fabrication as well as to have sufficiently strong teeth for withstanding the forces during clamping, limiting the number of positional states that could be realized. Similar examples with decreased latch increments were also shown by Syms *et al.* (2004b, 2004c) and by Unamuno and Uttamchandani (2006). However, latch increments smaller than 0.5 μm could not be demonstrated. If smaller fixation increments than in the range of 0.5-1 μm are required, generally friction-based clamping is applied.

Friction-based clamping is typically employed in a direction normal to the fine positioning directions. As a result, depending on the fine positioning directions relative to the chip surface, in- or out-of-plane clamping is desired. In general, it is considered beneficial if the clamping functionality could be integrated into the same component as used for the fine positioning functionality, since this would allow for a significant reduction of processing cost, and eliminates the need for additional assembly steps. However, especially realizing a configuration with in-plane part positioning and out-of-plane clamping in a single chip appears challenging, so most likely the need for multiple-chip solutions cannot always be avoided.

Examples of MST-based clamping mechanisms using friction-based clamping are shown by Grade *et al.* (2005) and Brouwer (2007). The device by Grade *et al.* is shown in Figure 7.3.

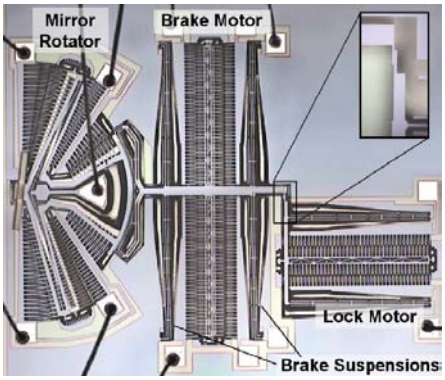

Figure 7.3 Microscope image of a rotational optical switch including brake motor and lock motor for powerless clamping (Grade *et al.* 2005). The inset shows an expanded view of the lock pin pressing the brake motor leftward against the rotator.

A mirror is rotated and subsequently clamped in the desired orientation by an electrostatic clamp acting perpendicular to the primary rotational mirror movement. The measured clamping accuracy was 0.1 mdeg, which was 0.0025% of the full-scale deflection. At an approximate radius of 3 mm, this was estimated to be in the order of 5 nm displacement. In both the examples by Grade *et al.* and Brouwer a locking mechanism was used to maintain the clamp force without power consumption.

Powerless clamping

An important requirement for mechanical clamping as fine fixation method in a PIAF approach is that the clamp force can be maintained without power consumption. In the previous examples, this either required form closure or additional separate locking actuators, which are both not very favourable. An alternative approach to achieve powerless clamping is by creating a normally-closed clamp, and by reversing the clamp operation, such that that the clamp is released upon actuation, and the clamp is engaged by powering down the actuator. Creating such a normally-closed clamp may be achieved by introducing pre-stress into the device, which could either be performed by pressing individual parts against each other during assembly, or alternatively by creating the pre-stressed structure inside the clamping chip itself.

Examples of internal pre-stressed structures by applying thermally-curable polyimide were shown by Kuribayashi and Fujii (1998) and Baba *et al.* (2003). Baba *et al.* showed a rotational micro-mirror with a holding structure containing two electrothermal U-beam actuators that was deformed by a locally applied quantity of polyimide, which after curing caused the U-beams to push against the sides of the micro-mirror. Releasing of the micro-mirror could be achieved by heating the U-beam actuators, see Figure 7.4.

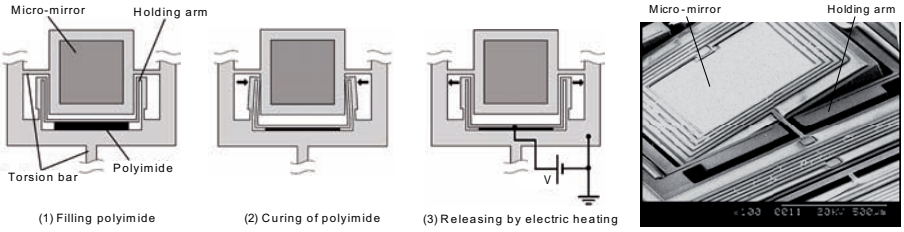

Figure 7.4 Creation of passively deformed U-beam actuators by thermally-curable polyimide (Baba *et al.* 2003)

Two other possible methods of achieving pre-stress are by using bistable mechanisms and by so-called snap fasteners or snap-fit structures, which are commonly applied in plastics, *e.g.* for bottle caps. Examples of bistable

mechanisms are shown by Qiu *et al.* (2004) and Boyle *et al.* (2004). Boyle *et al.* showed a bistable mechanism for clamping discrete optical components against fixed mechanical stops, with integrated electrothermal V-beam actuators for switching the bistable bent beam between the stable locking and unlocking states. Snap fasteners are for example shown by Prasad *et al.* (1995), Beamesderfer *et al.* (2001), and Dechev *et al.* (2004). A more comprehensive treatment of possible methods of achieving MST-based powerless mechanical clamping can be found in Van der Burgh (2007).

7.2 Selection fine fixation method 2-D fibre positioning concept

In this section, the selection of the fine fixation method for the 2-D fibre positioning concept presented in the previous chapter is discussed. Specific aspects for the selected fibre coupling case are the exceptionally strict position requirements, which are ± 0.1 μm in the fine positioned directions, perpendicular to the fibre axis, and the large restoring forces of the fibre and the fibre support structure in the order of several mN. As a consequence, the stiffness of the part fixation should be considerable. However, none of the discussed fixation methods are expected to have difficulties achieving the required stiffness.

The strict accuracy requirements in the fine positioned directions on the other hand are considered extremely challenging for solder and adhesive bonding. No examples have been found in literature of solder or adhesive joints with position shifts below ± 0.1 μm in the most critical directions. Therefore, although mechanical clamping requires significantly more space and design effort than the other two methods, it was decided to select mechanical clamping for fixation of the fibre in the selected coupling case.

An additional motive for selecting mechanical clamping in this project was that it enabled us to investigate the interactions of MST-based fine positioning and fine fixation functionality for use in the PIAF concept. Furthermore, a practical consideration was its easy releasability, which is potentially desirable for industrial yield improvement, but which was also convenient with regard to testing of demonstrators.

7.3 Design mechanical clamping functionality[1]

In this section, the conceptual and detailed design of the mechanical clamping functionality suitable for cooperation with the 2-D fibre tip positioning concept presented in the previous chapter are discussed. The adaptations

on the basic positioning concept shown in Figure 6.3 required to accommodate for the clamping mechanisms and to reduce the fibre overhang are also discussed.

The 2-D fibre positioning concept was taken as starting point for the design of the mechanical clamping functionality. The clamping functionality was integrated with the positioning chip, since this allowed for a reduction of processing cost, and eliminated the need for additional assembly steps. Instead of clamping the fibre directly, the clamp force was applied on the fibre mechanisms, thereby indirectly controlling the fibre position. Since integrated in-plane clamping is more easily implemented than out-of-plane clamping, clamping was applied in-plane with the positioning chip, on the end faces of the fibre mechanisms, perpendicular to their directions of movement.

Thermal actuation was selected for the clamp, because this facilitates its integration into the positioning chip, and it is capable of providing large in-plane forces and displacements at moderate voltage and current levels. In addition, experience was already gained with thermal actuators for fine positioning, allowing us to implement thermal actuators for the clamp functionality with relatively little additional effort.

As was discussed in Subsection 7.1.3, preferably the clamp force is maintained without power consumption. However, most shown methods for achieving powerless clamping are rather complicated or require quite large chip area. Fortunately, based on the specific characteristics of the positioning functionality, yet another method could be used for achieving powerless clamping, which was selected for its simplicity. It uses the movement of the fibre mechanism caused by the pretension force of the loaded fibre (around 4 mN, see Sassen (2007)), as shown in Figure 6.4. In this way a clamp tooth can move beyond a tooth on the fibre mechanism, and can subsequently lock after fibre positioning. This results in friction-based powerless clamping of the fibre mechanism at any position within the positioning window.

Clamping the fibre mechanism can be described in the following four steps, as shown in Figure 7.5. In the position after fabrication, the tooth of the clamp cannot move beyond the tooth on the fibre mechanism. When the fibre is loaded, the fibre mechanism moves aside (1) and the clamp is actuated until the tooth passes the tooth of the fibre mechanism (2). The positioning actuator then moves the fibre to the desired position (3) and the mechanical clamp is then powered down, thereby engaging the clamp (4).

[1] With some alterations, Sections 7.3 until 7.5 have previously been published in Henneken *et al.* (2008) in the Journal of Microelectromechanical Systems.

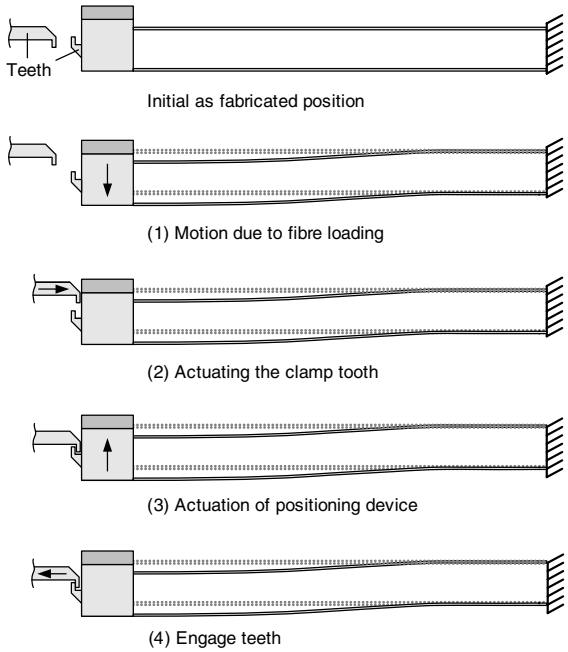

Figure 7.5 Four-step clamping sequence using the fibre loading to allow the clamp tooth to pass the tooth on the fibre mechanism and enable powerless clamping inside the positioning window

To maintain the clamp teeth in stable contact by friction, a sufficiently large clamping force should be exerted onto the fibre mechanisms. Because both the friction coefficients between fibre and fibre mechanism, and between the DRIE-processed clamping teeth were uncertain, a worst-case clamping situation was assumed, with a resulting clamping force of approximately 25 mN. As was indicated in Chapter 6, for determining the required force for the positioning actuators, a worst-case friction coefficient of 0.4 between fibre and <111> wedge surface was taken, resulting in a calculated actuation force of around 10 mN. However, to hold the fibre in position, a much smaller force in the order of only 2 mN is required, because in this situation the friction between fibre and fibre mechanisms actually helps in keeping the fibre in position. If this friction force would be ignored, the holding force would increase to approximately 3.5 mN, which would have to be provided via friction by a clamping force on the fibre mechanism normal to its positioning direction. Recent studies on friction between DRIE silicon sidewalls resulted in widely varying static friction coefficients from 0.15-0.35 (Hwang *et al.* 2006) to 0.9 (Guo *et al.* 2007). These were all obtained at much lower normal forces than required for our clamping situation, and for that reason a worst-case friction coefficient of 0.15 was chosen, resulting in a clamping force of approximately 25 mN.

Both the structural width of the teeth and the initial fabrication gap between the teeth were 10 μm, combined with a safety margin of 5 μm resulting in a required clamping actuation range of 35 μm.

The clamp functionality was developed separately from the 2-D positioning functionality including the <111> wedge structures. In the used process for fabricating the clamp structures, KOH etching on the front side was not performed and, consequently, only vertical sidewalls could be created in the wafer. Therefore, only in-plane fibre movements were possible. For this reason, an *in-plane* wedge was fabricated on the fibre mechanism (instead of an out-of-plane wedge) to obtain closing of the fabrication gap between the fibre mechanism and the positioning actuator tip by pushing of the fibre.

Figure 7.6 presents one side of the total positioning device on which the clamping structure, positioning actuator, and fibre mechanism can be recognized as all in-plane moving structures. For the actual device, this can be mirrored allowing for 2-D positioning motions. Figure 7.7 presents a zoomed image of the final design of the tooth of the mechanical clamp and the tooth in the fibre mechanism.

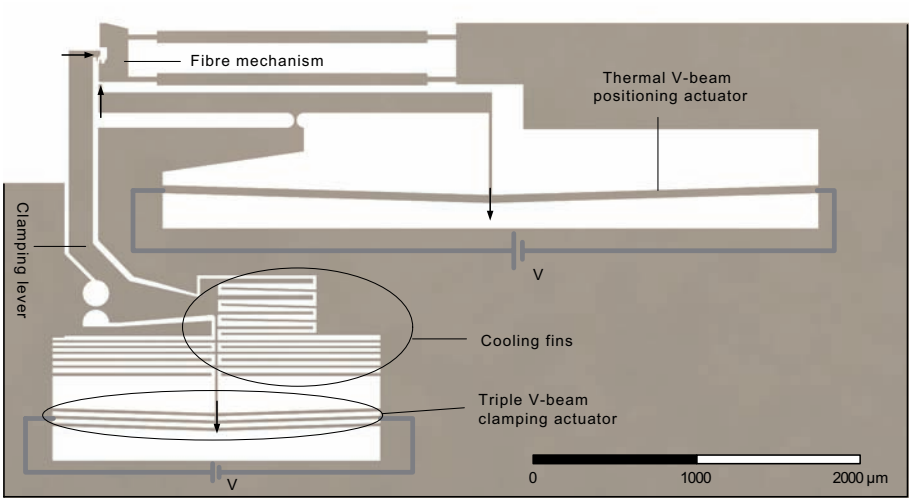

Figure 7.6 Top view of single side positioning and clamping concept

The positioning mechanism contained a 4000 μm long by 50 μm wide V-beam actuator which was connected to a lever on a circular flexure hinge reversing the movement of the actuator, see Figure 7.6. The mechanical clamp consisted of an angled lever to enlarge the actuator stroke by a factor of two. It was connected to a 2000 μm long triple V-beam stack for a large clamping stiffness. Cooling fins were included between the lever and the

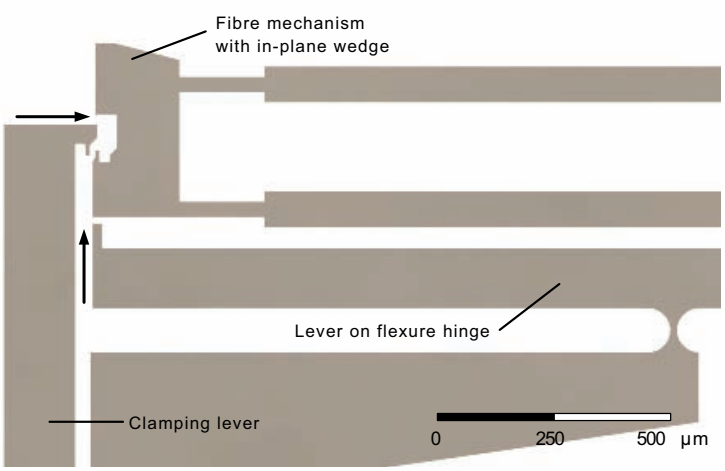

Figure 7.7 Close up image of fibre mechanism and clamp with in-plane wedge

actuator to limit the heat flow towards the lever tip, which would otherwise have caused expansion of the lever during actuation and shrinkage while powering down, leading to undesired fibre alignment errors. Air gaps of around 200-300 µm were included on either side of both actuators to reduce heat transfer to the neighbouring substrate by means of conduction through air. The fibre mechanism slender beams were reinforced to increase their out-of-plane and longitudinal in-plane stiffness while keeping a low stiffness in the actuated direction.

The fabrication gap was increased to 13 µm, and the tooth overlap was chosen such that in the least actuated fibre position, at least a 5 µm tooth overlap was achieved, and that in the centre of the positioning window - the nominal LD position - the fibre mechanism support beams were exactly straight. This resulted in minimal bending of the support beams across the entire positioning range, which was beneficial for minimizing the position shift upon engagement of the mechanical clamps. A 1-µm clearance was taken for allowing the teeth to pass each other for initiating the clamp. In order to enable this 5 µm tooth overlap and 1 µm clearance, the actuation range of the positioning actuators was increased from 14 µm to 20 µm.

The overall dimensions for the double-sided positioning device, including mechanical clamps, were approximately 5 × 6 mm, which could easily fit inside a standard optical fibre package.

7.4 Fabrication and test results clamping functionality

Fabrication of the mechanical clamping concept shown in Figure 7.6 was performed in nearly the same way as the basic 2-D positioning concept discussed in Chapter 6. The main difference was that the third step, KOH patterning and etching on the front side, did not take place. SEM images of the clamping mechanism and part of the positioning structure, and a close-up of the clamping teeth are shown in Figure 7.8 (see also Appendix E).

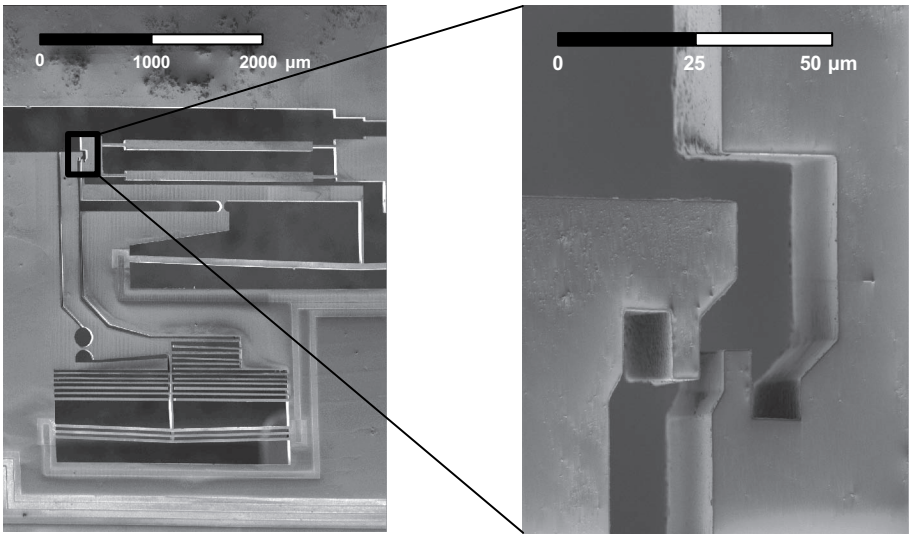

(a) (b)

Figure 7.8 The fabricated mechanical clamp and positioning device (a), and (b) close-up of the tooth mechanism

For determining the in-plane fibre positioning range and the clamp performance, the same measurement setup was used as for measuring the 2-D positioning window, described in Section 6.2. The measured fibre positioning range is shown in Figure 7.9. The displacement was measured for both a 10 µm and 1000 µm overhang. The results indeed show a significant difference in fibre tip displacement between situations with a small or large fibre overhang as was indicated before.

The measured fibre positioning range with 1000 µm fibre overhang was 26 µm at 33 V, just below the required positioning range of 27 µm, which can be reached by slightly increasing the actuator voltage. The thermal modelling, presented in the next section, showed that this can be safely done without overheating the structure.

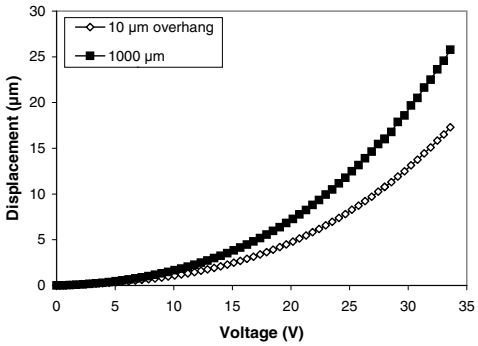

Figure 7.9 Measured in-plane fibre displacement with 10 µm and 1000 µm fibre overhangs

The clamping sequence is shown in Figure 7.10. Figure 7.10(a) shows the fibre mechanism being pushed against the positioning actuator by the inserted fibre. A voltage was then applied to the clamping actuator in order to allow the tooth of the clamping lever to pass the tooth of the fibre mechanism (b). Next, the fibre was aligned with respect to the opposing fibre end (c) and the actual clamping started. First, the clamp actuator was shut off, after which the positioning actuator was powered down, leaving the device completely without power (d). As shown in Figure 7.10(d), the fibre remained aligned with the second fibre, even when both the positioning actuator and clamping actuator were switched off.

Measurements on the step response behaviour of the thermal positioning actuator showed settling times of approximately 0.5 s, which is fast enough for assembly purposes. The total optimization including constraining the final position can take place in a matter of seconds.

The position shift during clamping was tested at different positions of the fibre. After fine positioning of the fibre, the clamping sequence (powering down both clamp and positioning device) was performed and the fibre displacement was measured. From repeated measurements it was determined that the clamping displacement at all tested positions was less than 0.1 µm and therefore, met the fibre-to-laser coupling requirements.

The devices were also tested for their resistance against vibrations, from 0 to 2000 Hz up to 15g. The lowest resonance frequencies of the structures were calculated to be much higher than 2000 Hz (7 kHz for the fibre mechanism, 27.9 kHz for the positioning actuator, and 25.8 kHz for the clamping structure), and therefore little damage, if any, to the structure was expected. The device was tested both in clamped and unclamped state in three orthogonal directions, see Figure 7.11. No visible failure or shift in clamping position

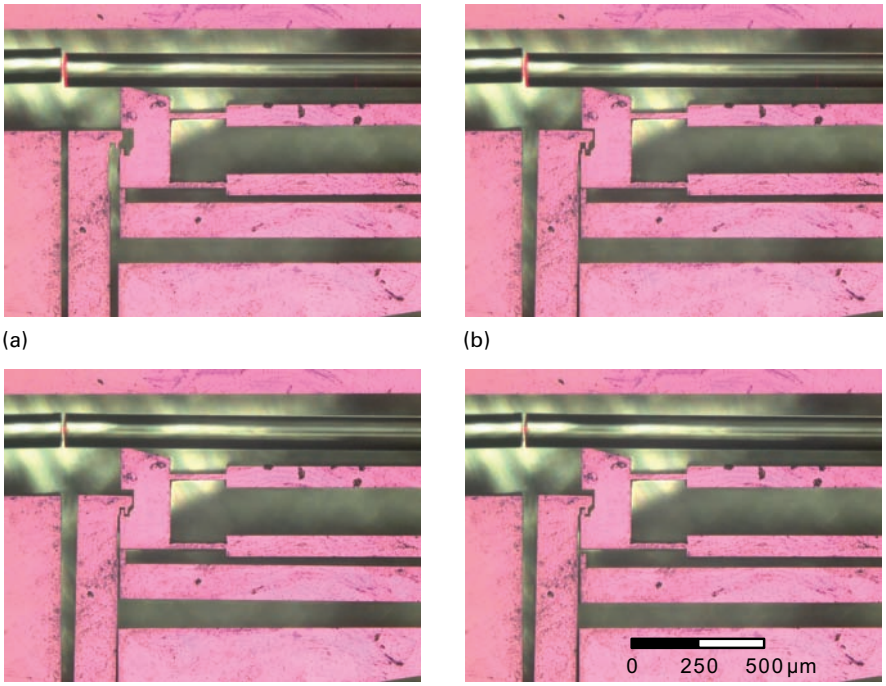

Figure 7.10 Fibre positioning and clamping sequence: (a) position without power including inserted fibre; (b) actuation of the clamp; (c) moving the fibre to the desired position; (d) engaging the clamp by powering down the voltage followed by powering down the positioning actuator. The fibre remained aligned without power.

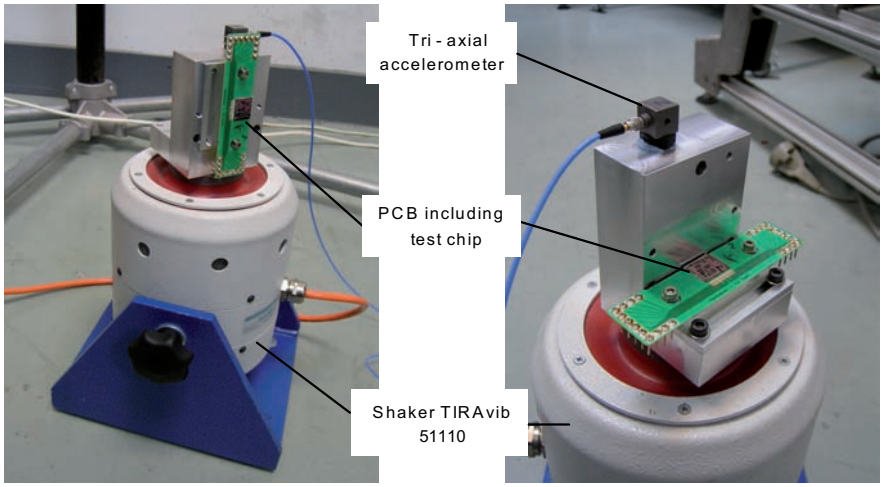

Figure 7.11 Vertically placed shaker with mounted PCB including test chip, in vertical (left), and in horizontal position

was observed after the experiments, indicating that the device will not be affected by vibrations that might be experienced under working conditions.

7.5 Thermal modelling

As for the in-plane actuators discussed in Chapter 4, for the devices presented in this chapter also the electrical, thermal, and mechanical behaviour and their coupling was modelled. Comsol Multiphysics^{TM} Finite Element (FE) modelling software was used, which enabled easier incorporation of temperature-dependent heat convection and radiation contributions. To investigate the temperatures in the actuators, the FE model was adjusted to match the fabrication parameters. In order to avoid possible unwanted high-temperature effects in the actuators leading to unpredictable behaviour, the temperatures in the actuators needed to remain below 870 K, as discussed in Chapter 4.

The model was further simplified by using only 2-D geometries to significantly decrease calculation time. As for the modelling presented before, the thin polysilicon resistor layer was not modelled separately, instead an equivalent electrical resistivity for the bulk silicon was calculated, which was admissible since the Biot number for the cross-section of the structures was much smaller than unity. In general, the electrical resistivity is strongly dependent on temperature and differs depending on the doping type and level. With a phosphorous doping concentration of approximately 10^{20} atoms/cm^3 in the polysilicon resistor layer, the equivalent electrical resistivity over the bulk silicon cross-section was calculated to be 3.0×10^{-3} $\Omega\cdot$m at room temperature. A linear expression for the electrical resistivity as a function of temperature was used to fit the modelled resistance to the measured values, which was determined to be adequate for these simulations. The thermal conductivity and the thermal expansion coefficient of single crystal silicon are also strongly temperature dependent and their values were taken from Lide (2006) and Okada and Tokomaru (1984), respectively.

In addition to heat conduction through the solid material, conductive and convective heat transfer through air and radiation were included. Temperature dependent values of density and thermal conductivity of air were taken from Mills (1999), as well as formulas for the convection coefficient for macro systems, which were extrapolated to the micro domain. For the radiation estimation, the structures were modelled as gray bodies with an emissivity of 0.7 (Hickey *et al.* 2003, Mankame and Ananthasuresh 2001). For more detailed information about the modelling parameters and boundary conditions the reader is referred to Sassen (2007).

The resistivity and displacement curves were in agreement with the experimental data and therefore, the modelled temperatures were assumed to be correct. The modelled temperature of the positioning actuator at 35 V is shown in Figure 7.12. To determine the displacement a force was applied to the actuator tip equivalent to the force exerted on the fibre mechanism by the fibre. The maximum displacement of approximately 16.5 μm is comparable to the experimental result for the case of a 10 μm overhang presented in Figure 7.9. This displacement was achieved at less than the maximum temperature, indicating that the actuator could have been manufactured more compactly.

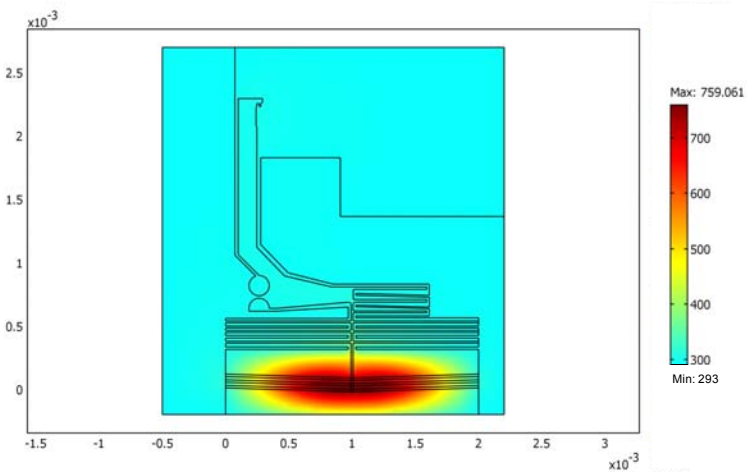

Figure 7.12 Temperature plot of modelled positioning structure at 35 V (in kelvin)

The temperature level in the mechanical clamp was also investigated. The temperature profile at 41 V is shown in Figure 7.13. From this simulation, there is only a very small heat flow into the lever thanks to the cooling fins. The clamp design was optimized such that the modelled vertical position shift upon cooling was zero. The required 35 μm horizontal displacement for passing the tooth is achieved at approximately 760 K, which is sufficiently below the allowable temperature of 870 K.

From Figure 7.12 and Figure 7.13 it can be seen that the heat induced zones remain very local, so, based on these results, thermal crosstalk is not expected. This was supported by the measurements, during which also no effects of crosstalk were observed between the individual components.

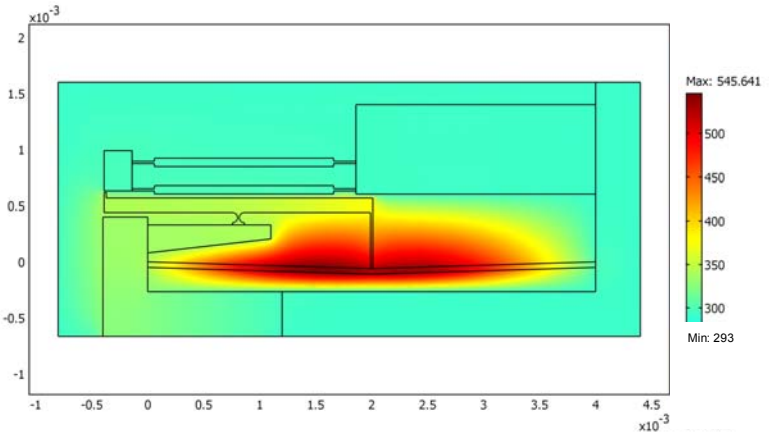

Figure 7.13 Temperature plot of modelled clamping structure at 41 V (in kelvin)

7.6 Consequences for the coarse assembly

When taking a broader look at the positioning and clamping functionality presented in the previous sections, it can be understood that they have a high potential of being combined with the laser diode attachment area in the same chip. The position of the fibre in a shallow V-groove with the tip pointing slightly upwards due to the force from the fibre mechanisms, enables the fibre tip to rise above the chip surface. This allows the active-side down placement of the laser diode on the top surface of the chip with the laser facet nominally aligned with the centre of the positioning window, as is schematically shown in Figure 7.14.

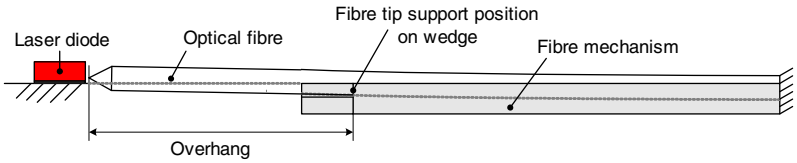

Figure 7.14 Schematic fibre overhang: side view of fibre mechanism

This means, that if the processing steps for creating the positioning and clamping functionality can be combined with those for the metal layers for the LD attachment, the silicon base part and the positioning chip can be integrated into a single silicon chip. This would result in the presence of

only a single component between the laser diode and the fibre. In Figure 7.15 an impression of the resulting simplified device layout is shown.

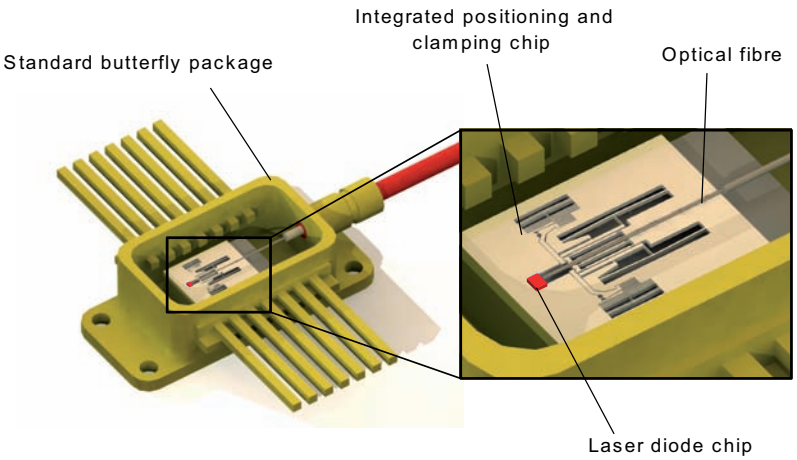

Figure 7.15 Schematic impression of fibre coupled laser diode package with integrated MST-based 2-D fibre positioning and fixation functionality in single silicon chip supporting both fibre and LD

This configuration was already identified in earlier chapters as being highly favourable, for its significantly reduced tolerance build up in x and y direction. Consequently, a significant reduction of the required fibre tip displacement range could be achieved, from 13.5 × 17.5 μm to 6.5 × 9.5 μm (see Section 5.4). This allows considerably reduced positioning actuator ranges and forces, and thus also smaller actuators. Because initially the emphasis in the development of the positioning and clamping functionality was primarily on verifying their manufacturability and whether they could function, this was realized in a relatively late stage of the project, and the positioning requirements were not adapted accordingly. Since the minimum tooth overlap and the clearance for the teeth to pass each other remain unaltered, the positioning actuator range is decreased somewhat less but still significantly, from 20 μm to 13 μm. The fabrication gap between actuator tip and fibre mechanism is reduced from 13 μm to 10 μm. The positioning force is also decreased, from 10 mN to a little over 5 mN. This reduction of actuator range and force could for example be achieved with a significantly smaller V-beam actuator of only 2500 μm long and 30 μm wide.

The clamping actuation range remains unchanged because this depends only on fabrication possibilities. However, due to the reduced positioning range, the clamping force can also be decreased. The maximum holding force in positioning direction is reduced from 3.5 mN to approximately

2 mN, resulting in a clamping force on the fibre mechanism normal to this direction of around 13-14 mN. This is slightly more than half of the initial clamping force of 25 mN, both calculated with an assumed worst-case friction coefficient of 0.15.

In addition, qualitative clamping experiments showed that at much lower clamping forces the clamps could still maintain the fibre mechanisms in place. Although additional tests should be performed to investigate the performance of the clamps at these lower clamping forces, this indicates that, indeed a higher friction coefficient can be used for calculating the required clamping force normal to the positioning direction. In any case, less stiff clamping mechanisms could be employed, with significantly reduced power consumption - and therefore, heat dissipation, which may allow for a reduction in clamp actuator area, by reducing or even eliminating the cooling fins between the lever and the actuator. Combined with the reduced size of the positioning actuators, this may quite easily result in a reduced chip area of 4 × 5 mm, a reduction of 33%. For comparison, the main parameters for the used configuration with separate base part and positioning chip and the adapted configuration with simplified device layout are summarized in Table 7.1.

	Used configuration with separate base part and positioning chip	**Adapted configuration with simplified device layout**
Fibre positioning range	13.5 × 17.5 µm	6.5 × 9.5 µm
Fabrication gap	13 µm	10 µm
Positioning actuator range	20 µm	13 µm
Positioning actuator force	10 mN	5 mN
Positioning actuator dimensions	4000 × 50 µm	2500 × 30 µm
Clamping force	25 mN	13-14 mN
Chip area	5 × 6 mm	4 × 5 mm

Table 7.1 Comparison main parameters internal assembly functionality used and simplified LD-fibre configuration

7.7 Discussion

The measurement results indicate that the presented mechanical clamping concept can be successfully applied for powerless clamping of the fibre in

cooperation with the concept for 2-D fibre positioning presented in the previous chapter.

The developed clamp was able to take over and indirectly hold the fibre in position, by applying a clamp force on the fibre mechanism, intended for use as intermediate body for in- and out-of-plane positioning of the fibre tip. Powering down the clamping actuator and positioning actuator showed an average shift in fibre position of less than 0.1 μm. No visible shift in clamping position was observed after a series of vibration tests. Therefore, the final position was assumed to be stable. Clamping was adequately fast, allowing alignment to be performed in a matter of seconds.

Since clamping could only be investigated in combination with 1-D fibre positioning, additional investigations should be performed on combined 2-D fibre positioning and clamping to verify their joint performance. Problems such as thermal crosstalk are not expected based on the obtained modelling and test results. During the measurements, no crosstalk was observed between the individual functions in the same chip.

The positioning and clamping functionalities can most likely be further optimized, based on a simplification of the device layout, allowing for a decrease in tolerance build up between laser and fibre. It is expected that with minor modifications of the processing, the laser diode can be placed directly on the positioning chip instead of on a separate substrate, as was assumed to be necessary before having decided upon the exact positioning and fixation layout. A smaller fibre positioning window is then allowed, and consequently also smaller actuator ranges and forces. Accordingly, the device can be made significantly more compact, thereby considerably reducing cost (see also Section 8.2). This example clearly confirms the importance of concurrently taking all relevant aspects in the PIAF design process into account in order to achieve the best possible overall result.

In this chapter, besides mechanical clamping we have discussed the two other most promising methods for fine fixation as part of the PIAF concept: soldering and adhesive joining.

Adhesive joining is the most versatile of the three methods. However, typically the achievable fixation accuracy and long-term stability of the other two methods are better. Mechanical clamping, if carefully applied, may provide the best accuracy and long-term stability, most likely at the expense of a larger required building space and higher development effort. When mechanical clamping is selected, it is preferred to integrate the clamp functionality with the positioning chip to reduce fabrication cost and to prevent the need for additional assembly steps.

Compared to mechanical clamping, which is considered more suited for in-plane use, soldering and adhesive joining are more suitable for use out-of-plane relative to the positioning chip surface. For most solder and adhesive bonds, the gap height direction is usually difficult to control. It is best not to let this direction coincide with one of the fine positioned directions, since these are generally the directions having the tightest positional tolerances. For mechanical clamping, the most convenient clamp direction is generally also perpendicular to the fine positioned directions. As a consequence, besides on the specific accuracy and stability requirements, the choice of fixation method is dependent on the orientation of the fine positioning directions relative to the positioning chip surface.

8

Conclusions and outlook

In this chapter, the main conclusions are presented regarding the investigation of the technical feasibility of applying MST-based product-internal assembly functions for the selected fibre coupling case.

Additionally, in Section 8.2, a limited assessment is presented of the economic viability of PIAF applied to this specific case, after which is zoomed out to discuss the potential of the PIAF method for possible other applications in Section 8.3. Finally, this chapter is concluded with suggestions for further research in Section 8.4.

8.1 Conclusions

The conclusions of this work are organized following the main research questions presented in the introductory chapter of this thesis.

Technical feasibility MST-based PIAF for fibre coupling

Based on the results presented in Chapter 6 and 7, it can be concluded that it is technically feasible to employ MST-based product-internal assembly functions for accurate assembly of an optical fibre with respect to the laser diode in the considered product case. Although some of the desired features could not be achieved, such as relaxed coarse assembly requirements in all directions and a maximum width of 250 μm for potential use in a fibre array, integrated MST-based functionality was successfully created for 2-D fibre positioning and powerless clamping at arbitrary positions in a 25×40 μm diamond-shaped positioning window perpendicular to the optical fibre

axis. In addition, positioning resolutions and fibre position shifts upon clamping both smaller than 0.1 μm were obtained, thereby meeting all requirements for the main performance aspects.

The developed internal assembly functionality was application specific. Their working principle was based on specific characteristics of the fibre (mainly its length and bending flexibility) and the structures were mostly non-standard, requiring quite considerable engineering effort.

Portion of assembly functionality performed internally and its level of integration with the overall system

Fibre tip positioning was restricted to the two most critical directions - the two translations perpendicular to the fibre tip - to keep the complexity manageable, although this meant that the required coarse assembly accuracy in the longitudinal direction was still relatively strict. Fine fixation was performed product-internally, based on the expected superior fixation accuracy of the selected MST-based mechanical clamping method compared to other available methods for fine fixation. Position sensing was performed externally, since it was too challenging to include this in the internal assembly functionality. However, this was not considered problematic for application of PIAF for this case.

The internal assembly functionality was integrated with the overall system in a hybrid way, due to the dissimilar functional and material requirements of the components. It was possible to replace the original parts supporting the laser and holding the fibre by silicon components in which the MST-based internal assembly functionality could be created, without too strongly affecting the primary device functionality.

Initially, a configuration was selected having two discrete silicon components in the mechanical link between laser diode and optical fibre, one to hold and fine position the fibre, and another to support the laser diode and the silicon positioning chip containing the fibre. This was chosen based on expected difficulties in process integration in case of combining these two components into one. The consequence of this choice was an increased position tolerance build up as compared to the ideal situation with only one silicon component between LD and fibre, requiring a larger fine positioning range, and therefore also a larger positioning chip area.

Only at a relatively late stage in the design process it was noticed that, despite the expectations, all internal assembly functionality most likely could have been integrated into a single chip, allowing for a significantly smaller fine positioning window. If this would have been realized in an earlier stage after defining the positioning concept and its associated processing steps, this could have been taken into account in the subsequent

development steps, reducing the overall development time. This example clearly indicates the importance of concurrently considering all influential factors in the PIAF design process in order to achieve the most timely and best possible overall result.

Coarse assembly of the optical components

In the proposed coarse assembly design, solder self-assembly and mechanical alignment features have been used to reduce the required initial placement accuracy for the assembly equipment, while still achieving sufficiently accurate coarse positioning of the laser diode and the fibre to enable fine positioning with acceptably small positioning ranges. In these methods, the required positioning accuracy is obtained from accurate MST-based alignment features in the positioning chip (and in the LD) that may be included at relatively low cost, since MST was also used for the internal assembly functionality.

The initial coarse placement requirements could be relaxed in all directions except the *z*-direction, in which the optical fibre could not be constrained at sufficient accuracy without risking damage to its tip. Therefore, in this direction still a relatively accurate positioning step was required, supported by visual feedback. Once in the desired longitudinal position, the fibre could simply be glued into a fixed V-groove in the positioning chip, aligned with the fibre tip contact areas of the fine positioning structures, resulting in well-defined fibre tip placement without risking damage to the fibre or the fine positioning structures.

Fine fibre tip positioning

MST-based electrothermal actuation was selected for fine positioning of the fibre, based on its relatively high attainable forces and displacements, and its simple construction, requiring no special materials. Although electrostatic actuation is also promising for internal fine part positioning, its attainable forces are too low for deflecting the fibre while maintaining a compact build up.

Two in-plane thermal V-beam actuators were combined with two wedge mechanisms for converting the actuator motions into in- and out-of-plane fibre tip movements. Although sliding between the fibre tip and the contact areas on the wedge mechanisms was unavoidable, fibre tip displacements in a diamond shaped positioning window of over 25 μm in-plane and more than 40 μm in the out-of-plane direction were shown with only a small visible hysteresis effect. Positioning resolutions smaller than 0.1 μm were measured, indicating that potential stick-slip due to the sliding of the fibre over the <111> surfaces was not a problem.

Final fibre tip fixation

Of the three most promising methods for fine part fixation as part of the PIAF concept - soldering, adhesive joining and MST-based mechanical clamping - mechanical clamping was selected for fixing the fibre tip. This choice was based on the superior fixation accuracy and the (potentially) favourable integration with the fibre positioning concept, since clamping could be performed in-plane using similar thermal actuators and mechanisms as employed for the positioning functionality.

The developed mechanical clamp was successfully tested for powerless clamping of the fibre with one half of the 2-D fibre positioning concept. The clamp was able to take over and indirectly hold the fibre in position, by applying a clamp force on the fibre mechanism perpendicular to its fine positioning direction. Powering down both clamp and positioning actuator (the latter could return unobstructed to its rest position without exerting force on the clamp) showed a fibre position shift of less than 0.1 μm. Furthermore, no visible shift in clamping position was observed after a series of vibration tests, indicating that the clamping function realises a stable final position. Clamping was adequately fast, allowing alignment to be performed in a matter of seconds. During the measurements, no thermal cross-talk was observed between the individual functions in the same chip.

8.2 Economic considerations

In order to assess the economic viability of the developed PIAF chip for LD to fibre alignment in an industrial setting, the cost of the novel PIAF alignment approach should be compared to that of presently employed assembly methods.

- For a full comparison, at least required are:
- production volume information;
- estimated unit cost of the PIAF chip;
- cost savings of the replaced components and process equipment;
- yield and cycle time information of the individual assembly processes.

Since most of this information cannot be estimated realistically, only a qualitative discussion is presented of the economic viability of the PIAF method applied to this case.

Estimated unit cost of the PIAF chip

The main contributors to MST device cost are development cost and production cost. Based on the low level of standardization, MST development

cost is generally high, typically in the order of 1 M€ (J.F.L. Goosen[1], personal communication, May 21, 2008), which should be divided over sufficiently large production quantities to result in reasonable unit costs.

In addition to development cost, production cost may also be quite significant. For example, with small wafer batches in the order of 50 to 100 wafers, fixed costs such as the cost for the mask sets and for setting up the process may lead to production costs in the order of several thousands of Euros per wafer. At higher production volumes, combined with relatively low processing complexity, the cost of a 150 mm wafer, which is standard in most commercial MST foundries, may remain below one thousand Euros.

Combined, unit prices range from fractions of a Euro to hundreds of Euros, depending on the chip size and the quantity produced. For our PIAF device, assuming a yearly production volume of 50,000 to 200,000 and 5 years of production, the estimated unit development cost would be in the range of € 1-4. Following, to obtain the production cost, the wafer production cost is divided by the number of good die on the wafer. With an estimated die size of 4×5 mm and a wafer diameter of 150 mm, over 600 die can be produced from a single wafer. Discarding yield loss, and estimating the wafer production cost at € 3000, the production cost per die is approximately € 5. Together with the development cost, this would result in a total estimated PIAF chip cost in the range of € 6-9.

Cost savings of the replaced components

Although including the PIAF chip seems an expensive addition to the laser device, as indicated above, compared to the overall device cost of well over a hundred Euros, it is still quite acceptable. According to Flanagan *et al.* (2003), who replaced laser welding for the fibre attachment by soldering, as was discussed in Subsection 7.1.1, savings in unit material cost of over € 35 per package can be obtained by elimination of the weld clip, weld platform, and fibre ferrule. Therefore, in the fibre coupling case, replacement by the PIAF chip in fact seems to *reduce* instead of increase the unit material cost.

Yield and cycle time

No yield and cycle time information is available about the PIAF method applied to the fibre coupling case. Based on the observed positioning reproducibility and the possibility to reapply the clamp if desired, the attainable yield is expected to be better than a process employing laser welding, which is still relatively difficult to control. In addition, both positioning and

[1] Assistant professor Microsystems and Microfabrication, Delft University of Technology.

clamping were adequately fast, allowing alignment to be performed in a matter of seconds. Therefore, the achievable cycle time is expected to be shorter than the cycle time reported for laser welding by Mobarhan *et al.* (2000) discussed in Chapter 3.

The above information seems to indicate that the PIAF method may be economically viable for application in this case, given sufficiently large production volumes. As mentioned earlier, this indication is only based on partial information, and conclusive statements cannot be made here.

8.3 Broader PIAF application potential

Up to this point, we have considered the PIAF method in the context of the specific fibre coupling case. Based on the insights gained, in this section an attempt is made to consider the broader application potential of the PIAF method for micro-assembly, both from technical and economic perspective.

The applicability of the PIAF method is on one side dependent on the technical possibilities of the internal functionality that can be created, and on the other on the specific technical demands for potential PIAF cases.

Technical possibilities of applying PIAF

Starting with the technical possibilities, we have learnt that both the attainable number of degrees of freedom that can be actively controlled as well as the attainable actuation ranges using MST-based functionality are rather limited. From force perspective, the considered case with its high fibre tip positioning forces was very specific. Generally for discrete components much smaller forces in the μN range will be required, which is not considered challenging for most MST-based actuators. However, sufficiently robust structures should be created *e.g.* to withstand external component placement forces, practically excluding the use of fragile surface micromachined structures with typical structural heights in the order of a few μm. Based on the results presented in this thesis, achieving useful actuation in more than two degrees of freedom with translations of over a few tens of microns is considered very challenging.[1] Larger actuation ranges are possi-

[1] Theoretically, in certain situations it may be possible to move not only one component, but for example two components with respect to each other, in order to achieve *relative* positioning in a higher number of directions. However, this option is not considered very likely, based on the significantly higher expected complexity of this approach.

ble, but generally at the expense of higher cost, due to the larger chip area required for the actuation structure.

With regard to sub-μm fine fixation, quite promising methods are available that may each be applied advantageously in specific situations, such as different orientations with respect to the positioning chip surface. However, as accuracy requirements in the most critical directions approach 0.1 μm, only a few fine fixation options are eligible.

Most challenging is the internal sensing for position feedback. This is not considered crucial for application of the PIAF method in the case considered in this thesis. On the other hand, this does entail that fully self-assembling, '*plug-and-play*'-like, PIAF modules are not easily created, and that continuous position control during product life is less likely than final fixation after positioning.

As we have seen, a technical limitation can be in the coarse assembly process, which may influence the economical applicability of the method. If high accuracies are required in more directions than can be fine positioned, ideally the position accuracy is obtained from accurately defined features in the parts to be mated. If this is not possible, as was observed in the longitudinal fibre direction, then more accurate and expensive coarse assembly must be used, negatively influencing the cost-effectiveness of the overall assembly procedure.

In the fibre coupling case, two aspects were relatively advantageous that may provide more difficulties in other cases:

- packaging was straightforward;
- the fibre length and flexibility allowed simple tip positioning in combination with permanent coarse fibre fixation.

The laser housing did not require adaptations for protection of the PIAF chip. However, one could imagine that in other situations a redesign of the package would be required, which may be challenging, particularly if interaction of the assembled component with the environment is necessary.

As explained in Chapter 6, the fibre flexibility allowed fibre tip positioning using two independent simple 1-D positioning mechanisms with sliding fibre contact, in combination with permanent coarse fibre fixation. For positioning discrete, rigid components in multiple directions this cannot be used. The most likely option is to create a structure inside the positioning chip onto which the component is permanently fixed, capable of performing multiple, independently controlled, motions for positioning the component. This is more difficult than realizing a number of independent 1-D positioning mechanisms. Therefore, applying PIAF in more than one direc-

tion for discrete, rigid components is expected to be more challenging than for the fibre coupling case.

Potential demand for PIAF application

Thus far, no examples are known of the PIAF method being carried out on commercial products. Future demand for application of this method is expected in products requiring accurate assembly of micro-parts, and that have sufficiently large volumes to justify the high non-recurring MST development and production cost. We have seen that positioning accuracies between directly connected components in the order of one to a few μm can be achieved using passive alignment features, which are generally easier implemented than active internal positioning functionality. Therefore, it is logical that the use of PIAF is mainly limited to products requiring sub-μm positioning accuracies in up to a few directions. Production volumes should at least be in the 10 to 100 thousands per year, depending on the allowable unit cost.

In addition to telecommunications, and other optical domains, applicability may be expected in areas such as consumer electronics and the automotive industry, potentially stimulated by the increasing employment of MST-based functionality in these domains. Although not necessarily being high-volume markets, also in bio-medical instrumentation and in high-end professional equipment, opportunities for application of this method could be expected.

As almost all PIAF examples in literature are from the optical domain, it is very difficult to predict which and how many degrees of freedom would be desirable to be internally positioned in possible applications from other domains. In practice, generally not all directions are equally critical, so most likely 6-D internal positioning is not necessary. For fibre tip manipulation, mostly devices capable of performing two orthogonal translations are shown. However, even from these examples it is difficult to infer what would ideally be desired, because they are limited by technical possibilities, as was also observed in our case investigation. All these considerations reduce trying to predict in which directions PIAF could be desired to guesswork.

Aside from a low awareness of the PIAF method, a number of aspects have been identified that could potentially impede proliferation of this method. The most important are the high required MST development expertise and the availability of alternative assembly methods.

Many companies who may wish to employ MST-based PIAF have no capability or expertise in micro fabrication technology. Currently, for designing a MST device a high level of fabrication knowledge is required in order to

create a successful design. Often the development of MST devices requires a significant dedicated research effort to find a suitable process sequence for its fabrication. However, as mentioned, the fact that composed products are increasingly equipped with MST-based components for their primary functionality, may be considered positive for the applicability prospect of the method in the longer term.

Compared to available alternative assembly methods, the PIAF method may involve more design adaptations to the primary device, which could be seen as complicated, particularly when the product and production development are executed in different departments or even in entirely separate companies.

In addition, the innovative character of the PIAF method combined with the high MST development effort may be seen as a high economical risk. Generally, unless the application for which PIAF is considered is totally new, there is an existing assembly process that the PIAF method attempts to replace. Only if this or potentially other conventional, seemingly less complicated, methods do not provide the desired performance, the willingness arises to look beyond the familiar and focus on less well-established methods, such as by PIAF.

Lastly, the addition of costly functionality into the product to reduce the overall production cost is rather counterintuitive. Therefore, accurate cost calculations may be required to convince potential users of the benefit of the method. These calculations are not easily made, because usually most of the required information cannot be estimated realistically.

8.4 Suggestions for further research

Recommendations for additional investigations are provided on two levels:

- on case level regarding possible further device development and testing;
- on a general level concerning applicability of the PIAF method.

On case level, additional investigations should be performed on the combined functions to verify their joint performance. It is recommended to fabricate the optimized 2-D fibre positioning and clamping functionality integrated in a single chip, and to include solder metallization layers for LD attachment. This way, functioning assembled demonstrators may be realized including optical fibre that allow for testing of the position stability under Telcordia GR-468-CORE test conditions.

In addition, it is recommended to verify the level of out-of-plane bending of the fibre mechanisms resulting from the fibre pretension. This could

influence the fibre position when the mechanism position is taken over by the clamp.

To reduce the chip area, smaller actuators with comparable performances are desired. Improved electrothermal in-plane V-beam actuator configurations, which were developed in the context of this research project and that may be here considered are presented in Sassen *et al.* (2008). Additionally, it may be investigated if the actuators could be safely powered up to higher temperatures than here reported (see Chapters 4 and 7).

Finally, despite adhesive bonding was not selected for the fine fixation, it may be attractive, either as safety measure by adding adhesive for definitively securing the clamp, or as a *replacement* of the mechanical clamps. Both options are recommended for further investigation. In the latter option, the adhesive could be applied in-plane between the fibre mechanism end faces and opposing parallel surfaces fabricated in the chip substrate, with the gap height normal to the motion direction of the fibre mechanisms. In this orientation, moderate adhesive shrinkage theoretically does not affect the fibre mechanism position, and much smaller chip area is required than with mechanical clamping. A careful design of the joint, however, is needed to ensure meeting the alignment demands.

On a general level, it is important for increased applicability of the PIAF method that the performance and design flexibility of MST-based actuators is improved. In particular the limited possibilities for multiple degree of freedom positioning functionality in a single chip are a restriction for employment of the PIAF method. This issue can only be addressed by developing novel MST-based fabrication technologies.

Increased actuator performance is both dependent on fabrication and geometric design. The level of standardization in geometric actuator design is quite low, resulting in significant design effort to create actuators with acceptable performances. By increasing the number of available actuator 'building blocks' having more or less standardized dimensions, and that may be tailored to a specific need, this design effort may be reduced quite significantly. Similarly, the increased availability of geometric optimization methods may aid the MST design process in the future. Unfortunately, *topology optimization*, despite being a popular research area in the past years, is still far from practically applicable *e.g.* for electro-thermo-mechanical design cases such as presented in this thesis (M. Langelaar[1], personal communication, March 26, 2007).

[1] Assistant professor Design Optimization, Delft University of Technology.

In addition to applicable actuator examples, additional PIAF implementations should be realized as they may serve as examples for designers contemplating its use in similar product cases. Although internal assembly functionality is generally case specific, successful example implementations may provide valuable insights as well as concrete ideas for implementation. It would be interesting to investigate a product case in which PIAF including fine positioning functionality in at least two directions is applied for assembling a discrete, rigid micro-part. This is considered particularly useful because of the distinctly dissimilar characteristics of such a part compared to those of the optical fibre considered in the presented research. Possibly the fibre coupling case as was studied in this research, but with in- and out-of-plane discrete lens positioning instead of fibre tip positioning, is a suitable product case for consideration.

A

Process flows and mask layouts

A.1 Short process flow first demonstrator series (DIMES identification code WB1241)

In this section a short process flow description is provided for fabrication of the in-plane actuation structures presented in Chapter 4. For a brief process description the reader is referred to Section 4.4 and the schematic fabrication sequence is shown in Figure 4.4.

Front side design: (4 ASM masks)

- PS, CO, IC, RIE (polysilicon definition, contacts, metallization and Si RIE etching)

Back side design (1 full wafer mask)

- KOH (to define the 120 μm thick structures, *i.e.* to etch ~ 405 μm of bulk silicon)

Starting material: (100) **n-type** and **p-type** Si wafers with measured thickness (525 μm thick ± 2 μm)

Front side processing (based on DIMES-03)

ZERO layer for ASM wafer stepper and for ELVIS: all wafers

- Coating and baking (resist thickness: 1.4 μm)

- Litho job: Sensor/ ZEFWAM , masks FWAM (alignment marks for ELVIS) + COMURK (alignment marks for ASM/ DIMES-03)
- Development
- Dry etching of silicon (Trikon Omega 201 plasma etcher, etching depth: 200 nm)
- Cleaning procedure (oxygen plasma and HNO_3 based cleaning)
- Thermal oxidation 300 nm
- LPCVD low stress SiN: 300 nm

Poly Si Resistors implantation (n-type wafers):

- LPCVD low stress poly: 300 nm
- Boron implantation: B^+, 40 keV, $1.0\times10^{16}/cm^2$
- Cleaning procedure (HNO_3 based cleaning)
- Coating and baking (resist thickness: 1.4 μm)
- Alignment and exposure: **mask PS** (litho job MA6×6)
- Development
- PolySi dry etching Drytek 384T plasma etcher (stop on nitride)
- Cleaning procedure (oxygen plasma and HNO_3 based cleaning)
- LPCVD TEOS oxide: 300 nm
- Anneal: 1000°C, 35 min, in Ar)

Poly Si Resistors diffusion (p-type wafers):

Follow CMOS flow chart

- LPCVD low stress poly: 500 nm
- Phosphorous diffusion ($POCl_3$ source, 950°C, 42 min)
- Oxide stripping (BHF, 30 s)
- Cleaning procedure (HNO_3 based cleaning)
- Coating and baking (resist thickness: 1.4 μm)
- Alignment and exposure: **mask PS** (litho job MA6×6)
- Development
- Poly dry etching Drytek 384T plasma etcher (stop on nitride)

- Cleaning procedure (oxygen plasma and HNO_3 based cleaning)
- LPCVD TEOS oxide: 300 nm

Contact windows and metallization: all wafers

- Coating and baking (resist thickness: 2 μm)
- Alignment and exposure: **mask CO** (litho job MA6×6)
- Development
- Plasma etching of oxide (stop on poly): Drytek 384T plasma etcher
- Cleaning procedure (oxygen plasma and HNO_3 based cleaning)
- Dip etching (HF 0.55%, 4 min)
- Metallization: TRIKON SIGMA sputter coater 0.6 μm Al/1%Si @ 350°C
- Coating and baking (resist thickness: 1.4 μm)
- Alignment and exposure: **mask IC** (litho job MA6×6)
- Development
- Plasma etching of metal: Trikon Omega plasma etcher, platen temperature 25°C + aluminium fence removal
- Cleaning procedure (oxygen plasma and HNO_3 based cleaning)

Backside processing:

Membrane definition:

- Coating and baking (resist thickness: 1.4 μm)
- Alignment and exposure: ELVIS : **mask KOH**
- Development
- Dry etching of silicon nitride Drytek 384T plasma etcher: stop on silicon
- Cleaning procedure (oxygen plasma and HNO_3 based cleaning)

Front side processing:

Silicon etching from front side:

- PECVD oxide: 2 μm
- Coating and baking (resist thickness: 3 μm)
- Alignment and exposure: **mask RIE** (litho job MA6×6)

- Development
- Plasma etching of oxide + nitride + oxide: Drytek 384T plasma etcher (stop on silicon)
- Cleaning procedure (oxygen plasma and HNO_3 based cleaning)
- Alloying: 400°C, 50 min

Backside processing:

Membrane etching:

- Silicon etching in KOH (33wt% @ 85°C): ~ 405 μm, 120 μm left
- Cleaning procedure (HNO_3 based cleaning)

Front side processing:

Structures release:

- DRIE of silicon from front side (120 μm) until etch through of structures (ADIXEN, oxide or resist layer on the back as stop layer)

A.2 Schematic mask layout WB1241

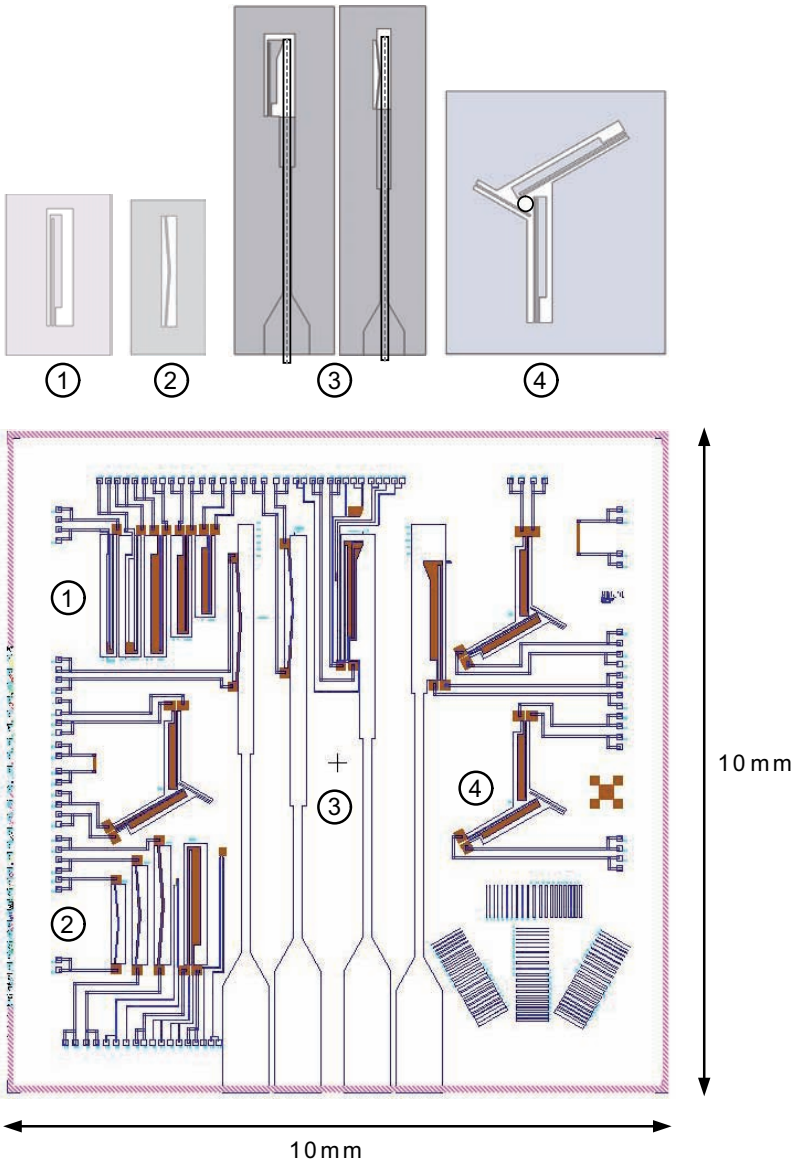

Figure A.1 Schematic mask layout of the first test chip containing in-plane moving actuators and various other test structures (in gray (red in the digital version): polysilicon resistor structures that act as heater elements)

A.3 Short process flow 2-D positioning concepts (WB1345)

Front side design: (5 ASM masks +1 full wafer mask)

- PS, CO, IC, KOH1, RIE + RIE 2 (polysilicon definition, contacts, metallization, Si wet etching and Si RIE etching). Litho job MA4×4 (15 × 15 mm die) in a 4×4 layout. KOH1 defines the 100 μm deep grooves in which fibres are placed; RIE defines the 150 μm deep silicon microstructures.

Back side design (full wafer masks)

- KOH2 (to define the 150 μm thick structures, *i.e.* to etch ~ 375 μm of bulk silicon)

Starting material: (100) **p-type** Si wafers with measured thickness (525 μm thick ± 2 μm)

Front side processing

ZERO layer for ASM wafer stepper and for ELVIS

- Coating and baking (resist thickness 1.4 μm)
- Litho job: Sensor/ ZEFWAM , masks FWAM (alignment marks for ELVIS) + COMURK (alignment marks for ASM/ DIMES-03)
- Development
- Dry etching of silicon (Trikon Omega 201 plasma etcher, etching depth: 200 nm)
- Cleaning procedure (oxygen plasma and HNO_3 based cleaning)
- Thermal oxidation 300 nm
- LPCVD low stress SiN: 300 nm

Poly Si Resistors diffusion (p-type wafers):

Follow CMOS flow chart

- LPCVD low stress poly: 500 nm
- Phosphorous diffusion ($POCl_3$ source, 950°C, 42 min)
- Oxide stripping (BHF, 30 s)
- Cleaning procedure (HNO_3 based cleaning)
- Coating and baking (resist thickness: 2 μm)

- Alignment and exposure: **mask PS** (litho job MA4×4)
- Development
- Poly dry etching Drytek 384T plasma etcher (stop on nitride)
- Cleaning procedure (oxygen plasma and HNO_3 based cleaning)

KOH1 definition:

- 300 nm LPCVD SiN
- Coating and baking (resist thickness 2 μm)
- Alignment and exposure: **mask KOH1** (litho job MA4×4)
- Developing
- 600 nm LPCVD low stress SiN + 300 nm thermal oxide etching (Drytek 384T plasma etcher)
- Dry etching of polySi from backside (Alcatel GIR 300 Fluorine etcher)
- Cleaning procedure (oxygen plasma and HNO_3 based cleaning)
- Silicon etching in KOH (33wt% @ 85°C): 100 μm
- Cleaning procedure (HNO_3 based cleaning)

Contact windows and metallization: all wafers

- Coating and baking: spray coating (Electronic Vision) resist thickness 2 μm
- Alignment and exposure: **mask CO** (litho job MA4×4)
- Development: AZ 400 K 1:4
- Plasma etching of SiN (stop on poly): Drytek 384T plasma etcher
- Cleaning procedure (oxygen plasma and HNO_3 based cleaning)
- Metallization: TRIKON SIGMA sputter coater, 1 μm Al/1%Si @ 350°C
- Coating and baking: spray coating (Electronic Vision) resist thickness 3 μm
- Alignment and exposure: **mask IC** (litho job MA4×4)
- Development: AZ 400 K 1:4
- Plasma etching of metal: Trikon Omega plasma etcher, platen temperature 25°C + aluminium fence removal
- Cleaning procedure (oxygen plasma and HNO_3 based cleaning)

Backside processing:

Membrane definition:

- Coating and baking (resist thickness: 1.4 μm)
- Alignment and exposure: ELVIS : **mask KOH2**; development
- Dry etching of 600 nm silicon nitride + 300 nm oxide, Drytek 384T plasma etcher: stop on silicon
- Cleaning procedure (oxygen plasma and HNO_3 based cleaning)

Front side processing:

Silicon DRIE pattern definition:

- PECVD oxide (Novellus): 3 μm
- Coating and baking: spray coating (Electronic Vision)
- Alignment and exposure **mask RIE + RIE2** (mask RIE2 contains the overlapping RIE + KOH1 structure definitions) litho job MA4×4
- Development: AZ 400 K 1: 4
- Plasma etching of 3 μm PECVD oxide + 600 nm nitride + 300 nm oxide: Drytek 384T plasma etcher, stop on silicon
- Cleaning procedure (oxygen plasma and HNO_3 based cleaning)
- Alloying: 400°C, 50 min

Backside processing:

Membrane etching:

- Silicon etching in KOH (33wt% @ 85°C): ~ 375 μm, 150 μm left
- Cleaning procedure (oxygen plasma + HNO_3 based cleaning)
- Al/1%Si sputtering TRIKON SIGMA sputter coater, 500 nm @ 25°C (use special wafer holder with grooves)

Front side processing:

Silicon etching from FRONT SIDE:

- Plasma etching of silicon: 150 μm in Adixen
- Cleaning procedure (oxygen plasma + HNO_3 based cleaning)
- Strip Al stop layer (wet)
- Strip oxide from front side in BHF 1:7

A.4 Schematic mask layout WB1345

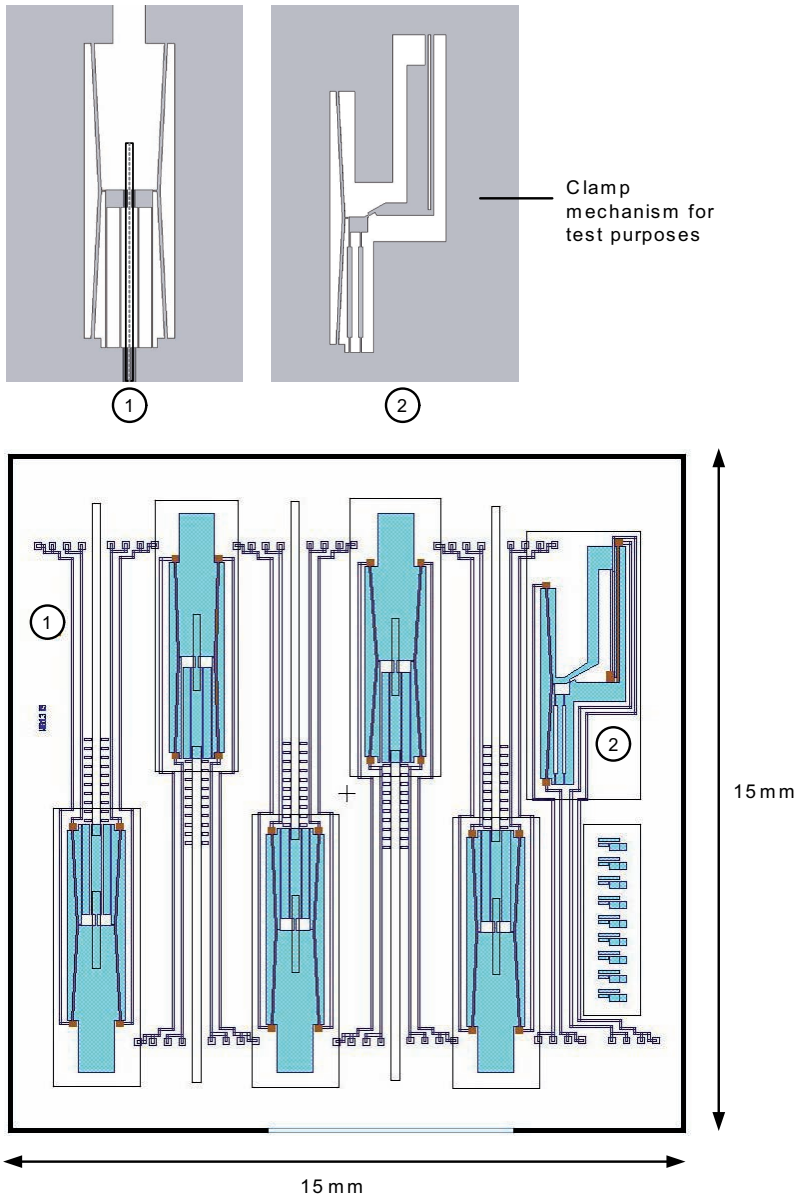

Figure A.2 Schematic mask layout of the second chip containing five geometrically different 2-D in- and out-of-plane moving actuators and a few other test structures

A.5 Short process flow clamp concepts (WB1406)

Front side design: (4 ASM mask)

- PS, CO, IC, RIE (polysilicon definition, contacts, metallization, Si RIE etching). Litho job MA4×4 (15 × 15 mm die) in a 4×4 layout. RIE defines the 150 μm deep silicon microstructures.

Back side design (1 Full wafer mask)

- KOH (to define the 150 μm thick structures, *i.e.* to etch ~ 375 μm of bulk silicon)

Starting material: (100) **p-type** Si wafers with measured thickness (525 μm thick ± 2 μm)

Front side processing

ZERO layer for ASM wafer stepper and for ELVIS

- Coating and baking (resist thickness 1.4 μm)
- Litho job: Sensor/ ZEFWAM, masks FWAM (alignment marks for ELVIS) + COMURK (alignment marks for ASM/ DIMES-03)
- Development
- Dry etching of silicon (Trikon Omega 201 plasma etcher, etching depth: 200 nm)
- Cleaning procedure (oxygen plasma and HNO_3 based cleaning)
- LPCVD low stress SiN: 300 nm

Poly Si Resistors diffusion (p-type wafers):

Follow CMOS flow chart

- LPCVD low stress poly: 500 nm
- Phosphorous diffusion ($POCl_3$ source, 950°C, 42 min)
- Oxide stripping (BHF, 30 s)
- Cleaning procedure (HNO_3 based cleaning)
- Coating and baking (resist thickness: 2 μm)
- Alignment and exposure: **mask PS** (litho job MA4×4)
- Development
- Poly dry etching Drytek 384T plasma etcher (stop on nitride)

- Dry etching of polySi from backside (Alcatel GIR 300 Fluorine etcher)
- Cleaning procedure (oxygen plasma and HNO3 based cleaning)
- LPCVD low stress SiN: 100 nm

Backside processing:

Membrane definition

- Coating and baking: resist thickness 1.4 μm
- Alignment and exposure: ELVIS: **mask KOH**
- Development
- Dry etching of 400 nm silicon nitride, Drytek 384T plasma etcher: stop on silicon
- Cleaning procedure (oxygen plasma and HNO_3 based cleaning)

Front side processing:

Contact windows and metallization

- Coating and baking: resist thickness 2 μm
- Alignment and exposure: **mask CO** (litho job MA4×4)
- Development
- Plasma etching of SiN (stop on poly): Drytek 384T plasma etcher
- Cleaning procedure (oxygen plasma and HNO_3 based cleaning)
- Dip etching (HF 0.55%, 4 min)
- Metallization: TRIKON SIGMA sputter coater 1 μm Al/1%Si @ 350°C
- Coating and baking (resist thickness: 1.4 μm)
- Alignment and exposure: **mask IC** (litho job MA4×4)
- Development
- Plasma etching of metal: Trikon Omega plasma etcher, platen temperature 25°C + aluminium fence removal
- Cleaning procedure (oxygen plasma and HNO_3 based cleaning)

Silicon DRIE pattern definition:

PECVD oxide (Novellus): 3 μm

Coating and baking: resist thickness 2 μm

- Alignment and exposure: mask RIE (litho job MA4×4)
- Development
- Plasma etching of 3 μm PECVD oxide + 300 nm nitride: Drytek 384T plasma etcher, stop on silicon
- Cleaning procedure (oxygen plasma and HNO_3 based cleaning)
- Alloying: 400°C, 50 min

Backside processing:

Membrane etching:

- Silicon etching in KOH (33wt% @ 85°C): ~ 375 μm, 150 μm left
- Cleaning procedure (oxygen plasma + HNO_3 based cleaning)
- Al/1%Si sputtering TRIKON SIGMA sputter coater, 500 nm @ 25°C (use special wafer holder with grooves)

Front side processing:

Silicon etching from FRONT SIDE:

- Plasma etching of silicon: 150 μm in Adixen
- Cleaning procedure (oxygen plasma + HNO_3 based cleaning)
- Strip Al stop layer (wet)
- Strip oxide from front side in BHF 1:7
- Cleaning procedure (oxygen plasma + HNO_3 based cleaning)

A.6 Schematic mask layout WB1406

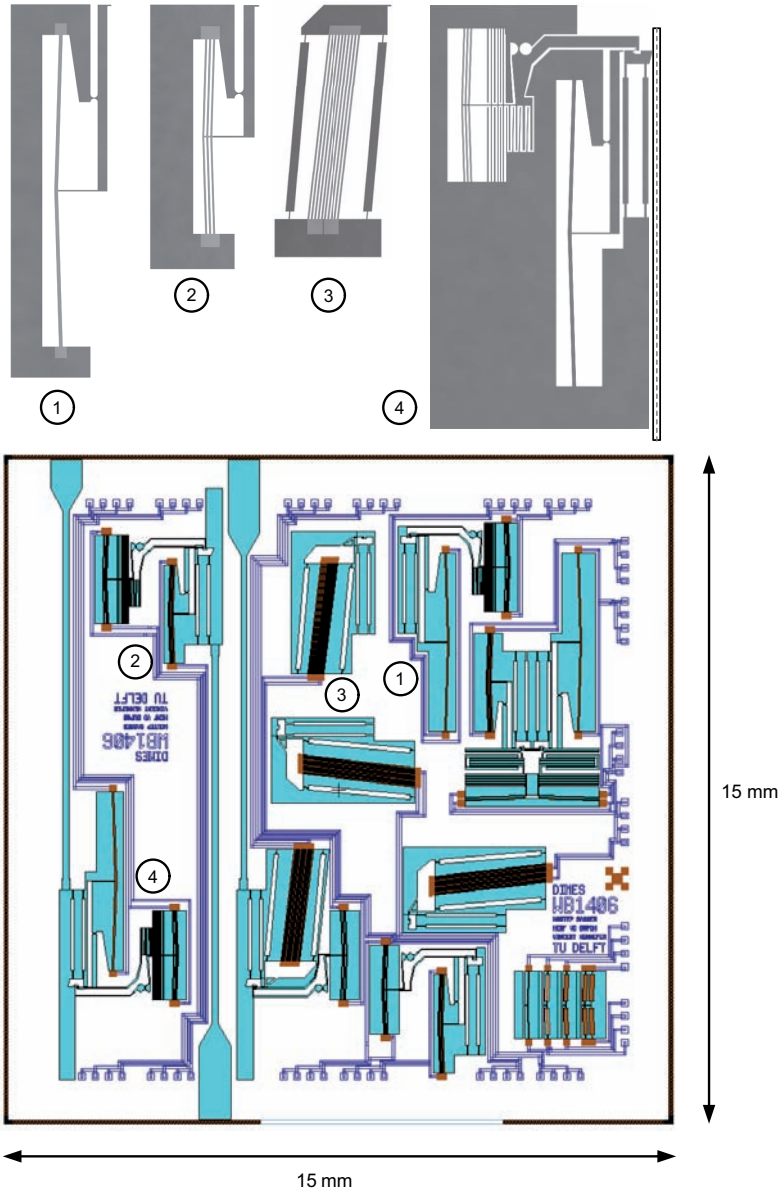

Figure A.3 Schematic mask layout of the third chip design containing various in-plane thermal actuation and clamp structures

B

Rejected MST-based thermal 2-D fibre positioning concepts

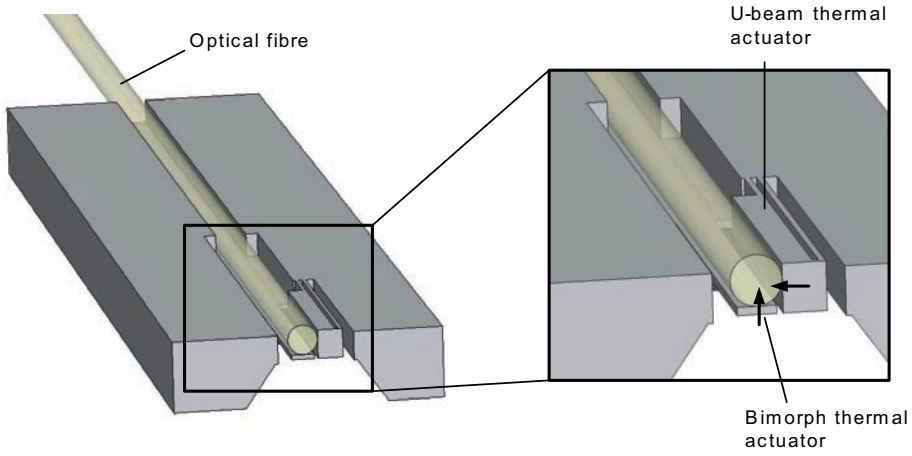

Figure B.1 Concept A. The fibre is inserted in a U-shaped groove and its tip is moved sideways by a U-beam or V-beam thermal actuator; vertical motion is performed by a bimorph thermal actuator with a metal layer on the bottom side.

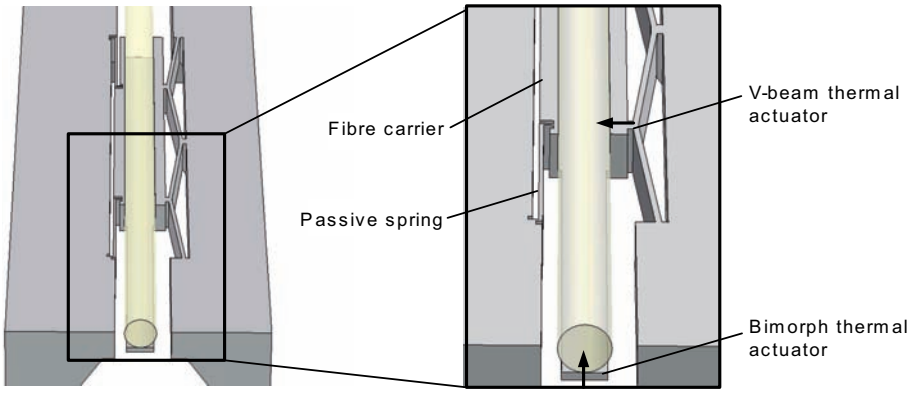

Figure B.2 Concept B. Similar to concept A, except for the sled supporting the fibre that is moved in its entirety, and therefore the relative fibre position on the actuator remains fixed.

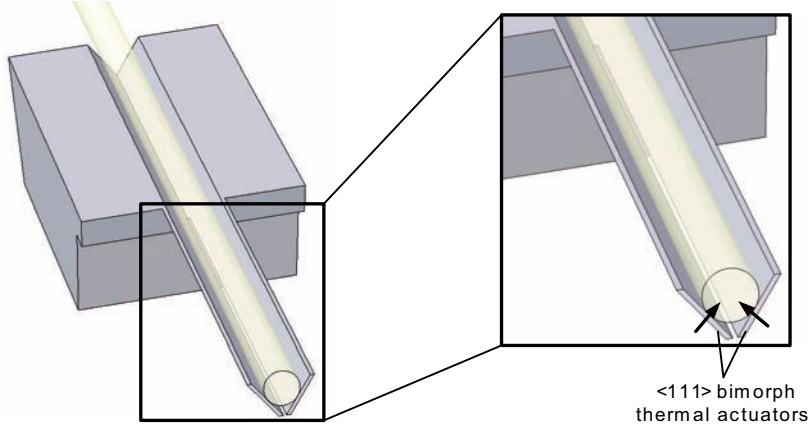

Figure B.3 Concept C. Two bimorph beams are oriented along the <111> crystallographic directions and can be actuated independently.

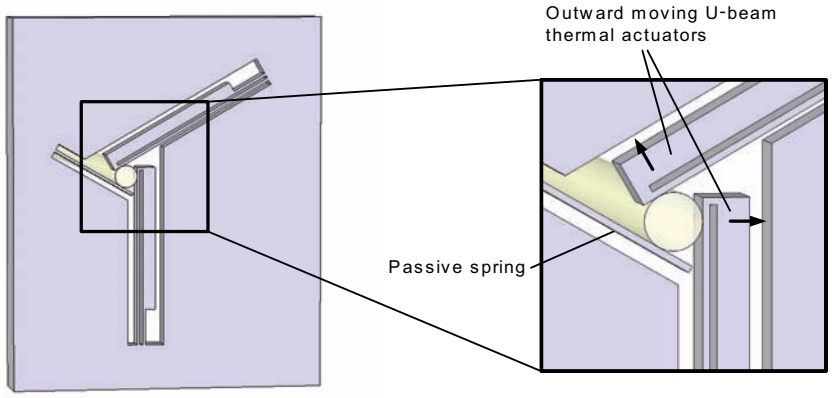

Figure B.4 Concept D. The fibre is clamped between two U-beam actuators and a passive spring. Upon heating, the U-beams move sideways, thereby releasing the preload in the spring. The fibre can be inserted with both actuators in fully deflected state. See also Appendix C.

Concept	Orientation	Actuators	Actuation direction	Relation fibre - end-effecter
A	In-plane	V-beam / U-beam Bimorph	In-plane Out-of-plane	Free (friction)
B	In-plane	V-beam Bimorph	In-plane Out-of-plane	Fixed
C	In-plane	Bimorphs	Out-of-plane	Free (friction)
D	Through-plane	U-beams	In-plane	Free (friction)

Table B.1 Comparison positioning concepts

C

Through-plane 2-D thermal fibre positioning concept

In the same chip as for the individual U- and V-beam actuators presented in Chapter 4, also a 2-D through-plane fibre positioning concept was included, which is schematically shown in Figure C.1.

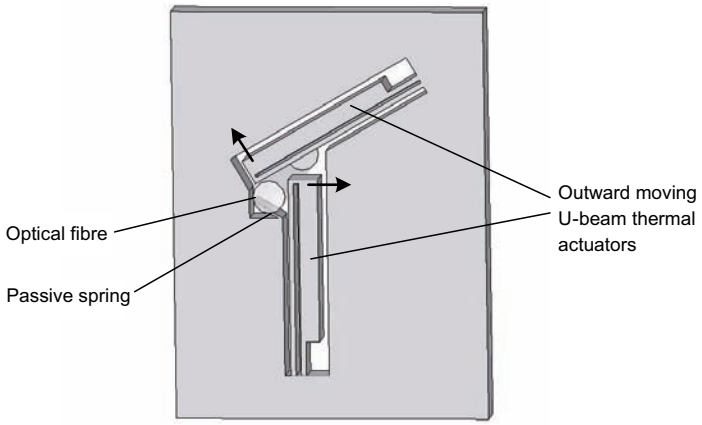

Figure C.1 Through-plane thermal 2-D fibre positioning concept

In this concept, the fibre tip is clamped between two U-beam actuators and a passive spring, each placed at a 60° angle relative to each other. Upon heating the U-beams move outward, thereby enlarging the triangular opening between the actuators and the passive spring. The fibre can be inserted with both U-beams in fully deflected state, and the fibre tip is clamped against the passive spring by decreasing the actuation voltages until the maximum passive spring preload is reached when the voltages are reduced to zero. Fol-

lowing, by independently moving the U-beam actuators, the fibre tip can be positioned in the chip plane while maintaining sliding contact with the passive spring and the sides of both U-beam actuators. The fibre tip position remains relatively well-defined as long as a non-zero spring preload is present to maintain contact between the fibre and both U-beam actuators.

In Figure C.2 an overview and a close-up SEM image are shown of one of the fabricated through-plane fibre positioning devices. The overall U-beam length was 1200 μm, and the passive spring had a length of 590 μm and a width of 20 μm, so that it theoretically possessed the same bending stiffness as the two U-beam actuators.

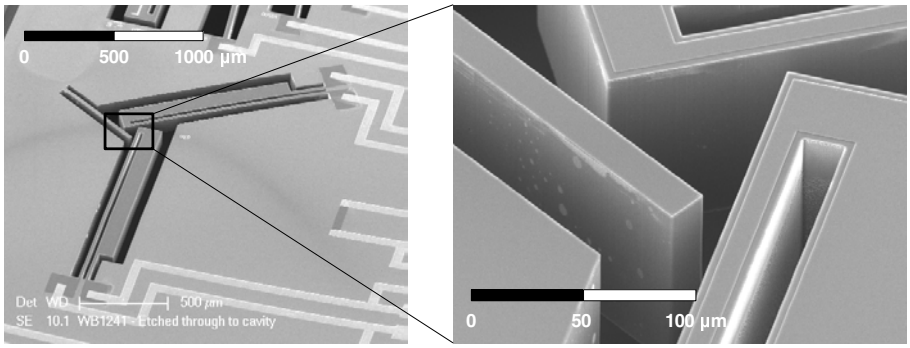

(a) (b)

Figure C.2 SEM images of the fabricated through-plane fibre positioning device, (a) overview image, and (b) close up of the fibre clamping opening, both at a 45° viewing angle

Tests were performed on a through-plane concept having a fibre opening with an inner diameter of 105 μm in rest position. By fully deflecting both U-beam actuators, the opening diameter could be enlarged to approximately 130 μm, allowing for insertion of a standard fibre having a 125 μm diameter. In Figure C.3 an overview and a close-up microscope image are shown of a through-plane concept with a successfully inserted optical fibre.

After insertion it was possible to position the fibre tip in a 2-D positioning window of approximately 10×10 μm. The movement was smooth, with no observable stick-slip during sliding of the fibre. Since only microscope observations were made, no detailed positioning information was obtained.

After the positioning tests, the fibre was taken out of the device and both the fibre surface and the actuator side walls were examined for possible damage; however no observable damage to the fibre or to the device was found. Although the device performance was quite good and scaling of the actuators is expected to render larger positioning windows, inserting the fibre

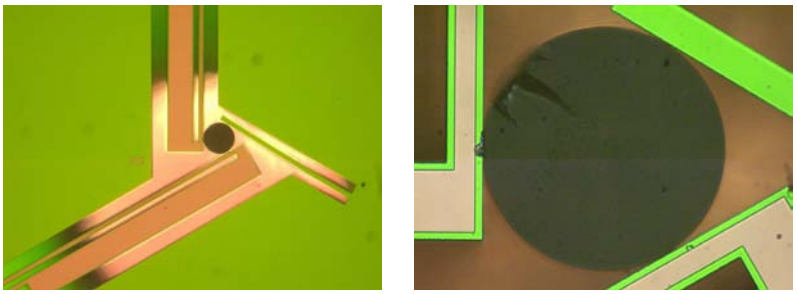

(a) (b)

Figure C.3 Top view microscope images of the through-plane concept including clamped 125 µm diameter optical fibre, (a) overview, (b) close-up

into the device was experienced to be highly challenging based on the limited depth of view of the microscope at the high magnifications required for this task. In a few instances even the passive spring or one or more of the actuators were broken due to the fibre being misplaced and pushing part of the silicon structures out of the chip plane until breaking occurred.

As discussed in Chapter 5, a through-plane build up was not selected due to its more complicated assembly and its lower potential for achieving an acceptably small tolerance build up, requiring the fine positioning travel ranges to be very large.

D

Equipment and experimental setup

(a)

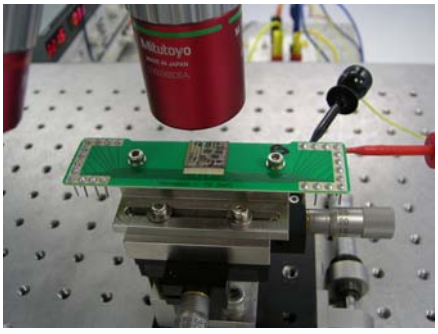

(b)

Figure D.1 Polytec MSA-400 Micro system analyzer, used for characterizing the in-plane displacement performance of the MST-based actuation structures (Polytec 2008)

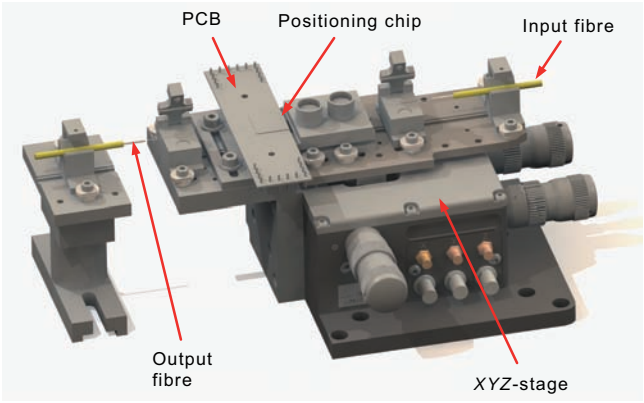

(a)

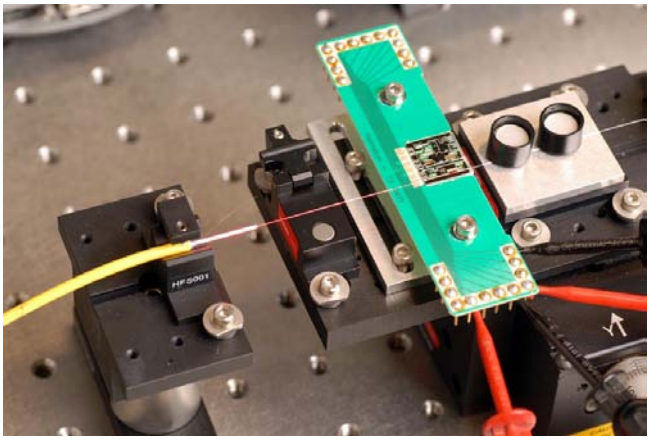

(b)

Figure D.2 (a) Thorlabs MAX311/M piezoelectric *xyz* micropositioning stage with mounted PCB including positioning chip and optical fibres. (b) Close-up of the test setup with positioning chip and optical fibres on the *xyz* positioning stage.

E

SEM images fabricated structures

E.1 First demonstrator series (WB1241)

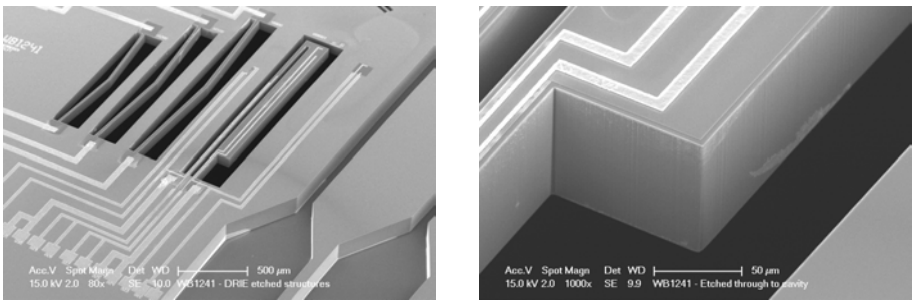

(a) (b)

Figure E.1 (a) SEM image of three V-beam actuators and one U-beam actuator; (b) detail image of the U-beam actuator close to its base

E.2 Second demonstrator series (WB1345)

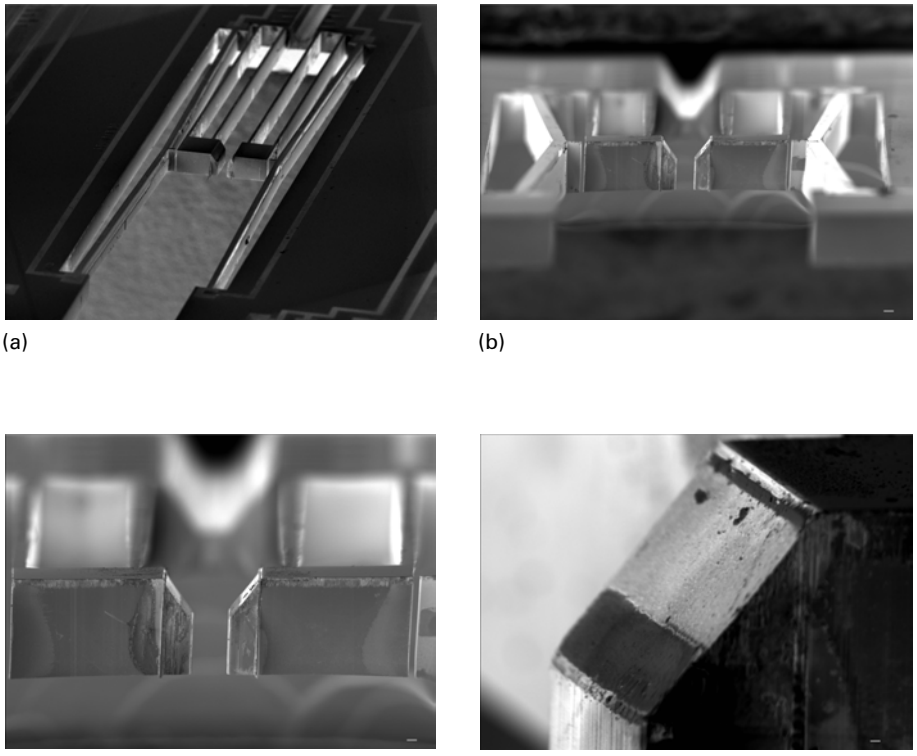

(a) (b)

(c) (d)

Figure E.2 Overview and detail SEM images of a fabricated 2-D fibre positioning device including <111> wedges for out-of-plane movement

E.3 Third demonstrator series (WB1406)

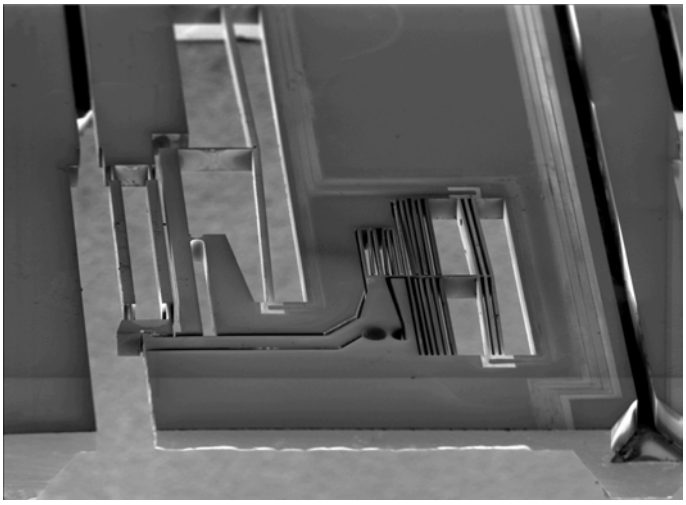

(a)

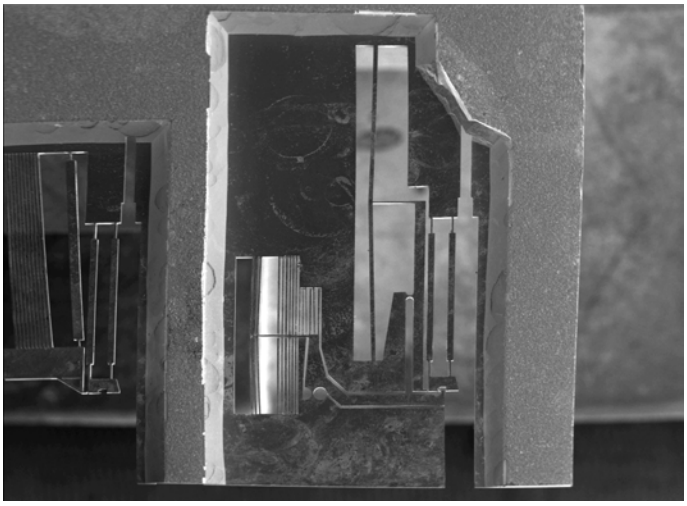

(b)

Figure E.3 Front side and back side views of one of the fabricated in-plane thermal actuation and clamp structures

F

Relevant student reports

Van den Bedem, S.P.W. (2004, Nov). *Design of a 2-DOF MST-based micro-positioning device for in-package optical fibre-chip coupling.* MSc Thesis, TU Delft, Internal report nr. PT 04.103.

- not selected alternative MST-based 2-D fibre positioning concepts;
- design first in-plane thermal actuator test chip.

Sassen, W.P. (2006, Jan). *Experimentation of thermal micro actuator performance.* Research assignment report, TU Delft, Internal report nr. PT 06.001.

- information experimental setup;
- description LabVIEW programmes for automated testing using fibre-to-fibre alignment.

Sassen, W.P. (2007, Apr). *Design and modelling of an improved MST-based 2 DOF positioning device.* MSc Thesis, TU Delft, Internal report nr. PT 07.009.

- design improved 2-D MST-based fibre fine positioning concept variants;
- engineering calculations and Comsol Multiphysics^{TM} FE models positioning functionality.

Van der Burgh, H.J. (2007, Apr). *Design of an MST-based mechanical clamp for in-package optical fibre-chip coupling.* MSc Thesis, TU Delft, Internal report nr. PT 07.012.

- description available MST-based powerless mechanical clamping solutions;
- design MST-based mechanical clamps for integration with improved 2-D fibre positioning concept;
- engineering calculations and Comsol Multiphysics^{TM} FE models clamp functionality.

Bibliography

Akiyama, T., U. Staufer, and N.F. de Rooij (2002). Fast driving technique for integrated thermal bimorph actuator toward high-throughput atomic-force microscopy. *Review of Scientific Instruments 73*(7), 2643-2646.

Alting, L., F. Kimura, H.N. Hansen, and G. Bissacco (2003). Micro engineering. *Annals of the CIRP 52*(2), 1-23.

Aoshima, S., N. Yoshizawa, and T. Yabuta (1992). Compact mass axis alignment device with piezoelements for optical fibers. *IEEE Photonics Technology Letters 4*(5), 462-464.

Arai, F., D. Ando, T. Fukuda, Y. Nonoda, and T. Oota (1995). Micro manipulation based on micro physics - strategy based on attractive force reduction and stress measurement. In *IEEE/RSJ Int. Workshop on Intelligent Robots & Systems (IROS)*, Pittsburgh, PA, USA, pp. 236-241.

Armiento, C.A., A.J. Negri, M.J. Tabasky, R.A. Boudreau, M.A. Rothman, T.W. Fitzgerald, and P.O. Haugsjaa (1992). Gigabit transmitter array modules on silicon waferboard. *IEEE Transactions on Components, Hybrids, and Manufacturing Technology 15*(6), 1072-1080.

Assembléon (2008). *Technical specifications AX-201* (online). Available from: http://www.assembleon.com/surface-mount-assembly/pick-and-place-equipment/a-series/ax-201/specifications (last accessed 22 August 2008).

Baartman, J.P. (1995, Mar). *Automation of assembly operations on parts*. PhD Thesis, TU Delft, ISBN 90-370-0119-X.

Baba, A., H. Okano, H. Uetsuka, and M. Esashi (2003). 2 axes optical switch with holding mechanism. In *Proceedings IEEE Micro Electro Mechanical Systems (MEMS)*, 19-23 January, Kyoto, Japan, pp. 251- 254.

Beamesderfer, M.A., E. Litcher, and D.L. DeVoe (2001). Micromechanical clamps for optical fiber packaging of high aspect ratio MEMS devices. In *Proceedings ASME International Mechanical Engineering Congress and Exposition (IMECE)*, 11-16 November, New York, NY, USA, pp. 71-75.

Beranek, M.W., E.Y. Chan, C.-C. Chen, K.W. Davido, H.E. Hager, C.-S. Hong, D.G. Koshinz, M. Rassaian, H.P. Soares Jr., R.L. St. Pierre, P.Y. Anthony, M.A. Cappuzzo, J.V. Gates, L.T. Gomez, G.E. Henein, J. Shmulovich, M.A. Occhionero, and K.P. Fennessey (2000). Passive alignment optical subassemblies for military/aerospace fiber-optic transmitter/receiver modules. *IEEE Transactions on Advanced Packaging 23*(3), 461-469.

Böhringer, K.F., R.S. Fearing, and K.Y. Goldberg (1999). Microassembly. In S.Y. Nof (Ed.), *The Handbook of Industrial Robotics*, 2nd ed. New York: John Wiley & Sons, pp. 1045-1066.

Bostock, R.M., J.D. Collier, R.E. Jansen, R. Jones, D.F. Moore, and J.E. Townsend (1998). Silicon nitride microclips for the kinematic location of optic fibres in silicon V-shaped grooves. *Journal of Micromechanics and Microengineering 8*, 343-360.

Boudreau, R., P. Zhou, and T. Bowen (1998). Wafer scale photonic-die attachment. *IEEE Transactions on Components, Packaging, and Manufacturing Technology 21*(2), 136-139.

Boyle, P., D.F. Moore, R. Breen, R.R.A. Syms, H. Zou, and J. Stagg (2004). MEMS bistable clamp with electrical locking and release. In *Proceedings European Micromechanics Workshop (MME)*, 5-7 September, Leuven, Belgium, paper A10.

Breedis, J.B. (2001). Monte Carlo tolerance analysis of a passively aligned silicon waferboard package. In *Proceedings 51st Electronic Components and Technology Conference (ECTC)*, 29 May-1 June, Orlando, FL, USA, pp. 247-254.

Brouwer, D.M. (2007). *Design principles for six degrees-of-freedom MEMS-based precision manipulators*. PhD Thesis, Universiteit Twente, Enschede, The Netherlands. ISBN 978-90-365-2510-7.

Choi, M.H., H.J. Koh, E.S. Yoon, K.C. Shin, and K.C. Song (1999). Self-aligning silicon groove technology platform for the low cost optical module. In *Proceedings 49th Electronic Components and Technology Conference (ECTC)*, 1-4 June, San Diego, CA, USA, pp. 1140-1144.

Christiaans, H.H.C.M., A.L.A. Fraaij, E. De Graaff, and Ch.F. Hendriks (2004). *Methodologie van technisch-wetenschappelijk onderzoek*, Utrecht: Lemma BV. ISBN 90-5189-839-8 (in Dutch).

Chronis, N. and L.P. Lee (2005). Electrothermally activated SU-8 microgripper for single cell manipulation in solution. *IEEE Journal of Microelectromechanical Systems 14*(4), 857-863.

Chu, L.L. and Y.B. Gianchandani (2003). A micromachined 2D positioner with electrothermal actuation and sub-nanometer capacitive sensing. *Journal of Micromechanics and Microengineering 13*, 279-285.

Chu, L.L., L. Que, A.D. Oliver, and Y.B. Gianchandani (2006). Lifetime studies of electrothermal bent-beam actuators in single-crystal silicon and polysilicon. *IEEE Journal of Microelectromechanical Systems 15*(3), 498-506.

Chui, B.W., M. Ashegi, Y.S. Yu, K.E. Goodson, and T.W. Kenny (1999). Intrinsic-carrier thermal runaway in silicon microcantilevers. *Microscale Thermophysical Engineering 3*(3), 217-228.

Cohen, M.S., M.F. Cina, E. Bassous, M.M. Oprysko, and J.L. Speidell (1991). Passive laser-fiber alignment by index method. *IEEE Photonics Technology Letters 3*(11), 985-987.

Cohn, M.B., K.F. Böhringer, J.M. Noworolski, A. Singh, C.G. Keller, K.Y. Goldberg, and R.T. Howe (1998). Microassembly technologies for MEMS. In *Proceedings SPIE 3513*, pp. 2-16.

Comtois, J.H., V.M. Bright, and M.W. Phipps (1995). Thermal microactuators for surface-micromachining processes. In *Proceedings SPIE 2642*, pp. 10-21.

Daneman, M.J., N.C. Tien, O. Solgaard, A.P. Pisano, K.Y. Lau, and R.S. Muller (1996). Linear microvibromotor for positioning optical components. *IEEE Journal of Microelectromechanical Systems 5*(3), 159-165.

Datta, M., Z. Hu, and M. Dagenais (2003). A novel method for fabrication of a hybrid optoelectronic packaging platform utilizing passive-active alignment. *IEEE Photonics Technology Letters 15*(2), 299-301.

Dautartas, M.F., J. Fisher, H. Luo, P. Datta, and A. Jeantilus (2002). Hybrid optical packaging, challenges and opportunities. In *Proceedings 52nd Electronic Components and Technology Conference (ECTC)*, 28-31 May, San Diego, CA, USA, pp. 787-793.

Dechev, N., W.L. Cleghorn, and J.K. Mills (2004). Microassembly of 3-D microstructures using a compliant, passive microgripper. *IEEE Journal of Microelectromechanical Systems 13*(2), 176-189.

Deladi, S., G.J.M. Krijnen, and M.C. Elwenspoek (2004). Distinction of the irreversible and reversible actuation regions of B-doped poly-Si based electrothermal actuators. *Journal of Micromechanics and Microengineering 14*, S31-S36.

Deng, K. and W.H. Ko (1992). A study of static friction between silicon and silicon compounds. *Journal of Micromechanics and Microengineering 2*(1), 14-20.

Dilthey, U., A. Brandenburg, and M. Möller (2001). Study of factors influencing the microdosing of unfilled adhesives. *Journal of Micromechanics and Microengineering 11*, 474-480.

Doll, W.J. and M.A. Vonderembse (1991). The evolution of manufacturing systems: towards the post-industrial enterprise. *OMEGA International Journal of Management Science 19*(5), 401-411.

Draka (2008). *Single-mode optical fibre type G.652.B* (online). Available from: http://www.drakafibre.com/draka/DrakaComteq/Drakafibre/Languages/English/Navigation/Markets%26Products/Technical_Support/Datasheets/DCOF_G652B_SMF.pdf (last accessed 22 August 2008).

Dutton, H.J.R. (1998). *Understanding optical communications*, Upper Saddle River, New Jersey: Prentice Hall PTR. ISBN 0-13-020141-3.

Ebefors, T., E. Kälvesten, and G. Stemme (1998). New small radius joints based on thermal shrinkage of poyimide in V-grooves for robust self-assembly 3D microstructures. *Journal of Micromechanics and Microengineering 8*, 188-194.

Edwards, C.A. and H.M. Presby (1993). Coupling-sensitivity comparison of hemispheric and hyperbolic microlenses. *Applied Optics 32*(9), 1573-1577.

Edwards, C.A., H.M. Presby, and C. Dragone (1993). Ideal microlenses for laser-to-fiber coupling. *Journal of Lightwave Technology 11*(2), 252-257.

Ehmann, M, P. Ruther, M. von Arx and O. Paul (2001). Operation and short-term drift of polysilicon-heated CMOS microstructures at temperatures up to 1200 K. *Journal of Micromechanics and Microengineering 11*, 397-401.

Ehmann, M., F. Schubert, P. Ruther, and O. Paul (2002). Thermally activated ageing of polysilicon. In *Proceedings IEEE Sensors*, June 12-14, Orlando, FL, USA, pp. 602-606.

EV Group (2008a). *EVG620 double-side mask aligner* (online). Available from: http://www.evgroup.com/market_to_product.asp?MTP_id=1

(last accessed 22 August 2008).

EV Group (2008b). *EVG101 advanced resist processing system* (online). Available from: http://www.evgroup.com/market_to_product.asp?MTP_id=31 (last accessed 22 September 2008).

Fearing, R.S. (1995). Survey of sticking effects for micro parts handling. In *IEEE/RSJ Int. Workshop on Intelligent Robots & Systems (IROS)*, Pittsburgh, PA, USA, pp. 212-217.

Field, L.A., D.L. Burriesci, P.R. Robrish, and R.C. Ruby (1996). Micromachined 1×2 optical-fiber switch. *Sensors and Actuators A 53*, 311-315.

Flanagan, C., S. Trask, and R. Heyler (2003). Direct-coupling retention using laser soldering\: technical and economical benefits. In *Proceedings 53rd Electronic Components and Technology Conference (ECTC)*, 27-30 May, New Orleans, LA, USA, pp. 1308-1311.

Fujita, H. (1998). Microactuators and micromachines. *Proceedings of the IEEE 86*(8), 1721-1732.

Geisberger, A.A., N. Sarkar, M. Ellis, and G.D. Skidmore (2003). Electrothermal properties and modeling of polysilicon microthermal actuators. *IEEE Journal of Microelectromechanical Systems 12*(4), 513-523.

Gerlach, A., H. Lambach, and D. Seidel (1999). Propagation of adhesives in joints during capillary adhesive bonding of microcomponents. *Microsystem Technologies 6*, 19-22.

Gerlach, T., D. Enke, T. Frank, L. Hutschenreuther, H-J. Schacht, and R. Schüler (1997). Automatic adjustment of monomode optical waveguides by a microsystem. *Journal of Micromechanics and Microengineering 7*, 227-229.

González, C., R.L. Smith, D.G. Howitt, and S.D. Collins (1998). MicroJoinery: concept, definition, and application to microsystem development. *Sensors and Actuators A 66*, 315-332.

Goodrich, J. (2001). A silicon optical bench approach to low cost high speed transceivers. In *Proceedings 51st Electronic Components and Technology Conference (ECTC)*, 29 May-1 June, Orlando, FL, USA, pp. 238-241.

Grade, J.D., K.Y. Yasumura, and H. Jerman (2005). Micromachined actuators with braking mechanisms. *Sensors and Actuators A 122*, 1-8.

Greitmann, G. and R.A. Buser (1996). Tactile microgripper for automated handling of microparts. *Sensors and Actuators A 53*, 410-415.

Guckel, H., J. Klein, T. Christenson, K. Skrobis, M. Laudon, and E. Lovell (1992). Thermo-magnetic metal flexure actuators. In *Technical Digest 5th IEEE Solid-State Sensors and Actuators Workshop*, June 22-25, Hilton Head, SC, USA, pp. 73-75.

Guo, Z., Y. Meng, H. Wu, C. Su, and S. Wen (2007). Measurement of static and dynamic friction coefficients of sidewalls of bulk-microfabricated MEMS devices with an on-chip micro-tribotester. *Sensors and Actuators A 135*, 863-869.

Haake, J.M., R.L. Wood, and V.R. Dhuler (1998). In-package active fiber optic micro-aligner. In *Proceedings SPIE 3276*, pp. 207-219.

Han, H., L.E. Weiss, and M.L. Reed (1992). Micromechanical Velcro. *IEEE Journal of Microelectromechanical Systems 1*(1), 37-43.

Heikkinen, V. (2004, Jun). *Tunable laser module for fibre optic communications*. PhD Thesis, University of Oulu, Finland, ISBN 951-38-6375-1.

Henneken, V.A., M. Tichem, and P.M. Sarro (2006). In-package MEMS-based thermal actuators for micro-assembly. *Journal of Micromechanics and Microengineering 16*, S107-115.

Henneken, V.A., W.P. Sassen, W. van der Vlist, W.H.A. Wien, M. Tichem, and P.M. Sarro (2008). Two-dimensional fiber-positioning and clamping device for product-internal microassembly. *IEEE Journal of Microelectromechanical Systems 17*(3), 724-734.

Hickey, R., D. Sameoto, T. Hubbard, and M. Kujath (2003). Time and frequency response of two-arm micromachined thermal actuators. *Journal of Micromechanics and Microengineering 13*, 40-46.

Hirano, T., L-S. Fan, J.Q. Gao, and W. Lee (1998). MEMS milliactuator for hard-disk-drive tracking servo. *IEEE Journal of Microelectromechanical Systems 7*(2), 149-155.

Hoffmann, M., D. Nüsse, and E. Voges (2003a). An electrostatically actuated 1×2 moving-fiber switch. *IEEE Photonics Technology Letters 15*(1), 39-41.

Hoffmann, M., P. Kopka, D. Nüsse, and E. Voges (2003b). Fibre-optical MEMS switches based on bulk silicon micromachining. *Microsystem Technologies 9*, 299-303.

Horsley, D.A., A. Singh, A.P. Pisano, and R. Horowitz (1997). Angular micropositioners for disk drives. In *Proceedings IEEE Micro Electro Mechanical Systems (MEMS)*, 26-30 January, Nagoya, Japan, pp. 454-459.

Hoshino, K., K. Yamada, K. Matsumoto, and I. Shimoyama (2003). A diffraction-limited-resolution full color display with a 10-μm-square visu-

al field. In *Proceedings IEEE Micro Electro Mechanical Systems (MEMS)*, 19-23 January, Kyoto, Japan, pp. 283-286.

Hoving, W. (1997). Accurate manipulation using laser technology. In *Proceedings SPIE 3097*, pp. 284-295.

Huang, L.-S., S.-S. Lee, E. Motamedi, M.C. Wu, and C.-J. Kim (1998). MEMS packaging for micromirror switches. In *Proceedings 48th Electronic Components and Technology Conference (ECTC)*, 25-28 May, Seattle, WA, USA, pp. 592-597.

Huang, Q.-A. and N.K.S. Lee (1999). Analysis and design of polysilicon thermal flexure actuator. *Journal of Micromechanics and Microengineering 9*, 64-70.

Humpston, G. (1997). Flip-chip solder bonding for microsystems. In *Digest IEE Colloquium on Assembly and Connections in Microsystems*, 26 February, London, UK, pp. 1-3.

Hunziker, W., W. Vogt, H. Melchior, P. Buchmann, and P. Vettiger (1995). Passive self-aligned low-cost packaging of semiconductor laser arrays on Si motherboard. *IEEE Photonics Technology Letters 7*(11), 1324-1326.

Hutter, M., H. Oppermann, G. Engelmann, and H. Reichl (2004). High precision passive alignment flip chip assembly using self-alignment and micromechanical stops. In *Proceedings 6th Electronics Packaging Technology Conference (EPTC)*, 8-10 December, Singapore, pp. 385-389.

Hwang, I.-H., Y.-G. Lee, and J.-H. Lee (2006). A micromachined friction meter for silicon sidewalls with consideration of contact surface shape. *Journal of Micromechanics and Microengineering 16*, 2475-2481.

Ishikawa, K., J. Zhang, A. Tuantranont, V.M. Bright, and Y-C. Lee (2003). An integrated micro-optical system for VCSEL-to-fiber active alignment. *Sensors and Actuators A 103*, 109-115.

Itoh, M., J. Sasaki, A. Uda, I. Yoneda, H. Honmou, and K. Fukushima (1996). Use of AuSn solder bumps in three-dimensional passive aligned packaging of LD/PD arrays on Si optical benches. In *Proceedings 46th Electronic Components and Technology Conference (ECTC)*, 28-31 May, Orlando, FL, USA, pp. 1-7.

Jackson, K.P., E.B. Flint, M.F. Cina, D. Lacey, J.M. Trewhella, T. Caulfield, and S. Sibley (1992). A compact multichannel transceiver module using planar-processed optical waveguides and flip-chip optoelectronic components. In *Proceedings 42nd Electronic Components and Technology Conference (ECTC)*, 18-20 May, San Diego, CA, USA, pp. 93-97.

Jebens, R., W. Trimmer, and J. Walker (1989). Microactuators for aligning optical fibers. *Sensors and Actuators 20, 65-73.*

Joo, G.-C., S.-H. Lee, K.-S. Park, J.-S. Choi, N. Hwang, and M.-K. Song (2000). A novel bidirectional optical coupling module for subscribers. *IEEE Transactions on Advanced Packaging 23*(4), 681-685.

Joyce, W.B. and B.C. DeLoach (1984). Alignment of Gaussian beams. *Applied Optics 23*(23), 4187-4196.

Kaufmann, H., P. Buchmann, R. Hirter, H. Melchior, and G. Guekos (1986). Self-adjusted permanent attachment of fibers to GaAs waveguide components. *Electronics Letters 22*(12), 642-643.

Kikuya, Y., M. Hirano, K. Koyabu, and F. Ohira (1993). Micro alignment machine for optical coupling. In *Proceedings IEEE Micro Electro Mechanical Systems (MEMS)*, 7-10 February, Fort Lauderdale, FL, USA, pp. 36-41.

Kim, S-H., Y. Yee, J. Choi, H. Kwon, M-H. Ha, C. Oh, and J.U. Bu (2003). Integrated MEMS optical flying head with lens positioning actuator for small form factor optical data storage. *Sensors and Actuators A 114*, 429-437.

Koster, M.P. (2000). *Constructieprincipes voor het nauwkeurig bewegen en positioneren*. 3rd ed. (rev.) Enschede: Twente University Press. ISBN 9-0365-1455-X (in Dutch).

Kurata, K., K. Yamauchi, A. Kawatani, H. Tanaka, H. Honmou, and S. Ishikawa (1996). A surface mount single-mode laser module using passive alignment. *IEEE Transactions on Components, Packaging, and Manufacturing Technology 19*(3), 524-531.

Kuribayashi, K. and T. Fujii (1998). A new micro SMA thin film actuator prestrained by polyimide. In *Proceedings IEEE Micromechatronics and Human Science (MHS)*, 25-28 November, Nagoya, Japan, pp. 165-170.

Kurniawan, I. and M. Tichem (2008). Investigation of electrostatic self-alignment. In *Proceedings European Society for Precision Engineering and Technology Conference (EUSPEN)*, May 18-22, Zurich, Switzerland, II: 174-178.

Lambert, P. (2005). *A contribution to microassembly: a study of capillary forces as a gripping principle*. PhD Thesis, Université Libre de Bruxelles, Belgium.

Lang, D. (2008, Oct). *A study on micro-gripping technologies*. PhD Thesis, TU Delft, ISBN 978-90-9023424-3.

Langen, H.H., T. Masuzawa, and M. Fujino (1995). Modular method for microparts machining and assembly with self-alignment. *Annals of the CIRP 44*(1), 173-176.

Lau, G.-K. (2007, Dec). *Micro-electro-thermal actuators using confined polymers*. PhD Thesis, TU Delft, ISBN 90-902-2531-9.

Lee, J., T. Beechem, T.L. Wright, B.A. Nelson, S. Graham, and W.P. King (2006). Electrical, thermal, and mechanical characterization of silicon microcantilever heaters. *IEEE Journal of Microelectromechanical Systems 15*(6), 1644-1655.

Li, B., H. Wirz, and A. Sharon (2005). Optimizing fiber coupling with a quasi-passive microoptical bench. *IEEE Journal of Microelectromechanical Systems 14*(6), 1339-1346.

Lide, D.R. (2006). *Handbook of Chemistry and Physics*. 87th ed. Boca Raton: CRC Press.

Lin, L.Y. and E.L. Goldstein (2002). Opportunities and challenges for MEMS in lightwave communications. *IEEE Journal on Selected Topics in Quantum Electronics 8*(1), 163-172.

Lin, L.Y., J.L. Shen, S.S. Lee, G.D. Su, and M.C. Wu (1997). Microactuated micro-XYZ stages for free-space micro-optical bench. In *Proceedings IEEE Micro Electro Mechanical Systems (MEMS)*, 26-30 January, Nagoya, Japan, pp. 43-48.

Lin, L.Y., S.S. Lee, K.J. Pister, and M.C. Wu (1994). Micro-machined three-dimensional micro-optics for integrated free-space optical system. *IEEE Photonics Technology Letters 6*(12), 1445-1447.

Lin, Y., W. Liu, and F.G. Shi (2006). Adhesive joint design for minimizing fiber alignment shift during UV curing. *IEEE Transactions on Advanced Packaging 29*(3), 520-524.

Lindgren, S., H. Åhlfeldt, L. Bäcklin, L. Forssén, C. Vieider, H. Elderstig, M. Svensson, L. Granlund, L. Andersson, B. Kerzar, B. Broberg, O. Kjebon, R. Schatz, E. Forzelius, and S. Nilsson (1997). 24-GHz modulation bandwidth and passive alignment of flip-chip mounted DFB laser diodes. *IEEE Photonics Technology Letters 9*(3), 306-308.

Lo, J.C.C., S.W.R. Lee, S.H.K. Lee, J.S. Wu, and M.M.F. Yuen (2004). Modified passive alignment of optical fibers with low viscosity epoxy flow running in V-grooves. In *Proceedings 54th Electronic Components and Technology Conference (ECTC)*, 1-4 June, Las Vegas, NV, USA, pp. 830-834.

Lott, C.D., T.W. McLain, J.N. Harb, and L.L. Howell (2002). Modeling the thermal behaviour of a surface-micromachined linear-displacement thermomechanical microactuator. *Sensors and Actuators A 101*, 239-250.

Luetzelschwab, M., D. Weiland, and M.P.Y. Desmulliez (2005). Submicron alignment of a two-dimensional array of multiple single-mode fibers. *IEEE Photonics Technology Letters 17*(12), 2634-2636.

Madou, M.J. (2002). *Fundamentals of microfabrication: the science of miniaturization*. 2nd ed. Boca Raton: CRC Press LLC. ISBN 0-8493-0826-7.

Maloney, J.M., D.S. Schreiber, and D.L. DeVoe (2004). Large-force electrothermal linear micromotors. *Journal of Micromechanics and Microengineering 14*, 226-234.

Mankame, N.D. and G.K. Ananthasuresh (2001). Comprehensive thermal modelling and characterization of an electro-thermal-compliant microactuator. *Journal of Micromechanics and Microengineering 11*, 452-462.

McCarthy, B., V.M. Bright, and J.A. Neff (2003). A multi-component solder self-assembled micromirror. *Sensors and Actuators A 103*, 187-193.

MEMSCAP (2008). *MUMPs Multi-User MEMS Processes* (online). Available from: http://www.memscap.com/en_mumps.html (last accessed 22 August 2008).

Mickelson, A.R., N.R. Basavanhally, and Y-C. Lee (Eds.) (1997). *Optoelectronic packaging*. New York: John Wiley & Sons. ISBN 0-471-11188-0.

Mills, A.F. (1999). *Basic Heat and Mass Transfer*. 2nd ed. Upper Saddle River: Prentice Hall.

Mitsubishi (2008). *MELFA Robots - RP Series* (online). Available from: http://www.mitsubishi-automation.com/products/robots_RP.html (last accessed 22 August 2008).

Mitze, T., M. Schnarrenberger, L. Zimmermann, J. Bruns, F. Fidorra, K. Janiak, J. Kreissl, S. Fidorra, H. Heidrich, and K. Petermann (2006). CWDM transmitter module based on hybrid integration. *IEEE Journal of Selected Topics in Quantum Electronics 12*(5), 983-987.

Mobarhan, K.S., S. Jang, and R. Heyler (2000). Laser diode packaging technology: 980 nm EDFA pump lasers for telecommunication applications. *Application Note No. 3*, Newport Corporation, Irvine, USA, pp. 1-7.

Modavis, R.A. and T.W. Webb (1995). Anamorphic microlens for laser diode to single-mode fiber coupling. *IEEE Photonics Technology Letters 7*(7), 798-800.

Morgan, B., J. McGee, and R. Ghodssi (2007). Automated two-axes optical fiber alignment using grayscale technology. *IEEE Journal of Microelectromechanical Systems 16*(1), 102-110.

Motamedi, M.D. (Ed.) (2005). *MOEMS: micro-opto-electro-mechanical systems*. Bellingham: SPIE. ISBN 0-8194-5021-9.

Nakagawa, G., T. Yamamoto, S. Sasaki, M. Norimatsu, N. Yamamoto, T. Nosaka, K. Terada, K. Tanaka, K. Miura, and M. Yano (1998). High power and high sensitivity planar lightwave circuit module incorporating a novel passive alignment method. *Journal of Lightwave Technology 16*(1), 66-72.

Nokia (2008). *Nokia corporate information* (online). Available from: http://www.nokia.com/aboutnokia (last accessed 22 August 2008).

Okada, Y. and Y. Tokomaru (1984). Precise determination of lattice parameter and thermal expansion coefficient of silicon between 300 and 1500K. *Journal of Applied Physics 56*(2), 314-320.

Ou, S., G. Xu, Y. Xu, and K.N. Tu (2004). Optical fiber packaging by lead (Pb)-free solder in V-grooves. *Ceramics International 30*, 1115-1119.

Owen, M. (2000). Agilent Technologies' singlemode small form factor (SFF) module incorporates micromachined silicon, automated passive alignment, and non-hermetic packaging to enable the next generation of low-cost fiber optic transceivers. *IEEE Transactions on Advanced Packaging 23*(2), 182-187.

Pahl, G. and W. Beitz (K. Wallace Ed.) (1996). *Engineering design: a systematic approach*. 2nd ed. Berlin: Springer. ISBN 3-540-19917-9.

Pan, C.S. and W. Hsu (1997). An electro-thermally and laterally driven polysilicon microactuator. *Journal of Micromechanics and Microengineering 7*, 7-13.

Pétremand, Y., P.-A. Clerc, M. Epitaux, R. Hauffe, W. Noell, and N.F. de Rooij (2007). Optical beam steering using a 2D MEMS scanner. In *Proceedings SPIE 6715*.

Pham, N.P., E. Boellaard, J.N. Burghartz, and P.M. Sarro (2004). Photoresist coating methods for the integration of novel 3-D RF microstructures. *IEEE Journal of Microelectromechanical Systems 13*(3), 491-499.

Pichonat-Gallois, E., V. Petrini, and M. de Labachelerie (2004). Design and fabrication of thermal actuators used for a micro-optical bench: application to a tunable Fabry-Perot filter. *Sensors and Actuators A 114*, 260-266.

Polytec (2008). *Polytec MSA-400 Micro System Analyzer - Features* (online). Available from: http://www.polytec.com/eur/158_6392.asp (last accessed 22 August 2008).

Prasad, R., K.F. Böhringer, and N.C. MacDonald (1995). Design, fabrication, and characterization of single crystal silicon latching snap fasteners for micro assembly. In *Proceedings ASME International Mechanical Engineering Congress and Exposition (IMECE'95)*, November, San Francisco, CA, USA.

Priyadarshi, A., L.H. Fen, S.G. Mhaisalkar, V. Kripesh, and A.K. Asundi (2006). Fiber misalignment in silicon V-groove based optical modules. *Optical Fiber Technology 12*, 170-184.

Que, L., J.-S. Park, and Y.B. Gianchandani (1999). Bent-beam electro-thermal actuators for high force applications. In *Proceedings IEEE Micro Electro Mechanical Systems (MEMS)*, 17-21 January, Orlando, FL, USA, pp. 31-36.

Que, L., J.-S. Park, and Y.B. Gianchandani (2001). Bent-beam electrothermal actuators - part I: single beam and cascaded devices. *IEEE Journal of Microelectromechanical Systems 10*(2), 247-254.

Qui, J., J.H. Lang, and A.H. Slocum (2004). A curved-beam bistable mechanism. *IEEE Journal of Microelectromechanical Systems 13*(2), 137-146.

Rassaian, M. and M.W. Beranek (1999). Quantitative characterization of 96.5Sn3.5Ag and 80Au20Sn optical fiber solder bond joints on silicon microoptical bench substrates. *IEEE Transactions on Advanced Packaging 22*(1), 86-93.

Read, B.C., V.M. Bright and J.H. Comtois (1995). Mechanical and optical characterization of thermal microactuators fabricated in a CMOS process. In *Proceedings SPIE 2642*, pp. 22-32.

Rehm, W., K. Adam, A. Göth, W. Jörg, J. Lauckner, J. Scherb, P. Aribaud, C. Artigue, C. Duchemin, B. Fernier, E. Grard, D. Keller, S. Kerboeuf, S. Rabaron, J.M. Rainsant, D. Tregoat, J.L. Nicque, A. Tournereau, P.J. Laroulandie, and P. Berthier (2000). Low cost laser module for SMT. In *Proceedings 50th Electronic Components and Technology Conference (ECTC)*, 21-24 May, Las Vegas, NV, USA, pp. 736-741.

Reid, J.R., V.M. Bright, and J.T. Butler (1998). Automated assembly of flip-up micromirrors. *Sensors and Actuators A 66*, 292-298.

Reinhart, G. and M. Höhn (1997). Growth into miniaturization - flexible microassembly automation. *Annals of the CIRP 46*(1), 7-10.

Rho, B.S. and J.W. Lim (2007). Multichip integration on a PLC platform for 16×16 optical switch module using passive alignment technique. *IEEE Transactions on Advanced Packaging 30*(3), 457-461.

Riethmüller, W. and W. Benecke (1988). Thermally excited silicon microactuators. *IEEE Transactions on Electron Devices 35*(6), 758-763.

Robert Bosch GmbH, (Lärmer, F. and A. Schilp) 1994. *Method of anisotropically etching silicon*. European patent application EP625285.

S.E.T. SAS (2008). *TRIAD 05 AP high accuracy assembly cell* (online). Available from: http://www.set-sas.fr/en/multipage.xml?pg=1&id=174515 (last accessed 22 August 2008).

Saitou, K., D-A. Wang, and S.J. Wou (2000). Externally resonated linear microvibromotor for microassembly. *IEEE Journal of Microelectromechanical Systems 9*(3), 336-346.

Sasaki, J., M. Itoh, T. Tamanuki, H. Hatakeyama, S. Kitamura, T. Shimoda, and T. Kato (2001). Multiple-chip precise self-aligned assembly for hybrid integrated optical modules using Au-Sn solder bumps. *IEEE Transactions on Advanced Packaging 24*(4), 569-575.

Sassen, W.P. (2007, Apr). *Design and modelling of an improved MST-based 2 DOF positioning device*. MSc Thesis, TU Delft, Internal report nr. PT 07.009.

Sassen, W.P., V.A. Henneken, M. Tichem, and P.M. Sarro (2008). Contoured thermal V-beam actuator with improved temperature uniformity. *Sensors and Actuators A 144*, 341-347.

Schwab, P., T. Bowen, R. Perko, N. Delen, J. Goodrich, and R. Anderson (2004). A high throughput optoelectronic module assembly process. In *Proceedings 54th Electronic Components and Technology Conference (ECTC)*, 1-4 June, Las Vegas, NV, USA, pp. 1475-1478.

Sehr, H., A.G.R. Evans, A. Brunnschweiler, G.J. Ensell, and T.E.G. Niblock (2001). Fabrication and test of thermal vertical bimorph actuators for movement in the wafer plane. *Journal of Micromechanics and Microengineering 11*, 306-310.

Sernelius, B.E. (1990). Temperature-dependent resistivity of heavily doped silicon and germanium. *Physical Review B 41*, 3060-3068.

Shakespeare, W.J., R.A. Pearson, J.L. Grenestedt, P. Hutapea, and V. Gupta (2005). MEMS integrated submount alignment for optoelectronics. *Journal of Lightwave Technology 23*(2), 504-509.

Shivkumar, B. and C.-J. Kim (1997). Microrivets for MEMS packaging: concept, fabrication, and strength testing. *IEEE Journal of Microelectro-*

mechanical Systems 6(3), 217-225.

Silicon Valley Microelectronics (2008). *Specifications 100 mm diameter standard silicon wafers* (online). Available from: http://www.svmi.com/diameter.aspx?id=3 (last accessed 22 August 2008).

Sinclair, M.J. (2000). A high force low area MEMS thermal actuator. In *Proceedings IEEE Inter Society Conference on Thermal Phenomena*, May 23-26, Las Vegas, NV, USA, pp. 127-132.

Srinivasan, U., M.A. Helmbrecht, C. Rembe, R.S. Muller, and R.T. Howe (2002). Fluidic self-assembly of micromirrors onto microactuators using capillary forces. *IEEE Journal on Selected Topics in Quantum Electronics 8*(1), 4-11.

Strandman, C. and Y. Bäcklund (1997). Bulk silicon holding structures for mounting of optical fibers in V-grooves. *IEEE Journal of Microelectromechanical Systems 6*(1), 35-40.

Su, Y-C. and L. Lin (2005). Localized bonding processes for assembly and packaging of polymeric MEMS. *IEEE Transactions on Advanced Packaging 28*(4), 635-642.

Syms, R.R.A. (1999). Surface tension powered self-assembly of 3-D micro-optomechanical structures. *IEEE Journal of Microelectromechanical Systems 8*(4), 448-455.

Syms, R.R.A. (2002). Long-travel electrothermally driven resonant cantilever microactuators. *Journal of Micromechanics and Microengineering 12*, 211-218.

Syms, R.R.A., H. Zou, and J. Stagg (2004a). Robust latching MEMS translation stages for micro-optical systems. *Journal of Micromechanics and Microengineering 14*, 667-674.

Syms, R.R.A., H. Zou, J. Stagg, and D.F. Moore (2004b). Multistate latching MEMS variable optical attenuator. *IEEE Photonics Technology Letters 16*(1), 191-193.

Syms, R.R.A., H. Zou, J. Stagg, and D.F. Moore (2004c). MEMS variable optical attenuator with a compound latch. *Microelectronic Engineering 73-74*, 423-428.

Tabib-Azar, M. (2000). *Microactuators: electrical, magnetic, thermal, optical, mechanical, chemical, and smart structures*. 2nd ed. Boston: Kluwer Academic Publishers. ISBN 0-7923-8089-4.

Tan, Q. and Y.C. Lee (1996). Soldering technology for optoelectronic packaging. In *Proceedings 46th Electronic Components and Technology Conference (ECTC)*, 28-31 May, Orlando, FL, USA, pp. 26-36.

Tang, Z., R. Zhang, S.K. Mondal, and F.G. Shi (2001). Optimization of fiber-optic coupling and alignment tolerance for coupling between a laser diode and a wedged single-mode fiber. *Optics Communications 199*, 95-101.

Telcordia (2008). *GR-468-CORE General Reliability Assurance Requirements for Optoelectronic Devices Used in Telecommunications Equipment* (online). Available from: http://telecom-info.telcordia.com/site-cgi/ido/index.html (last accessed 22 August 2008).

Texas Instruments (2008). *Digital Light Processor (DLP) Technology* (online). Available from: http://www.dlp.com (last accessed 22 August 2008).

Tichem, M. and B. Karpuschewski (2002). Structuring of micro-assembly methods. In *CD-ROM Proceedings of the 33rd International Symposium on Robotics (ISR)*, 7-11 October, Stockholm, Sweden.

Tichem, M., B. Karpuschewski, and P.M. Sarro (2003). Self-adjustment of micro-mechatronic systems. *Annals of the CIRP 52*(1), 17-20.

Tichem, M., D. Lang, and B. Karpuschewski (2004). A classification scheme for quantitative analysis of micro-grip principles. *Assembly Automation 24*(1), 88-93.

Timoshenko, S.P. (1925). Analysis of bi-metal thermostats. *Journal of the Optical Society of America 11*(3), 233-255.

Unamuno, A. and D. Uttamchandani (2006). MEMS variable optical attenuator with vernier latching mechanism. *IEEE Photonics Technology Letters 18*(1), 88-90.

Unamuno, A., J. Yao, and D. Uttamchandani (2005). Alignment and fixing of fiber optics based on electrothermal MEMS actuators. *IEEE Photonics Technology Letters 17*(4), 816-818.

Van Brussel, H., J. Peirs, D. Reynaerts, A. Delchambre, G. Reinhart, N. Roth, M. Weck, and E. Zussman (2000). Assembly of Microsystems. *Annals of the CIRP 49*(2), 1-21.

Van der Burgh, H.J. (2007, Apr). *Design of an MST-based mechanical clamp for in-package optical fibre-chip coupling*. MSc Thesis, TU Delft, Internal report nr. PT 07.012.

Vereniging FME-CWM (1999). *Voorlichtingspublicatie Microlijmen VM 117*. ISBN 90-75740-16-6 (in Dutch).

Vos, J.A.W.M. (2001, Jun). *Module and system design in flexibly automated assembly*. PhD Thesis, TU Delft, ISBN 90-407-2195-5.

Wale, M.J. and C. Edge (1990). Self-aligned flip-chip assembly of photonic devices with electrical and optical connections. *IEEE Transactions on Components, Hybrids, and Manufacturing Technology 13*(4), 780-786.

Walker, J.A. (2000). The future of MEMS in telecommunications networks. *Journal of Micromechanics and Microengineering 10*, R1-R7.

Willemse, M.A. (1997, Sept). *Interactive product design tools for automated assembly*. PhD Thesis, TU Delft, ISBN 90-370-0126-9.

Witham, C.R., M.W. Beranek, B.R. Carlisle, E.Y. Chan, and D.G. Koshinz (2000). Fiber-optic pigtail assembly and attachment alignment shift using a low-cost robotic platform. In *Proceedings 50th Electronic Components and Technology Conference (ECTC)*, 21-24 May, Las Vegas, NV, USA, pp. 21-25.

Wittwer, J.W., M.S. Baker, and L.L. Howell (2006). Simulation, measurement, and asymmetric buckling of thermal microactuators. *Sensors and Actuators A 128*, 395-401.

Wu, M.C. (1997). Micromachining for optical and optoelectronic systems. *Proceedings of the IEEE 85*(11), 1833-1856.

Yamauchi, K., K. Kurata, M. Kurihara, Y. Sano, and Y. Sato (2000). Automated mass production line for optical module using passive alignment technique. In *Proceedings 50th Electronic Components and Technology Conference (ECTC)*, 21-24 May, Las Vegas, NV, USA, pp. 15-20.

Yang, H-A., M. Wu, and W. Fang (2005). Localized induction heating solder bonding for wafer level MEMS packaging. *Journal of Micromechanics and Microengineering 15*, 394-399.

Yeh, R. E.J.J. Kruglick, and K.S.J. Pister (1996). Surface-micromachined components for articulated microrobots. *IEEE Journal of Microelectromechanical Systems 5*(1), 10-17.

Zhang, R., S. K. Mondal, Z. Tang, and F. G. Shi (2001). Fiber-optic angular alignment automation: recent progress. In *Proceedings SMTA Conference on Optoelectronics and Telecom Revolution*, 14-15 November, Dallas, Texas, USA.

Summary

Product-internal assembly functions

A novel micro-assembly concept applied to optical interconnects

In recent decades, a major trend in production has been the continuing miniaturization of functions and devices. This leads to increased difficulties in the field of micro-assembly: the assembly of miniature parts into composed products. In addition to decreasing part and product dimensions, the positioning requirements have also become stricter. These increasing difficulties have led to the conception of a novel method to perform micro-assembly tasks, which is researched in this thesis: *micro-assembly using product-internal assembly functions* (PIAF). This method distinguishes itself from traditional assembly approaches by the fact that part of the assembly functionality is included into the product subject to assembly, and takes care of the fine assembly of parts, after an initial coarse assembly process. Although this added functionality may increase development cost, the overall cost including assembly can decrease, because of the expected reduction of the required accuracy, and hence the cost, of the preceding coarse assembly step. *Microsystem technology* (MST) was selected as enabling technology for the product-internal functionality, because of its capability to create very small structures with extremely high accuracies at potentially low cost, resulting from the batch processing.

The objective of the research has been to explore the technical feasibility to use MST-based product-internal assembly functions for the purpose of micro-assembly. The investigation was narrowed down to a realistic prod-

uct case, for which product-internal assembly functionality was designed, fabricated and tested: the accurate assembly of an optical fibre relative to a telecommunication laser diode. This case was selected for its alignment challenge with the strictest tolerances in the plane perpendicular to the light propagation direction.

For the fibre coupling case, solution principles for the main considered sub-functions *fine positioning*, *coarse assembly* and *final fixation* were investigated and developed in a step-wise approach, increasing in complexity from 1-D to 2-D fine positioning, and ultimately leading to a proposed overall design including integrated mechanical clamps for the final fixation. Demonstrators were developed and realized at the Delft Institute of Microsystems and Nanoelectronics (DIMES) of the TU Delft.

In-plane MST-based electrothermal actuators were selected for fine positioning and clamping of the fibre, based on their high attainable workloads and their simple construction. Two V-beam actuators were combined with two <111> plane wedge mechanisms to convert the in-plane actuator motions into in- and out-of-plane fibre tip movements. Fibre tip displacements in a diamond shaped positioning window of over 25 μm in-plane and more than 40 μm in the out-of-plane direction were shown with only a small visible hysteresis effect. Positioning resolutions smaller than 0.1 μm were measured, indicating that potential stick-slip due to the sliding of the fibre over the <111> surfaces was not relevant.

A fabricated mechanical clamp capable of powerless clamping was tested to function successfully in combination with the positioning concept. The clamp was able to take over and indirectly hold the fibre in position, by applying a clamp force on the fibre mechanism perpendicular to its fine positioning direction. Powering down both clamp and positioning actuator showed a fibre position shift of less than 0.1 μm. No visible shift in clamping position was observed after a series of vibration tests, indicating that the clamping function realises a stable final position. The developed wafer processing sequence allows both the position and clamping functionality to be realised in one monolithic chip.

A design is proposed for the coarse assembly process which precedes the fine assembly process using the developed chip. Solder self-alignment and lithographically defined mechanical alignment features reduce the required initial placement accuracy for the assembly equipment, while still achieving sufficiently accurate coarse positioning of the laser diode and the fibre to enable fine positioning with acceptably small positioning ranges. A tolerance analysis showed the feasibility of the proposed coarse assembly process, with the exception of the coarse alignment in the longitudinal fibre direction. This degree of freedom still requires a relatively accurately controlled assembly process using visual feedback.

Based on the results, it appears to be technically feasible to employ MST-based product-internal assembly functions for accurate assembly of an optical fibre relative to the laser diode in the considered product case. Some of the desired features could not be achieved, such as relaxed coarse assembly requirements in all directions. Position sensing was performed externally, however this was not considered problematic for application of the PIAF method. It is crucial to concurrently take all relevant aspects in the PIAF design process into account in order to achieve the best possible overall result.

Thus far, no examples are known of the PIAF method being carried out on commercial products. In general, future application is expected in products requiring micro-assembly steps with sub-μm accuracies in one or more degrees of freedom, and that have sufficiently large volumes to justify the relatively high non-recurring MST development cost. The fact that products containing MST-based components are increasingly applied in areas like consumer electronics, telecommunications, and the automotive industry appears promising for integration of MST-based product-internal assembly functionality in these types of products in the future.

Samenvatting

Product-interne assemblage functies

Een nieuw microassemblage concept toegepast op optische verbindingen

Een belangrijke trend in de afgelopen jaren is de voortgaande miniaturisering van functies en producten. Dit leidt tot toenemende moeilijkheden op het gebied van microassemblage: de assemblage van miniatuurcomponenten tot samengestelde producten. Naast afnemende onderdeel- en productdimensies zijn ook de positioneereisen strikter geworden. Deze toenemende moeilijkheden hebben geleid tot een nieuwe methode om microassemblagetaken uit te voeren, welke is onderzocht in deze studie: *microassemblage met behulp van productinterne assemblagefuncties* (PIAF). Deze methode onderscheidt zich van conventionele assemblagemethoden doordat een deel van de assemblagefunctionaliteit is geïntegreerd in het product dat wordt geassembleerd. Dit draagt bij aan de eindassemblage van onderdelen, na een initiële, minder nauwkeurige, assemblagestap. Hoewel deze toegevoegde functionaliteit de ontwikkelkosten mogelijk doet toenemen, kunnen de totale kosten inclusief assemblage *af*nemen door de verwachte afname van de benodigde nauwkeurigheid van de voorbereidende assemblagestap. *Microsysteemtechnologie* (MST) is geselecteerd als fabricagetechnologie voor de productinterne functionaliteit, vanwege de mogelijkheid om hiermee zeer kleine structuren te vervaardigen met extreem hoge nauwkeurigheden, tegen potentieel lage kosten door middel van parallelfabricage.

Het doel van het onderzoek was de exploratie van de technische haalbaarheid van het gebruik van MST-gebaseerde productinterne assemblagefuncties voor microassemblage. Het onderzoek is ingeperkt tot een realistische productsituatie, waarvoor productinterne assemblage functies zijn ontworpen, vervaardigd en getest: de nauwkeurige assemblage van een optische fiber ten opzichte van een laser diode voor telecommunicatiedoeleinden. Dit voorbeeld is geselecteerd vanwege de aanzienlijke uitlijnuitdaging met de meest strikte nauwkeurigheidseisen loodrecht op de voortbewegingsrichting van het licht.

Oplossingsprincipes voor de subfuncties *fijnpositionering*, *grove assemblage* en *eindfixatie* zijn onderzocht en stapsgewijs ontwikkeld voor het fiberuitlijningsvoorbeeld, toenemend in complexiteit van 1-D naar 2-D fijnpositionering, uiteindelijk resulterend in een totaalontwerp inclusief geïntegreerde mechanische klemmen voor de uiteindelijke fixatie. Demonstratieversies zijn ontwikkeld en gerealiseerd in het Delft Institute of Microsystems and Nanoelectronics (DIMES) van de TU Delft.

In het vlak werkende MST-gebaseerde elektrothermische actuatoren zijn geselecteerd voor fijnpositionering en klemmen van de fiber, vanwege de hoge haalbare arbeid en de eenvoudige constructie. Twee V-vormige actuatoren zijn gecombineerd met twee mechanismen met <111> vlakken. Deze werken als wigelementen voor het converteren van de in het vlak werkende actuatorbewegingen naar zowel in als uit het vlak positionering van de fibertip. Fibertipverplaatsingen in een ruitvormig positioneerbereik van meer dan 25 μm in het vlak en 40 μm uit het vlak zijn getoond met slechts een beperkte hoeveelheid hysterese zichtbaar. Positioneerresoluties kleiner dan 0.1 μm zijn gemeten, waaruit kan worden afgeleid dat mogelijke stick-slip ten gevolge van glijden van de fiber over de <111> vlakken niet van belang is.

Uit tests met een vervaardigde mechanische klem, geschikt om zonder vermogen klemkracht uit te oefenen, is gebleken dat deze succesvol kan worden toegepast in combinatie met het positioneerconcept. De klem was in staat om indirect de fiberpositie over te nemen, door een klemkracht aan te laten grijpen op het wigmechanisme loodrecht op zijn positioneerrichting. Uitschakelen van zowel de klemactuator als de positioneeractuator resulteerde in een fiberpositieverandering van minder dan 0.1 μm. Na een serie trillingstesten was de klempositie niet zichtbaar veranderd, wat aangeeft dat de klem een stabiele eindpositie waarborgt. Met het ontwikkelde fabricageproces kunnen de positioneerfunctionaliteit en de klemfunctionaliteit in dezelfde chip worden gerealiseerd.

Een ontwerp is gemaakt voor de grove assemblagestap die voorafgaat aan de fijnassemblage met behulp van de ontwikkelde chip. Zelfuitlijning met behulp van soldeer en gebruikmaking van lithografisch gedefinieerde

mechanische uitlijnstructuren kan de benodigde plaatsingsnauwkeurigheid van de gebruikte assemblage apparatuur reduceren, terwijl toch voldoende nauwkeurige positionering van de laser diode en de fiber wordt bereikt om de uiteindelijke fijnpositionering uit te kunnen voeren met in de chip ingebouwde microactuatoren. Een tolerantieanalyse toonde de haalbaarheid van het voorgestelde grove assemblageproces, met uitzondering van de grove uitlijning in de lengterichting van de fiber. In deze richting was nog steeds een relatief nauwkeurige uitlijningsstap nodig door middel van positieterugkoppeling met behulp van beeldherkenning.

Op basis van de resultaten is geconcludeerd dat het technisch mogelijk is om MST-gebaseerde productinterne assemblage functies toe te passen voor de nauwkeurige assemblage van een optische fiber ten opzichte van de laser diode in het beschouwde productvoorbeeld. Niet alle gewenste aspecten konden worden gerealiseerd, zoals ruimere grove assemblage-eisen in alle richtingen. Positiemeting was extern uitgevoerd, maar dit was geen bezwaar voor toepassing van de PIAF methode. Het is van groot belang gebleken om in het PIAF ontwerpproces met alle relevante aspecten gelijktijdig rekening te houden om het best mogelijke totaalresultaat te bereiken.

Tot op heden zijn geen voorbeelden bekend van toepassing van de PIAF methode in commerciële producten. Algemeen gesproken is toekomstige toepassing verwacht in producten waarvoor microassemblage met submicrometer nauwkeurigheden in één of meerdere richtingen vereist is, en die in voldoende grote hoeveelheden worden geproduceerd om de relatief hoge MST ontwikkelkosten te rechtvaardigen. Het feit dat steeds meer producten met MST-gebaseerde componenten worden toegepast in gebieden zoals consumentenelektronica, telecommunicatie en de automobielindustrie is veelbelovend voor de integratie van MST-gebaseerde productinterne assemblage functies in deze typen producten in de toekomst.

List of publications

Journal publications

Henneken, V.A., W.P. Sassen, W. van der Vlist, W.H.A. Wien, M. Tichem, and P.M. Sarro (2008). Two-dimensional fiber-positioning and clamping device for product-internal microassembly. *IEEE Journal of Microelectromechanical Systems 17*(3), 724-734.

Sassen, W.P., V.A. Henneken, M. Tichem, and P.M. Sarro (2008). An improved in-plane thermal folded V-beam actuator for optical fibre alignment. *Journal of Micromechanics and Microengineering 18*, doi: 10.1088/0960-1317/18/7/075033, 9 pp.

Sassen, W.P., V.A. Henneken, M. Tichem, and P.M. Sarro (2008). Contoured thermal V-beam actuator with improved temperature uniformity. *Sensors and Actuators A 144*, 341-347.

Henneken, V.A., M. Tichem, and P.M. Sarro (2006). In-package MEMS-based thermal actuators for micro-assembly. *Journal of Micromechanics and Microengineering 16*, S107-115.

Henneken, V.A., M. Tichem, and B. Karpuschewski (2004). Exploring the benefits of MEMS for micro assembly tasks. *Assembly Automation 24*(4), 416-421.

Refereed conference publications

Henneken, V.A., M. Tichem, and P.M. Sarro (2006). Improved thermal U-beam actuators for micro-assembly. In *CD-ROM Proceedings Eurosensors XX*, September 17-20, Göteborg, Sweden.

Henneken, V.A. and M. Tichem (2006). Tolerance budgeting in a novel coarse-fine strategy for micro-assembly. In *Proceedings 3rd Int. Precision Assembly Seminar*, February 19-21, Bad Hofgastein, Austria, pp. 155-166.

Henneken, V.A., M. Tichem, and P.M. Sarro (2005). In-package MEMS-based thermal actuators for micro-assembly. In *Proceedings 16th MicroMechanics Europe Workshop*, September 4-6, Göteborg, Sweden, pp. 284-287.

Henneken, V.A., S.P.W. van den Bedem, M. Tichem, B. Karpuschewski, and P.M. Sarro (2004). Design of in-package MST-based actuators for micro-assembly. In *CD-ROM Proceedings 7th SAFE Workshop*, November 25-26, Veldhoven, The Netherlands.

Patent

Technische Universiteit Delft, (V.A. Henneken) 2007, *Inrichting voor het uitlijnen van een glasfibervezel.* Dutch patent application 2000876.

Highlights

- *Uitlijnen van optische glasvezels met behulp van in-package MST actuatoren.* PT Jaarboek 2008, annual publication of the Dutch Society for Precision Engineering (NVPT).
- Clamping demonstration setup displayed at various trade fairs and conferences, *e.g.* Precision Fair 2007, Veldhoven, The Netherlands, and EUSPEN 2008, Zürich, Switzerland.
- *DIY chip.* Delft Outlook 24(4), 2007.
- *Gespierde chips en mini-machines met gevoel.* Delta 38 (2007).
- *Beweging in de chip.* Delta 31 (2007).
- Cover photo Mikroniek 45(6), 2005.
- Invited plenary presentation Precision Fair 2004, November 10, Veldhoven, The Netherlands.

About the author

Vincent Henneken was born in Leidschendam, The Netherlands, on October 1, 1976. He followed his secondary education at the Alfrink College in Zoetermeer from 1988 to 1994. He received his Master Degree in Mechanical Engineering with a specialization in Production Engineering from Delft University of Technology, Delft, The Netherlands, in 2002. During his study, he was active in the Delft student volleyball club 'Punch', of which he was chairman in 1997-98 (one year fulltime university scholarship). For his graduation thesis, he worked on the design of a MEMS *xy* micro stage for nanometre applications in a transmission electron microscope (TEM). This project was performed at the Philips Centre for Industrial Technology, Eindhoven, The Netherlands (later renamed Philips Applied Technologies).

In 2003, he started as a PhD researcher at the Laboratory for Micro and Nano Engineering (MNE), which is part of the Precision and Microsystems Engineering (PME) Department of the Faculty of Mechanical, Materials, and Maritime Engineering of Delft University of Technology. The research objective of the project was to explore the technical feasibility of using MST-based product-internal assembly functions for the purpose of micro-assembly, which was focused towards the development of MST-based internal assembly functionality for optical fibre-chip alignment. The study comprised the design, modelling, fabrication, and testing of MST demonstrators including on-chip electrothermal actuators for 2-D fibre tip positioning and fixation by means of integrated micromechanical clamps. The device fabrication was conducted at the Delft Institute of Microsystems and Nanoelectronics (DIMES). The research activities during the PhD period have resulted in this thesis, a total of nine scientific publications and

a Dutch patent application. During his PhD project he coached over a dozen university students in their bachelor or master phase, of which about half during their MSc assignment.